Development of Robust State of Charge Estimation Algorithms for Lithium-ion Batteries in Electric Vehicles

Gautam Sethia

Development of Robust State of Charge Estimation Algorithms for Lithium-ion Batteries in Electric Vehicles

A

Thesis Submitted

in Partial Fulfilment of the Requirements

for the Degree of

DOCTOR OF PHILOSOPHY

By

Gautam Sethia

Department of Electronics and Electrical Engineering

Indian Institute of Technology Guwahati

Guwahati - 781 039, INDIA.

July, 2022

Declaration

I hereby certify that the work presented in this thesis entitled "**Development of Robust State of Charge Estimation Algorithms for Lithium-ion Batteries in Electric Vehicles**"is entirely my own account of research performed under the guidance of Prof. Somanath Majhi and Prof. Sisir Kumar Nayak. Any part of this work has not earlier been submitted for the award of any degree, diploma, associate-ship, fellowship or its equivalent to any University or Institution.

Date: 01-08-2022

Place: Guwahati.

Gautam Sethia

Registration no: 146102041

Dept. of Electronics & Electrical Engg.

Indian Institute of Technology Guwahati

Guwahati - 781039, Assam, India.

Certificate

This is to certify that the thesis titled "**Development of Robust State of Charge Estimation Algorithms for Lithium-ion Batteries in Electric Vehicles**", submitted by **Gautam Sethia** (146102041), a research scholar in the *Department of Electronics & Electrical Engineering, Indian Institute of Technology Guwahati*, for the award of the degree of **Doctor of Philosophy**, has been carried out by him under my supervision and guidance. The thesis has fulfilled all requirements as per the regulations of the institute and in my opinion has reached the standard needed for submission. The results embodied in this thesis have not been submitted to any other University or Institute for the award of any degree or diploma.

Date: 01-08-2022

Place: Guwahati.

Prof. Somanath Majhi

Dept. of Electronics & Electrical Engg.

Indian Institute of Technology Guwahati

Guwahati - 781039, Assam, India.

Date: 01-08-2022

Place: Guwahati.

Prof. Sisir Kumar Nayak

Dept. of Electronics & Electrical Engg.

Indian Institute of Technology Guwahati

Guwahati - 781039, Assam, India.

Acknowledgements

I am deeply grateful to my supervisors Prof. Somanath Majhi and Prof. Sisir Kumar Nayak for their encouragement, support and meticulous guidance throughout the entire duration of my research. With great patience and careful instructions, they have guided me step by step in my research and inspired me to keep on learning and exploring the ever-evolving world of technology. They broadened my perspectives in research and provided invaluable assistance to overcome the challenges that I faced. In addition, the progress I achieved in writing was mostly due to their extensive and critical reviews on my manuscripts and thesis. It has been a privilege to work under their tutelage.

I will be forever grateful to my doctoral committee members, Dr. Indrani Kar, Dr. Ravindranath Adda, and Dr. Hanumant Singh Shekhawat, for taking out the time from their busy schedule to evaluate my thesis work. Their valuable suggestions have been extremely helpful in setting the proper course of my research. I would also like to take this chance to appreciate all the faculty members of the department for their support and training during my academic studies. My special thanks to non teaching staffs of department and all the members of the Control & Instrumentation Laboratory for providing the technical resources and help throughout my research. I am also thankful to IIT Guwahati and MHRD, India, for granting the scholarship for undertaking my research.

My sincere gratitude goes to my friends in IITG who have always been there for me. Their friendship, love, and support helped in every step of my research and my life. I thank all my friends for always helping me with their useful suggestions and for providing an excellent research environment.

Last but not the least, I would like to thank my family. My parents, my parents-in-law, my siblings, and my sisters-in-law are the rock of my life and their endless love and support have made it possible for me to forever keep on moving forward. My most sincere thanks to my dear wife for her unconditional love and support. Finally, I thank God for providing the strength to work hard during my PhD tenure.

(Gautam Sethia)

Abstract

With increasing innovation and environmental awareness, electric vehicles (EVs) are becoming more popular than the conventional fuel based vehicles for emission-free future transportation. Lithium-ion battery (LIB) is the most suitable choice of energy storage system that works as the core of an EV. Along with the battery, a micro-controller known as battery management system (BMS) is required for reliable and secure operation of the battery. In BMS, real-time access to the information of one of the most critical battery states, known as state of charge (SOC), is vital as it indicates the remaining capacity of the battery, helps to prevent overcharging and undercharging, increases capacity utilization and lifespan, improves reliability, reduces cost, and ensures safety of the battery and its surroundings. Being an internal state, SOC is not available for direct measurement by any sensor and estimating it accurately for an LIB is non-trivial due to the highly nonlinear nature of the battery and various uncertain operating conditions. The literature reports several different approaches to estimate SOC of an LIB with each having its own advantages and drawbacks. It is important to note that each method of SOC estimation in literature possess some drawbacks either in accuracy or in real-time implementation. Hence, there is a scope for further improvement of these methods to enhance the performance of SOC estimation.

This thesis primarily offers improved solution for estimating SOC under diverse real-time constraints and operating conditions. It carefully focuses on improving various performance parameters of SOC estimation algorithm such as accuracy, robustness, computational time, and convergence speed. It strives to minimize the information requirement to achieve the cost-effective performance of SOC estimation. The algorithms are designed such that they can be implemented on a low cost BMS. For this purpose, four different model based approaches for SOC estimation have been progressively proposed and developed, including modelling of the LIB and its identification techniques. The proposed SOC estimation approaches are based on conventional super twisting algorithm (STA), strict Lyapunov su-

per twisting STA, adaptive Lyapunov STA, and adaptive generalized integral STA. For designing the state estimators, the required battery model parameters are identified using relay feedback, recursive least square with forgetting, and adaptive forgetting factor based recursive least square approaches. The effectiveness of conventional STA along with relay feedback approach for SOC estimation is validated with numerical simulations. The other SOC estimation algorithms are executed on an actual battery using a real-time driving cycle current profile under diverse conditions. The obtained results demonstrate the efficacy of these proposed methods in terms of crucial performance parameters such as accuracy, chattering, robustness, computational complexity, and convergence speed compared to the well-established SOC estimation methods in the current state-of-the art.

Contents

List of Figures

List of Tables

List of Acronyms

RES	Renewable energy sources
EV	Electric vehicle
LIB	Lithium-ion battery
BMS	Battery management system
SOC	State of charge
STA	Super twisting algorithm
OCV	Open circuit voltage
SOH	State of health
SOP	State of power
SLSTA	Strict Lyapunov super twisting algorithm
RLSF	Recursive least square with forgetting
ALSTO	Adaptive Lyapunov super twisting observer
GSTA	Generalized super twisting algorithm
ALSTA	Adaptive Lyapunov super twisting algorithm
AGISTO	Adaptive generalized integral super twisting observer
P2D	Pseudo two dimensional
SPM	Single particle model
BECM	Battery equivalent circuit model
PNGV	Partnership for a new generation of vehicle
ANN	Artificial neural network
SVM	Support vector machine
NN	Neural network
RBFNN	Radial basis function neural network
DNN	Deep neural network
RNN	Recurrent neural network
CNN	Convolution neural network

KF	Kalman filter
EKF	Extended Kalman filter
IEKF	Iterated extended Kalman filter
UKF	Unscented Kalman filter
SPKF	Sigma point Kalman filter
CDKF	Central difference Kalman filter
AEKF	Adaptive extended Kalman filter
AUKF	Adaptive unscented Kalman filter
PF	Particle filter
UPF	Unscented particle filter
PI	Proportional-integral
SMO	Sliding mode observer
FOSMO	First order sliding mode observer
SOSMO	Second order sliding mode observer
AGSMO	Adaptive gain sliding mode observer
CSTA	Conventional super twisting algorithm
VSCS	Variable structure control system
SMC	Sliding mode control
HOSM	Higher order sliding mode
GA	Genetic algorithm
PSO	Particle swarm optimization
ORLS	Ordinary recursive least square
SLSTO	Strict Lyapunov super twisting observer
CDDS	Chassis dynamometer drive schedule
MAE	Maximum absolute error
RMSE	Root-mean-square error
TVDSMO	Time-varying discrete sliding mode observer
AFFRLS	Adaptive forgetting factor based recursive least square
RMS	Root-mean-square

List of Publications

Journal Publications

1. G. Sethia, S. Majhi, S. Nayak, and S. Mitra, Strict Lyapunov super twisting observer design for state of charge prediction of lithium-ion batteries, *IET Renewable Power Generation*, vol. 15, pp. 424-435, 2021.

2. G. Sethia, S. Nayak, and S. Majhi, An approach to estimate lithium-ion battery state of charge based on adaptive Lyapunov super twisting observer, *IEEE Transactions on Circuits and Systems I: Regular Papers*, vol. 68, no. 3, pp. 1319-1329, 2021.

3. G. Sethia, S. Nayak, and S. Majhi, Development of a fast convergent state of charge estimator with improved real-time parameter identification, manuscript under preparation for *IEEE Transactions on Control System Technology*.

Conference Publications

1. G. Sethia, S. Majhi, and S. Nayak, Estimation of state of charge of Li-ion battery in EVs using relay feedback approach and super twisting sliding mode observer, *IEEE Conference on Decision and Control, Melbourne, Australia,* vol. 4, pp. 5038-5043, 2017.

1

Introduction

1.1 Introduction to energy storage system and electric vehicle

The rising level of global warming is one of the most alarming issues in the present time. Global warming accounts for the gradual increase of temperature of earth's surface primarily due to human-activities such as burning of fossil fuel. The emission of carbon dioxide, methane, nitrous oxide, and other green-house gases into the atmosphere is considered the primary reason for global warming. The green-house gases are known to be heat-trapping and thus increase the average global temperature by absorbing the heat from the sun. The other adverse effects of global warming are rising sea levels, floods, wildfires, droughts, hurricanes, melting of ice at glaciers and the poles of the earth, etc [1].

According to United States Environmental Protection Agency, the electricity sector is a major source of global warming, contributing 25% of the total green-house gases to the environment, as evident from Figure 1.1 [2]. Due to the environmental awareness and low operating cost, there is a

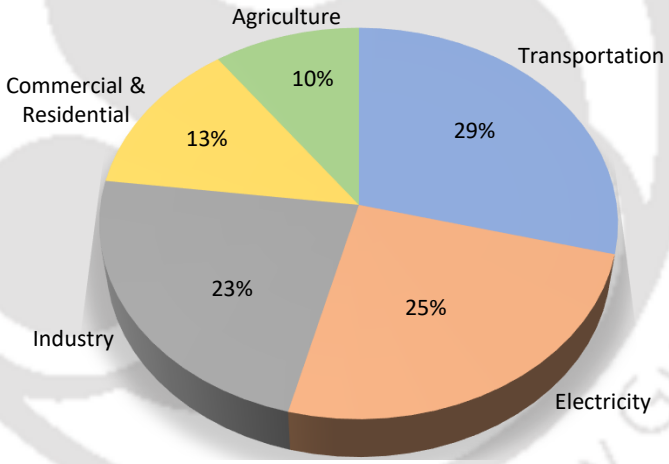

Figure 1.1: Sectors contributing to the emission of green-house gases.

swift increase in the use of renewable energy sources (RES) in smart grids and micro grids in recent years. The RES, such as solar and wind energy, are considered to be clean energy sources and do not contribute to the global warming. However, the availability of both wind and solar energy is intermittent in nature. Hence, an energy storage system such as battery is required to store the energy when available and use it later when needed. The battery can also assist in some emergency situations to increase the reliability of the smart grids and micro grids [3, 4]. In smart grids, battery can also be used for the purpose of peak shaving, voltage regulation, and frequency regulation by storing or feeding energy. Hence, the energy storage system such as battery has become an integral part of present smart grids and micro grids.

The high consumption of conventional fossil fuel in the transportation sector has made it the largest source of green-house gases, as shown in Figure 1.1 [2]. In 2014, the electricity sector was the highest contributor of green-house gases [2]. But in 2019, the transportation sector has surpassed the electricity sector to become its highest contributor (29%). Besides, the increasing price of fossil fuel also causes severe setback for the automobile sector and advocates the need to develop unconventional fuel-driven vehicles. In order to address these issues, the implementation of electric vehicles (EVs) has received significant attention and become an attractive alternative for vehicle industries and researchers. The EVs provide high torque, strong acceleration, and quiet operation. They also require less maintenance than the internal combustion engines. The battery storage system is a vital part of an EV and acts as its primary source of energy which powers the electric motors of the vehicle. It accounts for a significant part of the cost of an EV. Since the cost of the EV battery (especially lithium-ion battery) has been falling sharply since 2010, as shown in Figure 1.2, the market share of EVs has been continuously increasing and is expected to continue its growth [5]. Moreover, the operating cost of electricity to

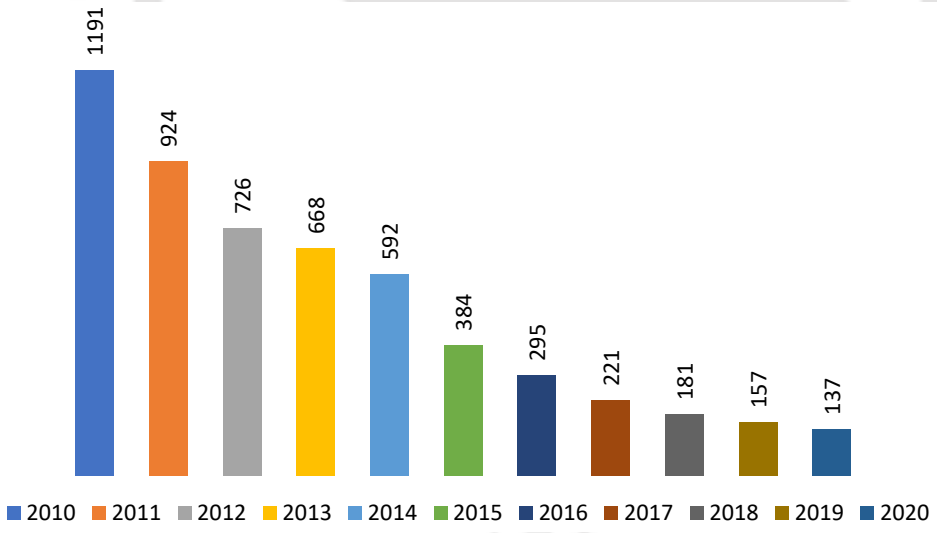

Figure 1.2: Volume-weighted average of lithium-ion battery price in USD since 2010.

run an EV is much smaller than the cost of fuel needed to propel an equivalent internal combustion engine. In recent years, various infrastructures for charging of EV batteries have also been developed. The charging of the EV batteries can be done either using stand-alone charging stations or power grids. Hence, the range of EVs is not a significant issue anymore as it was before. Since the battery is a vital and costly part of an EV, its proper management is essential. This thesis focuses on the management of various aspects of the battery used in EVs.

1.2 Batteries for EVs

The commercial batteries are broadly classified into two categories: (i) primary batteries and (ii) secondary batteries. The primary batteries are also known as single use batteries and can not be used again once they are completely discharged. In this case, the electrochemical reaction that occurred at the electrodes during the discharge of the battery is not reversible. The secondary batteries have the ability to get recharged and can be used several times. Hence, they are also known as rechargeable batteries. In this case, the electrochemical reactions at the electrodes are at least partially reversible. It is important to note that these reactions are not entirely reversible, which further degrades the battery capacity and reduces the lifetime. However, they can be safely recharged over many cycles before becoming inappropriate for further uses. In order to have an increased battery lifetime, it is important that the battery should be capable of recharging over a large number of cycles.

1.2.1 Types of batteries for EVs

Due to the recharging capability over several cycles, secondary batteries are utilized in electric vehicles. Smaller and lighter batteries are preferred so that they can reduce the overall weight of the vehicle and eventually improve its performance. There are several kinds of rechargeable batteries available in the market that use different combinations of chemicals, such as lead-acid battery, nickel-metal hydride (Ni-MH) battery, nickel-cadmium (Ni-Cd) battery, lithium-ion battery (LIB), etc [6]. Compared to other battery chemistries, lithium is one of the most electro-positive and lightest metals. Hence, LIBs generally deliver a high electrode potential and low weight. In recent years, LIBs have become the most suitable energy storage device for EV applications due to their various advantages, such as high energy density, high power density, long life cycle, and low self-discharge [7]. For the same capacity, the weight and volume of LIBs are significantly lower compared to other rechargeable batteries. In addition, they demand less maintenance and have no memory effect. The memory effect is most prominent in the Ni-Cd and Ni-MH batteries. If we repeatedly recharge them after discharging partially, they tend to lose their maximum usable capacity gradually [8]. The battery seems to remember the depth of discharge of the recent cycles. Therefore, memory effect causes rechargeable batteries to store less power and reduces operating time of the batteries. Considering the above mentioned advantages, LIBs are excellent choice for EV applications. Owing to its attractive features, a huge amount of investment has already been made to improve reliability and stability of

LIBs. The performance comparison of LIB with some other rechargeable batteries is shown in Table 1.1 [9].

Table 1.1: Performance comparison of four key types of rechargeable batteries

Parameters	Lead-acid	Ni-Cd	Ni-MH	Lithium-ion
Cell voltage (V)	2	1.2	1.2	3.7
Weight energy density (Wh/kg)	30-50	40-60	60-120	170-250
Volume energy density (Wh/L)	60-110	150-190	140-300	350-700
Cycle Life (times)	300	1500	1000	500-2000
Self discharge per month (%)	5	20	30	< 10
Toxicity	High	High	Low	Low
Overcharge tolerance	High	Moderate	Low	Low

1.2.2 Structure and working principle of LIBs

The LIB is a family of rechargeable batteries that is composed of positive and negative electrodes, electrolyte, separator, and current collectors, as shown in Figure 1.3 [10]. The negative electrode of

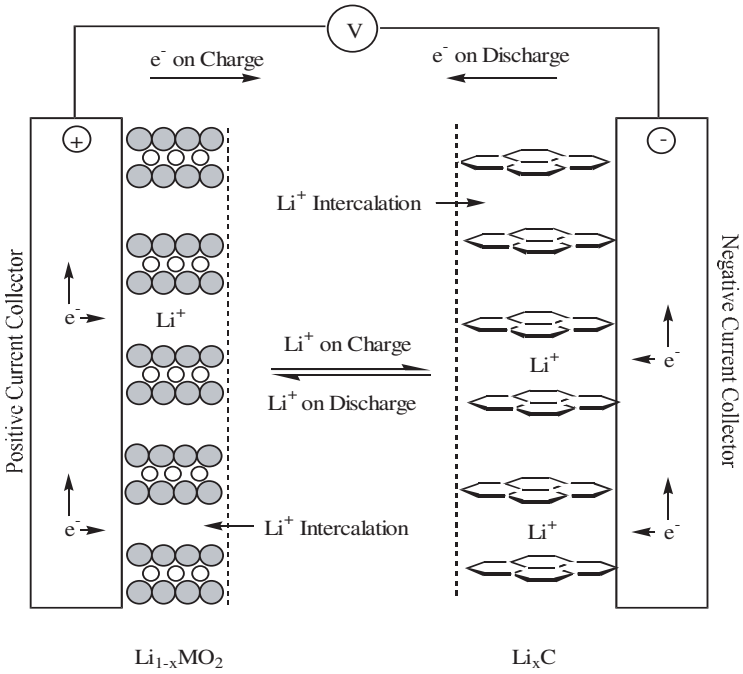

Figure 1.3: Schematic diagram of LIB.

a standard LIB is made from carbon compounds. The positive electrode is a lithium metal oxide or lithium compound. The LIB is generally named by the material used in the positive electrode. The electrolyte is an organic solvent with dissolved lithium salt that provides media for the movement of

lithium ions from one electrode to the other during charging or discharging. A separator is a thin porous membrane that separates the alternating layers of cathode and anode present in the LIB. It prevents any physical contact between anode and cathode while facilitating the movement of lithium ions. There are two current collectors which work as the bridging components that collect electrical current generated at the electrodes and connect with external circuits.

In LIBs, lithium ions move from one electrode material to the other and are intercalated into the host electrode. Intercalation means the insertion of lithium ions into voids present in the crystallographic structure of electrode. The movement of the lithium ions is from negative electrode (anode) to positive electrode (cathode) during discharging and vice-versa during charging. Due to intercalation, there is no free lithium metal present within a lithium-ion cell. During the discharging process, the battery supplies a current and delivers electrical energy to the external circuit. The electrical energy is generated by converting the internal chemical energy stored in the battery. The supplied current is governed by the transfer of electrons from anode to cathode that corresponds to the transport of lithium ions. Lithium atoms are oxidised at the anode. At the cathode, the reduction occurs which combines the lithium ions and electrons that are transported from the anode through the electrolyte and the external circuit, respectively. The electrode reactions during charging and discharging are given as [10]:

$$\text{Positive: } \mathrm{LiMO_2} \underset{\text{Discharging}}{\overset{\text{Charging}}{\rightleftharpoons}} \mathrm{Li_{1\text{-}x}MO_2} + \mathrm{xLi^+} + \mathrm{xe^-}$$

$$\text{Negative: } \mathrm{C + xLi^+ + xe^-} \underset{\text{Discharging}}{\overset{\text{Charging}}{\rightleftharpoons}} \mathrm{Li_x\,C}$$

$$\text{Overall: } \mathrm{LiMO_2 + C} \underset{\text{Discharging}}{\overset{\text{Charging}}{\rightleftharpoons}} \mathrm{Li_x\,C} + \mathrm{Li_{1\text{-}x}MO_2}$$

When a current is injected to the battery, the concentration of lithium ions inside the electrode and at the surface differ, which creates concentration gradient and causes lithium ion diffusion [11]. The lithium ion diffusion is a slow process and takes time, which causes diffusion polarization. The diffusion process determines the performance of electrodes by using the reaction velocity of electrode materials [12].

1.2.3 Important battery terminologies

In literature, various terminologies associated with LIB have been reported to express its distinct characteristics. In this subsection, some important terms relevant to this thesis are discussed which will be used repeatedly throughout the thesis.

(i) Open circuit voltage (OCV): It is the terminal voltage of the battery when the battery system is subjected to no load and in equilibrium state [13]. Equilibrium state means that the battery is entirely relaxed which is achieved by a long resting time after the battery is disconnected from the load.

(ii) Nominal capacity: It is the maximum amount of charge that can be extracted from a battery when it is fully charged [14]. The unit to represent capacity is known as Ampere-hour (Ah). The nominal capacity can also be defined as the total Ah released when a battery is completely discharged at a certain discharge current from its fully charged state.

(iii) C-rate: It is defined as the magnitude of constant discharge current required to completely discharge a battery from its fully charged state in exactly one hour time. It is another representation of charging or discharging current. To illustrate this, consider a battery with nominal capacity 5Ah. In this case, 5A and 2.5 A currents are considered as 1C and 0.5C, respectively.

(iv) Safe operating area: There is a range of voltage, current and temperature in which the battery can operate safely. This is known as the safe operating area of the battery. This range is generally given by the manufacturer and should not be violated during operation.

(v) Peak voltage, cut-off voltage, and nominal voltage: Peak voltage is the open circuit voltage of the battery when the battery is in fully charged state. Whereas, the cut-off voltage is defined as the open circuit voltage when the battery is in fully discharged state. Nominal voltage is the reference voltage of the battery and is generally lies in between peak voltage and cut-off voltage with satisfactory safety margins.

(vi) State of charge (SOC): The SOC is defined as "the ratio of remaining capacity to the nominal capacity" of the battery [14]. It works like the fuel gauge of the battery which indicates how much energy is left inside a battery to power a vehicle before it gets fully discharged. It is measured in %, where 100% SOC means the battery is fully charged and 0% means it is fully discharged.

Mathematically, SOC can be represented as:

$$\text{SOC}(\%) = \frac{C_{rem}}{C_{nom}} \times 100 \tag{1.1}$$

where C_{rem} is the remaining capacity of the battery and C_{nom} is the nominal capacity of the battery.

(vii) State of health (SOH): There is no consensus definition of SOH present in literature. However, it can be related to irreversible degradation of the battery and the loss of capacity of the battery [15]. It provides remaining useful life and allows the users to compare the current condition of the battery with the new one (beginning of life). The ageing and cycling are main reasons for the permanent degradation of the capacity of the battery. The battery is called to reach its end of life when the capacity reduces to 80% of that of the new battery.

(viii) State of power (SOP): The amount of electrical power that can be delivered by the battery under certain condition is estimated by a parameter known as SOP [16]. The main factors directly affecting the peak power capability of the battery are SOC, SOH, and temperature.

1.2.4 Challenges in using LIBs

Despite the various advantages of LIBs, there are some challenges associated with their implementation which need to be addressed for safe and efficient utilization of them. The major challenges associated with using LIBs are:

(i) Overcharging and overdischarging: The overcharging of a battery occurs when the battery is charged beyond a specified voltage limit. In such a situation, the battery operates at a high stress level beyond its safe limit [17, 18]. Overcharging causes a small decrease in the battery capacity and frequent overcharging may lead to the large decrease in its capacity [19]. It also increases the resistance sharply due to injection of the overcharge energy while intercalation hardly takes place anymore. The electrical energy is dissipated in the form of heat and increases the temperature of the battery [20]. Hence, the severe effects of high temperatures are also associated with overcharge. Another problem created by overcharging is the decomposition of electrolyte, which may generate insoluble products and release certain gases. The generation of gases further increases the stress on the battery and may cause safety hazards to the battery and its surroundings. It also causes lithium plating on the anode which degrades the life of the battery. Overdischarging or deep discharging occurs when a battery is discharged beyond a specified voltage limit known as cut-off voltage. It causes capacity fade of the

battery [21]. It also induces the corrosion of the current collectors, resulting in loss of contacts with electrodes and causes power fade.

(ii) Effect of temperature and thermal runaway: Temperature plays a very important role in the battery operation and highly influences the battery capacity. In general, a battery works in a certain range of operating temperature. Beyond this limit, the capacity of the battery is severely affected [21, 22]. The capacity loss may be temporary or permanent. At low temperatures, the battery requires a higher amount of activation energy while there is less movement of lithium ions. This induces lithium plating and temporary capacity loss which restores when the temperature rises and comes within the range [23]. In case of operating the battery at higher temperature than the normal range, the effect is more severe and it may permanently fade the capacity or also damage the battery. Thermal runway is a phenomenon that takes place when the internal temperature of the battery becomes excessively high because of the increased consumption of power or any internal short circuit [22]. The exothermic chemical reactions also take place which causes severe reactions when the temperature approaches the melting point of lithium.

(iii) Ageing/degradation of battery: The movement of lithium ions from one electrode to another is not completely reversible in LIB [24]. During the movement, there may be energy losses due to the inter-facial and bulk resistances of both electrolyte and electrodes, chemical side reactions, and deformations of electrodes occurred by the intercalation and release of lithium. It changes the performance of the battery, such as reduced capacity and increased internal impedance over time [25, 26]. The long term storage of the battery at high SOC and temperature also causes fading of its capacity and power [27].

(iv) Cell imbalance: In general, a single battery cell has limited voltage and capacity. Hence, number of battery cells are connected in series or parallel to make a battery pack that acts as the desired energy storage system. However, there are inconsistencies among these cells which may be due to manufacturing issues such as different coulombic efficiency [28]. The SOC and capacity of each cell vary at different rates leading to the unequal SOC of each cell over the time [29,30]. The capability of charging/discharging of the pack decreases since each cell may have higher or lower SOC with respect to others. This influences the performance of the battery pack and reduces its capacity utilization.

1.2.5 Battery management system

There are several challenges associated with implementation of LIBs, as discussed in the previous section. They need careful monitoring which can improve these issues and boost the battery performance. The battery management system (BMS) serves this purpose which can monitor the various performance parameters and regulate them to enhance the efficacy of the battery [31]. The followings are the main tasks of an efficient BMS: (i) protecting the battery to prolong its life, (ii) operating the battery within a safe limit of voltage, current, and temperature, (iii) estimating and measuring the battery states accurately for better energy management, and (iv) handling thermal degradation and cell imbalance. For portable electronic devices such as cellular phones and laptops, the existing BMS are well-developed. However, the implementation of BMS in critical applications such as satellites and EVs still needs further development and is a popular area of research.

The BMS is a device consisting of a few hardware and software components. The basic framework of BMS is given in Figure 1.4. In general, the hardware part comprises of microcontrollers, sensors,

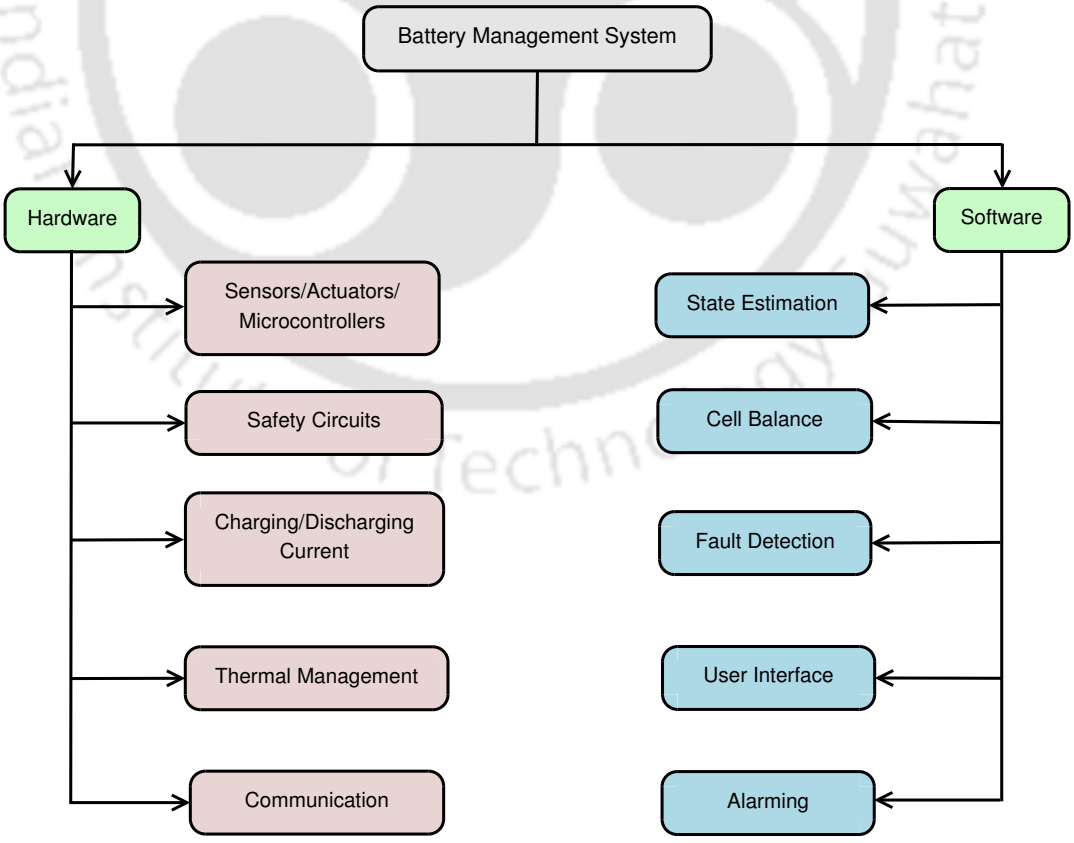

Figure 1.4: Basic framework of BMS.

conditioners (e.g. low pass filter), and actuators to control the operation of the battery and sense and condition various measuring quantities such as voltage, current, and temperature [31]. These measured data are then sent for the decision making process of BMS. The BMS is equipped with safety circuits that can prevent battery hazards such as overcharging and overdischarging by limiting the battery operation within the safe operating area. It provides thermal management which helps to prevent degradation of the battery as well as the thermal runaway. The BMS also helps to regulate the necessary charging and discharging current to the battery. It consists of communication circuits that enable the data transfer between hardware and software.

There are several tasks that need to be performed by the software part present in BMS, which generally comprises of well-developed algorithms [32]. Among them, estimation of battery states such as SOC, SOH, and SOP using various algorithms is vital. These algorithms utilize the measured data by the available sensors. The information of various predicted battery states is transmitted to the vehicle controller to take further decisions to improve the performance of the battery. The algorithms are also designed for the purpose of cell balancing and various fault detections. The software part also consists of an interface between user and BMS. The user interface provides all the necessary information to the user by showing it on the display present in BMS. For instance, the available driving range is displayed on the dashboard based on the value of the SOC. The BMS also regulates the alarms when battery replacement is required or in case of any abnormal condition to protect the battery from getting damaged.

1.3 Motivation

The importance of LIBs in electric vehicles has been discussed extensively in the earlier sections of this chapter. The SOC plays a vital role in enhancing the performance of LIBs through BMS. It provides an indication of the remaining capacity of the battery. SOC helps to prevent overcharging and overdischarging of the battery and thus increases its lifespan. It also assists in estimating the drive distance of EVs to optimize the size and cost of the battery. The accurate SOC is essential for maximizing the capacity utilization and guaranteeing the reliable functioning of LIBs. It aids in ensuring the safety of the battery and its surroundings. In addition, the SOC value also influences some other functions of the BMS and acts as an input for many algorithms developed for SOH estimation, cell balancing and power calculations. Unfortunately, such an important parameter is not available

for direct measurement by any sensor. It can be only inferred by using the available measurable quantities such as battery terminal voltage, current, and temperature which are strongly correlated to SOC. Despite the straightforward definition of SOC, estimating it accurately for the LIB is nontrivial due to the highly nonlinear nature of the battery. Moreover, various operating conditions such as temperature and pressure that may change the internal electrochemical characteristics of the battery make the estimation even more challenging.

Considering the above mentioned issues, a well-developed estimation algorithm is crucial, which can ensure precise, reliable, and computationally efficient SOC estimation such that it can be implemented on a low cost BMS. The importance of SOC estimation can also be established by the fact that the majority of the research on BMS is on estimating SOC of a battery [33]. The literature reports several different approaches to estimate SOC of the LIB with each having its own advantages and drawbacks. The detailed literature review of various existing SOC estimation approaches with their merits and demerits can be found in Chapter 2 of this thesis. It is important to note that none of them are able to fulfil all the performance parameters together required by the application. Hence, there is a scope for further improvement of these methods to enhance the performance of SOC estimation, which motivates this research work.

1.4 Research objectives

The aim of this thesis is to progressively develop efficient model-based SOC estimation algorithms in real-time that enhance the performance of BMS and boost the usage of LIBs in future EVs by making them a more appealing and safer choice. The research objectives of this thesis are as follows:

(i) A comprehensive review on the current state-of-the-art SOC estimation techniques.

(ii) To study different LIB equivalent models and selecting the suitable one for the application of interest considering the trade-off between simplicity and accuracy.

(iii) To develop systematic simplification framework for the selected LIB equivalent model and improve the real-time identification of battery model parameters which in turn plays an important role in achieving good accuracy in SOC estimation.

(iv) To develop SOC estimators which provide improvements upon the various current state-of-the-art SOC estimation algorithms by enhancing the performance indices such as robustness

against wider class of uncertainties, computation time, convergence speed, amount of information requirement, and adaptiveness to different operating conditions.

(v) To investigate the effects of sensor noise and modelling inaccuracy on estimation performance.

1.5 Contributions of the thesis

This thesis strives to develop improved SOC estimation algorithms under diverse real-time constraints and operating conditions. It carefully focuses on improving various performance parameters of SOC estimation algorithm such as accuracy, robustness, computational time, and convergence speed. This thesis contributes four research chapters on different progressively developed SOC estimation algorithms, including modelling of the LIB and its identification techniques. A brief summary of the contributions offered by this thesis is as follows:

1. Development of an SOC estimation algorithm based on relay feedback approach and conventional super twisting observer

A new SOC estimation approach is proposed and developed for LIBs that employs the conventional super twisting algorithm (STA) based observer. It resolves the various issues related to existing sliding mode based SOC observers such as chattering, discontinuous control injection, more number of sensor requirement, and the need for low pass filters. It also ensures finite-time convergence of the observer states to the actual states. A novel offline approach for parameter identification of type 1, second order, and minimum phase system using the state-space based relay feedback approach is proposed to identify the battery model parameters required for the observer design. This is a closed loop approach and provides good identification accuracy. The efficacy of the proposed method is established using numerical simulations. It is found that the proposed approach provides better estimation accuracy and lower chattering compared to the other sliding mode based SOC estimation approaches.

2. Development of strict Lyapunov super twisting SOC observer based on real-time identification of battery model parameters

A new method is proposed based on strict Lyapunov super twisting algorithm (SLSTA) for improved estimation of SOC of the LIB. This algorithm can provide robust finite-time stability for a much wider class of uncertainties than conventional STA based observer. Since the battery model parameters vary with different operating conditions, a standard online approach known as recursive least square with forgetting (RLSF) is employed for real-time identification of battery model parameters. A

strict Lyapunov function is used to prove the robust finite-time convergence of the proposed battery SOC observer. The proposed method is implemented on an actual battery setup by using a real-time driving cycle current profile. The results demonstrate that the proposed approach performs better than the various well-known approaches in terms of accuracy, robustness, computational complexity, and convergence time.

3. Development of SOC estimation algorithm based on adaptive Lyanuov super twisting observer

We propose a new approach for SOC estimation based on adaptive Lyapunov super twisting observer (ALSTO). The main advantage of the proposed approach is that unlike the conventional STA and SLSTA, it does not demand any information on the boundaries of various uncertainties except for their existence. The ALSTO adaptively minimizes the associated gains in such a way that the sliding is maintained and no overestimation of the observer gains take place. This further helps to reduce the chattering significantly. ALSTO can also deal with a more comprehensive class of uncertainties compared to conventional STA based observer. The finite-time convergence of estimation error and robustness of the battery SOC observer are demonstrated using Lyapunov stability theory. By implementing the proposed approach on an actual battery setup and utilizing a real-time driving cycle current profile, it is shown that the SOC estimation performance of the proposed approach outperforms that of SLSTA based algorithm and various other well-known approaches.

4. Development of a fast convergent SOC observer with improved real-time parameter identification

The advantages of generalized super twisting algorithm, adaptive algorithms, and integral sliding mode algorithms are combined together to develop a new and improved SOC estimation method. The proposed observer makes the convergence faster even when the trajectories are far from origin and works efficiently without the knowledge of the upper bounds of various uncertainties for both known and unknown initial conditions. The class of uncertainties for which the finite-time convergence of the system is guaranteed is also wider than the ALSTO. The convergence of the proposed observer is proven using a strong Lyapunov function. The required battery model parameters to design the observer are identified by developing an improved recursive least square approach with adaptive forgetting factor. This identification approach enhances the stability, convergence, and tracking ability of RLSF approach by varying the forgetting factor with the root-mean-square of the prediction error for a

window period. Using the experimental results, it is shown that the proposed approach provides high SOC estimation accuracy, low computational time, high convergence speed, and improved robustness against measurement noise and modelling uncertainties compared to other well-established methods.

1.6 Organization of the thesis

This thesis consists of seven chapters including this chapter of introduction. The remaining thesis is organized as follows:

Chapter 2: This chapter presents literature survey of various battery modelling techniques and SOC estimation methods.

Chapter 3: This chapter proposes a new SOC estimation technique based on conventional super twisting observer. A novel approach for parameter identification of type 1, second order, and minimum phase system using the state-space based relay feedback approach is proposed for battery model parameter identification. The numerical simulation results for validation of the proposed method are shown.

Chapter 4: This chapter proposes a new SLSTA based approach for precise estimation of SOC under a comprehensive range of uncertainties. A strict Lyapunov function is used to prove the robust finite-time convergence of the proposed battery SOC observer. A standard online method is employed for real-time identification of battery model parameters. The presented method is executed on an actual battery with the help of a real-time driving cycle current profile.

Chapter 5: This chapter proposes a new ALSTO based approach for precise estimation of SOC without overestimating the observer gains in the absence of knowledge of disturbance bounds. The finite-time convergence of estimation error and robustness of the battery SOC observer are demonstrated using Lyapunov stability theory. The experiments are conducted on an actual battery with a real-time current profile to verify the efficacy of the proposed method under different operating conditions.

Chapter 6: This chapter proposes a new SOC estimation approach based on adaptive generalized integral super twisting observer. A strong Lyapunov function is utilized to prove the convergence of the proposed observer. The recursive least square with adaptive forgetting factor approach for identification of required battery model parameters is developed. To establish the effectiveness of the proposed method, the experimental results are obtained under different operating conditions using an

actual physical battery and real-time driving cycle.

Chapter 7: This chapter concludes the thesis with a few works as future scope in this research area.

भारतीय प्रौद्योगिकी संस्थान गुवाहाटी
Indian Institute of Technology Guwahati

2

Literature Survey

2.1 Introduction

In recent years, efforts have been made by many researchers to develop several SOC estimation methods for LIBs. This chapter presents a comprehensive literature review of them. Among them, a majority of methods also require the knowledge of battery model for the purpose of SOC estimation. Hence, this chapter also covers the various battery modelling process for EV application.

2.2 Modelling of LIBs

In this section, a brief overview of some basic battery models is presented. Modelling of LIB is a vital part of many battery SOC estimation algorithms. In these algorithms, SOC estimation of a battery highly depends on the accuracy of the modelling. The model helps in anticipating performance of the battery under different working conditions. The battery model should be simple, easy to implement and accurate to ensure precise and computationally efficient estimation of battery states. As the battery is an electrochemical device and very highly nonlinear in nature, it is difficult to obtain its exact model. Recently, many attempts have been made to develop battery models describing the dynamic behaviour of the LIB. The battery models used for EV applications can be mainly classified into three categories: (i) empirical models, (ii) electrochemical models, and (iii) equivalent circuit models. The further classification of these models can be seen in Figure 2.1 and are detailed in the following subsections.

2.2.1 Empirical models

In empirical models, the electrochemical dynamics of the battery is represented as mathematical expressions. A mathematical function is employed to illustrate the relationship of terminal voltage with battery current and SOC [34]. In literature, various empirical battery models can be found. Among them, the Shepherd model [35], Nernst model [36], and Unnewehr universal model [37,38] are the most prominent. In [34], the accuracy of these models are compared in estimating the terminal voltage. It is found that the Nernst model shows the overall best accuracy. The Shepherd model performs better in the case of continuously discharging current. In [39], the combined model of all three of them is represented, which improves the accuracy as well as the computational burden associated with each individual model.

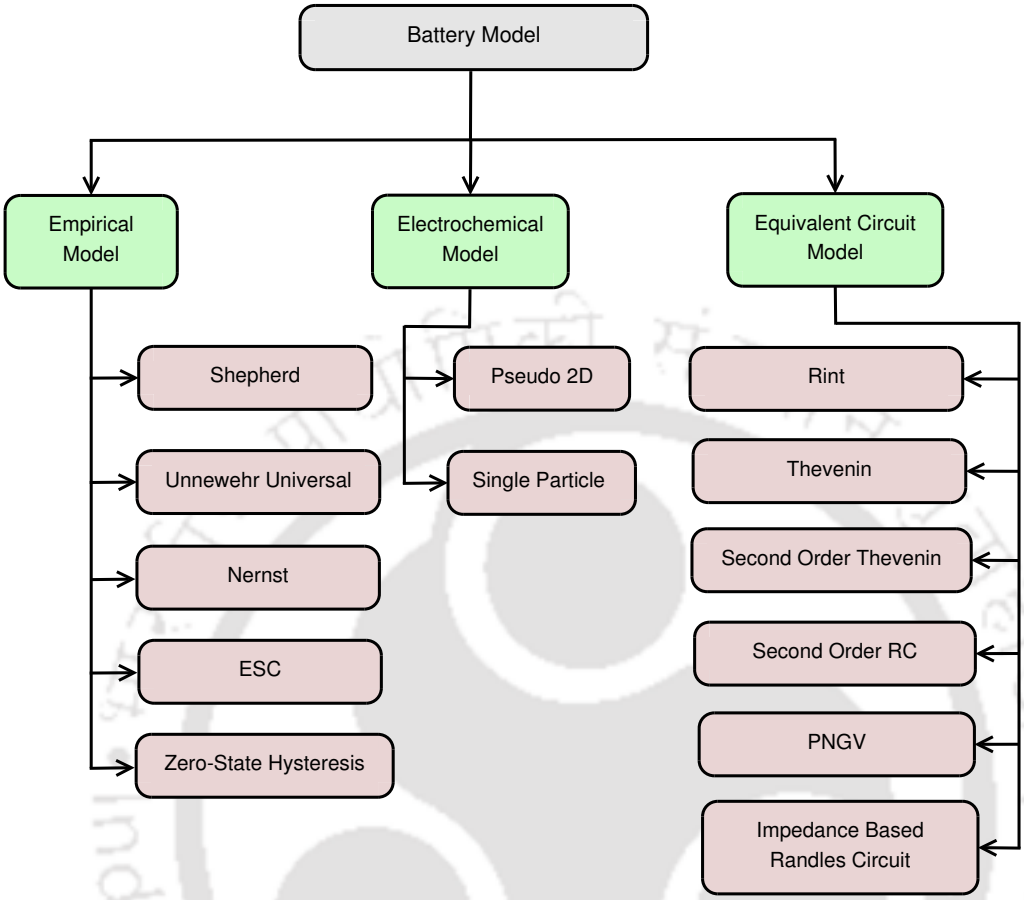

Figure 2.1: Types of battery models.

There are several other ways also to enhance the accuracy of the above mentioned three standard empirical models. The Shepherd model suffers from the problem of instability and algebraic loop in a real-time application. To address this issue, a modified version of Shepherd model is suggested in [40]. The effectiveness of this model is established using a constant current profile. To further improve the dynamic performance of this modified version of Shepherd model, the SOC-OCV relationship is considered in [41] and an additional term is added related to the polarization voltage. The singularity problem associated with the Shepherd model and its different variants is improved in [42]. In [36], the improved Nernst model is proposed which has stronger ability to represent the dynamics of terminal voltage. For that purpose, two additional constants are added in the standard Nernst model. Another problem with the standard models during the relaxation time is the hysteresis effect [43]. To consider the hysteresis effect, zero-state hysteresis model is proposed in [39] where a correction term is added to the standatd Nernst equation. Moreover, an enhanced self-correcting model is suggested in [44]

which considers the hysteresis voltage as a function of SOC.

2.2.2 Electrochemical models

The electrochemical models are obtained based on electrochemical dynamics inside the battery and its transport equations. These models are also known as physics based battery models. The electrochemical dynamics of the battery is represented by partial differential equations, which represent the physical phenomenon inside the battery during both charging and discharging. The order and number of partial differential equations describe the complexity of any electrochemical model. Higher number and order require higher memory and computational power. Among several choices of the electrochemical models, the pseudo two dimensional (P2D) model [45] is one of the most widely used battery models for LIBs, as shown in Figure 2.2 [45]. In this figure, L, L_p, L_n, and L_s are the thickness of the porous region, positive electrode, negative electrode, and separator, respectively; $\mathbf{c}_e$ denotes lithium ion concentration of electrolyte, while $\mathbf{c}_{s,y}$ denotes ionic concentration of active material in y electrode, where y = p (positive) or n (negative); $c_{s,y}^{surf}$ is the ionic concentration of active material in the surface of y electrode; x is position in porous region which varies from 0 to L, and r is the radial position of spherical solid particle which varies from 0 to R_y, where R_y is the radius of the spherical solid particle of y electrode. This model is mainly based on theories of porous electrodes and

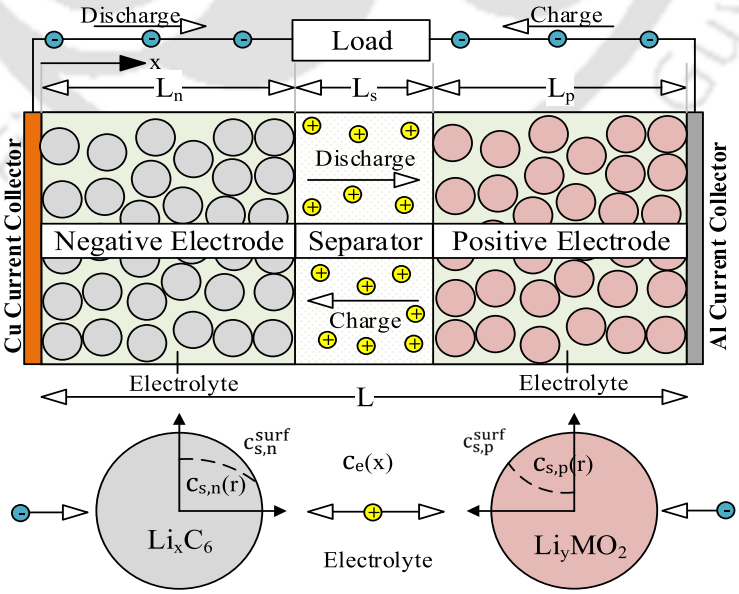

Figure 2.2: Schematic of P2D electrochemical model.

concentrated solutions [46]. This model includes a group of governing equations expressed in the form

of partial differential equations and algebraic equations. The detail of these equations can be found in [47]. The P2D is able to accurately describe not only the battery voltage but also the reaction kinetics and transport within the battery. However, this model is highly sophisticated and requires significant computational resources. Therefore, it is not applicable for real-time applications such as BMS present in EVs [48].

Several reduced order variants of P2D model have also been reported in literature [49, 50]. The single particle model (SPM) [51], as shown in Figure 2.3, is considered the simplest one among them. This model is achieved by assuming that the electrolyte does not vary with time and space. It

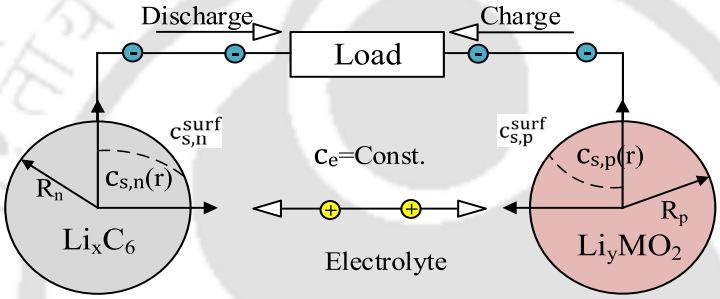

Figure 2.3: Schematic of SPM electrochemical model.

requires low computational effort compared to P2D model and can be applied in real-time applications. However, it comes at the expense of low SOC accuracy. This model also has a significant drawback if the battery has a thick electrode or operates under a high discharge current rate. The validation of the model for some applications operating at low current rate has been reported in a number of research papers [52]. In order to improve the accuracy of the SPM under high current rate, the extended SPM model has been proposed in [53]. In comparison with the SPM, the extended SPM involves variation of the electrolyte. In this model, the electrolyte potential and electrolyte concentration are approximated by polynomial functions.

2.2.3 Equivalent circuit models

Battery equivalent circuit models (BECMs) aim to accurately describe the battery operating characteristics using a network of electrical components such as resistors, capacitors, voltage sources, etc. The principle of the BECM is simple to work upon. For estimation and control, the BECMs are preferred as they can be analysed mathematically without having knowledge of the electrochemistry of the battery [54, 55]. Compared to the electrochemical models, the equivalent circuit models require

less computational effort, yet yields high accuracy in the SOC estimation. The BECMs are widely used in the application of SOC estimation of EV battery [56]. There are several BECMs presented in literature. The most common BECMs are Rint model [56, 57], Thevenin model [58, 59], second order Thevenin model [60, 61], second order RC model [62, 63], partnership for a new generation of vehicles (PNGV) model [64], improved PNGV model [65], and impedance based models [66].

Rint model makes a battery equivalent to a voltage source in series with an internal ohmic resistance, as shown in Figure 2.4(a) [56]. The voltage source is represented by the OCV of the battery. In

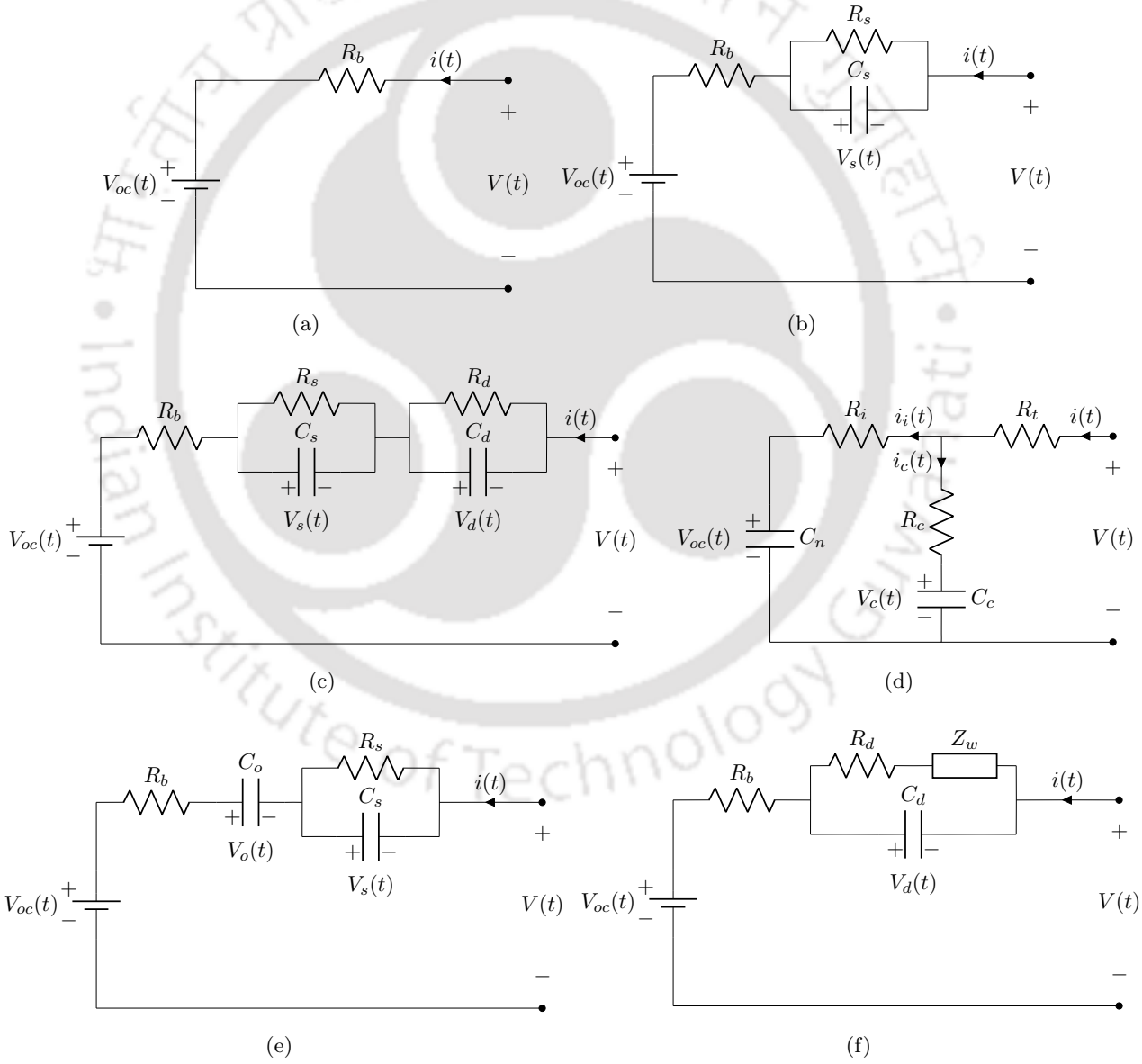

Figure 2.4: (a) Rint model (b) Thevenin model (c) second order Thevenin model (d) second order RC model (e) PNGV model, and (f) Randles model.

Figure 2.4(a), $V(t)$ represents the terminal voltage, $i(t)$ denotes terminal current (positive for charg-

ing), and $V_{oc}(t)$ represents OCV of the battery. When the current passes through the battery during discharging/charging, there is a drop/rise in terminal voltage due to electrolyte resistance and connectors which is represented as the parameter R_b. In practice, apart from the instantaneous response, the dynamic (non-instantaneous) response to the current step is also observed. However, Rint model can not explain the above phenomenon and also fails to reflect the various complex dynamic characteristics of LIB. Hence, this model is not sufficiently accurate for a real-time battery monitoring system under dynamic working conditions and is rarely used in BMS.

To improve the drawbacks of Rint model, an RC parallel network is added in series to it, as shown in Figure 2.4(b). It is known as Thevenin equivalent circuit model and has been most widely employed for long time in BMS. The dynamic characteristics shown by the RC parallel network, consisting of capacitor C_s and resistor R_s, during charging and discharging reflect the slow internal diffusion of lithium from one part of the LIB to the other which builds concentration gradient [58]. It induces a slowly changing voltage which is generally known as diffusion voltage ($V_s(t)$). Hence, the cell terminal voltage does not change instantly to its final value. In Thevenin equivalent circuit, apart from the instantaneous change in terminal voltage due to current step, the battery voltage continues to evolve slowly [59]. At the preliminary stage of the current step, the terminal voltage of LIB changes rapidly, which primarily occurs due to the ohmic resistance R_b. As the LIB discharges/charges continuously, its terminal voltage drops down/increases slowly in a continuous manner, which is characterized by the diffusion phenomenon. At the end of discharge/charge, the effect of internal ohmic resistance vanishes, and it will result in the rapid rise/drop of the terminal voltage followed by the slow relaxation process to reach equilibrium.

It is found that the accuracy of the Thevenin model increases by adding more number of parallel RC networks [60]. However, it also increases the complexity of the model. Hence, considering the second order Thevenin model which uses two RC parallel networks, as shown in Figure 2.4(c), is a good trade-off between the accuracy and complexity of the model for EV application. In this model, the first RC circuit (R_s, C_s) describes the long time-constant reactions associated with the diffusion phenomenon. Whereas, the additional RC circuit (R_d, C_d) describes the short time-constant reactions associated with the double-layer effect and charge-transfer phenomenon [61]. In Figure 2.4(c), R_d is the charge transfer resistance that models voltage drop over the electrode-electrolyte interface due to the load and C_d is double-layer capacitance that models the effect of charges building up in the

electrolyte at electrode surface. Some higher order models with more number of RC parallel networks are also proposed in literature in order to achieve higher accuracy at the cost of heavier computation.

For the application of EV battery, a second order RC model, as shown in Figure 2.4(d), is proposed in [62, 63]. This model was designed by SAFT, a famous battery company, and has good application accuracy [67]. This simplified second order model has good balance between simplicity and accuracy. In Figure 2.4(d), C_n is the bulk capacitance representing the ability of a battery to store the charge; C_c and R_c reflect the occurrence of diffusion and surface effects inside the battery. The resistance R_t and R_i represent the terminal resistance and end resistance of the battery, respectively. $V_{oc}(t)$ is the voltage across C_n, also known as OCV, and $V_c(t)$ is the voltage across C_c.

The PNGV equivalent circuit model, as shown in Figure 2.4(e), is a modified version of Thevenin model with addition of one extra capacitor [64]. The change in OCV with SOC is taken into account in the model itself with the help of capacitance C_o. The voltage across it is represented by $V_o(t)$. The improved PNGV model or second order PNGV model is also reported in [65] which includes one more RC circuit to PNGV model as the second order Thevenin model.

Impedance based equivalent circuit models have also been used for modelling of LIBs for EV applications. These types of models are constructed based on electrochemical impedance spectroscopy of the battery. Randles circuit model is an example of the impedance based models and is shown in Figure 2.4(f) [66]. In this model, Z_w is Warburg impedance representing the diffusion phenomenon. The Warburg impedance is a constant phase element having a phase of 45° (independent of frequency). The magnitude of this constant phase element depends on the frequency and is inversely proportional to the square root of it. There are no simple differential equation that represents a Warburg impedance. The impedance based models, in general, are more complicated and require higher computational resources compared to the Thevenin based models. Because of their complexity, the impedance based models have not been widely used in EV applications.

2.3 SOC estimation techniques

In a BMS, we can directly measure only three quantities: current, voltage, and temperature. Since SOC is not a directly measurable quantity, the BMS has to utilize the above mentioned measurable quantities to obtain a robust estimate of the battery SOC. In recent years, efforts have been made by many researchers to develop some indirect methods for predicting SOC of the LIB accurately. This

section reports various such estimation approaches present in the literature. Most of the reported approaches for SOC estimation can be broadly categorized into three groups: conventional methods, data driven methods, and model based methods. The further classification of these methods can be seen in Figure 2.5 and are detailed in the following subsections.

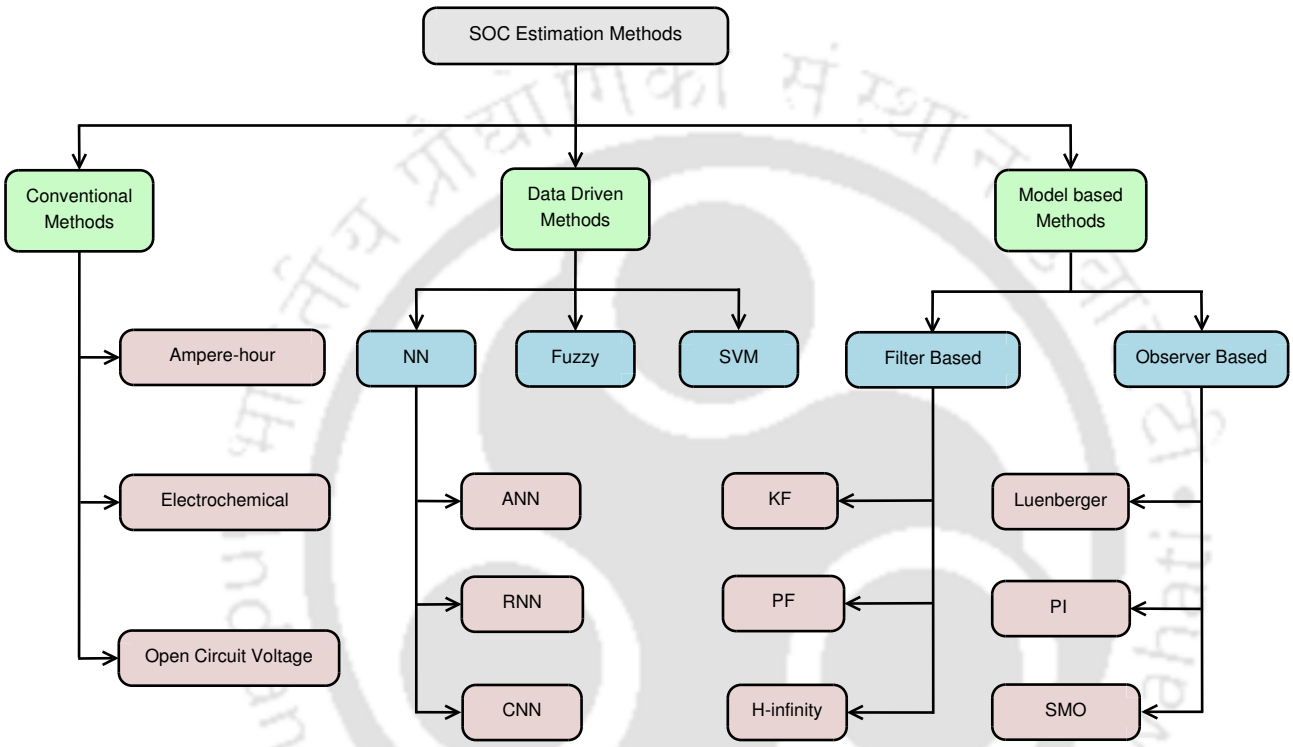

Figure 2.5: Types of SOC estimation methods.

2.3.1 Conventional methods

In this subsection, some important conventional methods to estimate the SOC, such as Ampere-hour method, open circuit voltage (OCV) method, and electrochemical method, are discussed. These methods are considered fundamental methods of estimating SOC and suitable for low cost applications.

Ampere-hour method is the most apparent technique by the definition of SOC [68, 69]. It is also known as charge balance method or coulomb counting method. In this method, SOC is calculated utilizing only the measured current signal. It simply uses current integration to obtain the SOC. In

this method, SOC is calculated as follows:

$$SOC(t) = SOC(t_0) + \int_{t_0}^{t} \frac{\eta I(\tau)}{C_{nom}} d\tau \tag{2.1}$$

where $SOC(t)$ = estimated SOC at time t, $SOC(t_0)$ = initial SOC at t_0, η = coulombic efficiency generally having a value unity for discharging and slightly less than unity for charging process depending on the electrochemistry of the battery, $I(\tau)$ = input current at time τ, and C_{nom} = nominal capacity of the battery. The current $I(\tau)$ is considered positive for charging and negative for discharging process of the battery. This method is very straightforward, concise, and easy to implement in practice. Hence, it is widely used in industrial applications, portable electronic devices, etc. However, this method is sensitive to the initial SOC and choice of coulombic efficiency. Also, due to the reliance on integration, the measurement errors due to current sensor noise and resolution are cumulative and eventually cause significant error in SOC estimation [70]. The estimation process may start when the battery is fully charged because initial SOC is known precisely at that time. However, it may not be suitable in case of various applications such as EVs or satellites, where the full charge is not always possible. Moreover, since this an open loop method, it can not reject inherent disturbances and noises present in the system.

In OCV method, SOC of the battery is estimated by measuring its terminal voltage only when the battery is disconnected from the circuit and is completely relaxed for a long period [71, 72]. The measured battery terminal voltage under such condition is known as OCV of the battery. It is well-known that there is an explicit relationship between SOC and OCV for each battery. Using the measured OCV and the OCV-SOC relationship, the SOC of a battery is estimated in this method. It is generally done using the lookup tables. However, measuring the OCV is not an easy task. Since OCV can only be measured while the battery is not in use or disconnected from the circuit for a long period, this method is not suitable for online applications such as EV, where SOC needs to be measured in real-time, i.e., while the vehicle is in running condition.

Electrochemical method utilizes the electrochemical characteristics of the battery and predicts the SOC from an electrochemical aspect. In this method, the impedance spectra of the battery is obtained at different states of the battery [73–75]. The battery impedances are correlated with known impedances at different SOC levels. The commonalities of the impedance spectra are utilized for estimating the battery SOC. Although this method provides good accuracy in estimating SOC, obtaining

impedance spectra of the battery is tedious and very time-consuming in real-time implementation [70]. Moreover, the battery impedances are generally obtained offline by injecting desired signals into it. Hence, it is difficult to apply this method to an online application. The need for costly and bulky equipment to implement this method is another disadvantage of this method.

2.3.2 Data driven methods

In literature, there have been several data driven methods utilized for estimating SOC of LIBs. Among them, the intelligent algorithms such as artificial neural network (ANN) and their variants, support vector machine (SVM), and fuzzy logic based algorithms are the most prominent. The main advantage of such methods is that a good understanding of battery model and the knowledge of initial value of SOC are not required [76].

ANN is a type of machine learning technique whose functioning and structure is similar to human brain [77]. It consists of artificial neurons called nodes. These nodes are generally placed in three layers, named as input layer, hidden layer(s), and output layer. The nodes in the hidden layers have activation functions that transform the input signal to the output signal. The algorithms train the network structure by learning from the large training dataset. During learning, the weights which connect the layers are determined based on the function minimization. In SOC estimation problem, data for the training are collected from the battery charging and discharging under different working conditions [76, 78].

For battery SOC estimation, a three layer feedforward neural network (NN) is proposed in [79], where the signal travels only in forward direction. In this approach, the input layer consists of the battery's voltage, its first and second derivatives, current, and temperature. The output layer consists of the SOC. To improve the dynamic adaptation of the conventional feedforward NN, the time delayed NN is proposed in [80]. In [81, 82], the radial basis function NN (RBFNN) has also been employed to improve the performance of the NN model. It is a type of feedforward NN with radial basis functions as activation functions. A deep neural network (DNN) is used for SOC estimation in [83]. Another type of DNN technique known as recurrent neural network (RNN) is utilized for estimation of battery SOC in [84]. In contrast to the conventional feedforward NN, hidden nodes are used to store information of past inputs in RNN. Another deep neural network known as convolution neural network (CNN) is employed for SOC estimation of a battery [85]. CNN has some additional layers such as convolution

layer, rectified linear unit layer, and pooling layer that are used to process and extract features from the data. Then the flattened data is fed as the input to the fully connected layer. Though the ANN and its variant based methods show good accuracy for SOC estimation, their performance strongly depends on the quantity and quality of the training data. Large datasets and time are required to train the NN for its good performance. Some joint estimation methods are also utilized to improve the robustness and accuracy further. For instance, the RBFNN is used in a joint close-loop SOC estimation with the adaptive sliding mode observer [61], extended Kalman filter (EKF) [86] and adaptive unscented Kalman filter (AUKF) [87] to overcome the uncertainties of the battery model. However, it brings some additional problems with it such as more computational power requirements and over-fitting.

The SVM is a kernel function-based machine learning algorithm that has been employed in various domains of pattern recognition, including SOC estimation. The benefit of the SVM is its capability to deal with nonlinear and high-dimensional models. In SVM based SOC estimation, the battery's voltage, current, and temperature are the inputs to the model [88–90]. The training data are obtained from experiments with different profiles of these inputs. However, the SOC can be rapidly and accurately predicted only if the training dataset is suitably chosen. Moreover, the SVM based approaches are open-loop estimations and require large amount of training data. Fuzzy logic has been used as the estimation algorithm for the SOC of different battery types [91–93]. Since the fuzzy system often deals with inaccurate inputs and data, the accuracy of these methods is generally lower than the NN based methods [94]. The selection of different fuzzy rules, membership functions, and inference algorithms also have a significant impact on the accuracy and depends on human expertise [95]. Fuzzy logic has also been utilized with ANN and SVM based methods to enhance the flexibility of the ANN-based and the SVM-based methods. The combined methods include a stochastic fuzzy NN in [96], a merged fuzzy NN in [97], and the fuzzy SVM in [98].

2.3.3 Model based methods

In recent years, the model based approaches have attracted significant interest from many researchers for the battery monitoring system. The model based SOC estimation approaches generally consist of two steps: (i) modelling of LIB and its identification and (ii) design of state estimator. The model based methods take advantage of some additional information of the battery provided by the battery models. Different battery models, such as empirical models, electrochemical models, and

the electrical equivalent models, have been discussed above in Section 2.2. Unlike the Ampere-hour and OCV based methods, both measured voltage and current signals are used in these methods. The measured voltage is provided as feedback to form a closed loop leading to a more precise estimation of battery SOC than Ampere-hour and OCV based methods. These methods are easier to implement in real-time applications compared to electrochemical method and data driven methods. The model based methods can be further broadly classified as filter based methods and observer based methods.

2.3.3.1 Filter based methods

In literature, there are several filter based methods that are used for SOC estimation of battery, such as Kalman filter based methods, particle filter based methods, and H-infinity filter based methods. Among them, Kalman filter (KF) based methods are the most popular. The notion behind KF based methods is to minimize the mean-square error in state estimation. In KF based SOC estimation methods, the SOC is one of the state variables to be estimated. The error between measured terminal voltage and the estimated terminal voltage acts as the closed-loop feedback to correct the estimation. The KF based methods do not require the knowledge of initial SOC.

In general, KF algorithm is primarily employed for estimation of states of linear systems. For the application of nonlinear systems such as battery, the other variants of KF algorithm such as EKF [99, 100] and iterated EKF (IEKF) [52] are used. The EKF algorithm first approximates the nonlinear model to the linear one by using Taylor series expansion, then uses the KF algorithm on the linearized model. This approximate linearization induces significant error in battery SOC prediction. The IEKF improves the linearization error of the EKF by recursively modifying the Taylor series expansion's centre point. The improvement of linearization error comes at the cost of increased computational requirements. Unscented Kalman filter (UKF) or sigma point Kalman filter (SPKF) also strives to reduce the linearization error and shows much better accuracy [101–104]. It utilizes the unscented transformation to linearize the nonlinear model, where a set of weighted properly chosen samples known as sigma points are used to represent the mean and the variance of the state distribution. Another variant of KF is central difference Kalman filter (CDKF) [105]. Instead of Taylor series expansion, it uses Sterlings polynomial interpolation formula to approximate the nonlinearity. Though UKF and CDKF are free from calculating Jacobian as in EKF, these algorithms have almost same computational time with EKF due to other computational complexities. The square root version

of CDKF eliminates calculation of square root of the state covariance matrix by directly updating the matrix square root rather than decomposing it. Due to the recursive computation of various matrices, KF based methods are computationally complex. In addition, both EKF and UKF require precise knowledge of statistical properties of measurement and process noise. The performance of these algorithms degrades in the absence of such knowledge. To improve this issue, adaptive versions of EKF (AEKF) [106–108] and UKF (AUKF) [63,109,110] are used to estimate SOC. The adaptive algorithms estimate the source of noise along with the estimation of the system states. These algorithms provide better accuracy of SOC estimation compared to the nonadaptive KF based approaches. However, the computational complexity further increases in the case of AEKF and AUKF. It is worth noting that KF based methods assume the noise as Gaussian for its effective implementation. Moreover, majority of the KF based methods need precise information about the battery model for accurate SOC estimation.

In [111–113], particle filter (PF) is utilized for estimation of battery SOC. In PF, a Monte Carlo approximation approach is utilized and a set of random particles have been selected for approximating the probability density function. Unlike KF based methods, this algorithm considers non-Gaussian distribution of noise for estimating the system states. This method has higher efficiency compared to KF based methods but at the cost of more complexity and memory consumption. Different variants of the PF have also been reported in literature. In [114], an unscented particle filter (UPF) algorithm is proposed for estimating SOC of LIBs. Recently, an online adaptive double scale particle filter is proposed in [115]. It slightly improves the computational cost of the PF algorithm by assuming that BECM parameters vary much slower than the SOC.

In [116–118], H-infinity filter based algorithm is utilized for estimation of SOC of the LIB. The design of the algorithm is simple and guarantees the boundedness of error in state estimation to a given attenuation level even in the worst case of system and measurement noises. Unlike KF based methods, H-infinity based method does not require the knowledge of statistical properties of system and measurement noises. In [119], an adaptive H-infinity filter is proposed for estimating SOC of the LIB. However, the performance of H-infinity based algorithm highly depends on the design parameters. Also, the nonlinear constraints are not well-handled in this method. Hence, effect of temperature, ageing, and hysteresis may deviate the SOC estimation accuracy of the method. The H-infinity has also been combined with some other approaches, such as EKF [120] and UKF [121], to improve the

accuracy of SOC estimation. The joint estimations improve the accuracy, but at the cost of increase in the complexity of the algorithms.

2.3.3.2 Observer based methods

The observer based methods are simple and generally have better computational efficiency than the KF based methods such as EKF and UKF [122]. In literature, there have been several observer based methods utilized for SOC estimation of LIBs. Among them, Luenberger observer, proportional-integral (PI) observer, and sliding mode observers are the most prominent and discussed below.

In 1966, the Luenberger observer was proposed [123] which later became very popular for its utility in different types of systems. Luenberger observer uses a proportional feedback gain to estimate the system states. In this method, the model output converges to system output by careful selection of the gain. For estimating SOC of the LIB by reducing the error between the estimated and the actual terminal voltages, an adaptive Luenberger observer is proposed in [124], which uses stochastic gradient approach to adaptively adjust the gain. It does not need any assumption for noise characteristics and covariance specifications of measurement noise and process noise. As Luenberger observer is a linear observer, its performance reduces when implemented on nonlinear systems. Similar to the KF based methods, an accurate battery model is required for the Luenberger observer approach without which this method cannot perform well.

In [125], SOC estimation is performed using the PI observer which is basically an extension of Luenberger observer. This observer has two feedback loops to be designed. It not only uses the term proportional to estimation error but also its integral that provides better estimation performance than Luenberger observer. However, the optimal tuning of the gains of PI observer is often tedious. In [126], the PI observer is also implemented in conjunction with a drift corrector where the problem of sensor error is resolved by splitting the measured current into actual value, current sensor drift, and zero-mean noise of the sensor.

Sliding mode theory has become a great tool for designing controllers, observers, and robust exact differentiators [127, 128]. The sliding mode observer (SMO) is one of the most simple and powerful nonlinear observer based methods known for its robustness property against modelling uncertainties, measurement noise, and external disturbances [129]. Hence, they have been the most widely used observer based methods for the purpose of SOC estimation. In order to control sliding regime, a

feedback switching gain is designed in this method to ensure the robustness characteristics. For SOC estimation application, the superiority of SMO in terms of computational time, code complexity, and memory usage over KF based methods is shown in [130]. In [129], the first order sliding mode observer (FOSMO) with constant gain is proposed to estimate the states of a battery by compensating the uncertainties due to the nonlinear dynamic characteristics of the battery. It has been shown in the work that the modelling uncertainties and the measurement noises are also compensated well and stability is guaranteed. In spite of several features of FOSMO, it suffers from the disadvantage of high switching frequency of finite amplitude known as chattering which occurs due to the discontinuous control injection and finite sampling frequency [131]. To reduce chattering, various methods have been proposed in literature [132]. Designing observers using higher order sliding mode algorithms is one of them that has received a lot of attention in recent times. These methods significantly reduce chattering due to the fact that they not only drive the sliding variable but also its higher derivatives to zero [133]. In [62], second order sliding mode observer (SOSMO) is used to estimate SOC, which drives both the sliding variable and its first derivative to zero. However, unlike the FOSMO, it necessitates additional information of the derivative of sliding variable along with the information of sliding mode itself. It gives rise to the need for additional sensors and hence increases the cost of the estimation process. Moreover, the above discussed sliding mode based methods require knowledge of the uncertainty boundaries for suitable selection of SMO parameters, such as switching gains, resulting in trade-off between the convergence time of SOC estimation and magnitude of chattering. In [134,135], SOC of a lithium polymer battery is estimated by utilizing adaptive gain SMO (AGSMO) algorithm. By using adjustable switching gains, this algorithm shows improvement in attenuating the chattering level to some extent without demanding the knowledge of disturbance bounds.

2.4 Summary

In this chapter, the state-of-the-art of various types of battery models and SOC estimation methods have been presented. The battery models introduced in this chapter are primarily categorized as: (i) empirical models, (ii) electrochemical models, and (iii) electrical equivalent circuit models. For estimation and control, the BECMs are preferred as they can be analysed mathematically without having knowledge of the electrochemistry of the battery. Depending upon the application, a few popular electrical equivalent circuit models of LIB have been presented in this chapter. However,

there exists a trade-off between complexity and accuracy in choosing the battery model. A good battery model is characterized by reasonably high accuracy and low complexity.

Among the SOC estimation methods, the Ampere-hour method is most widely used in portable electronics due to its simplicity and ease of implementation. However, this open-loop method fails to provide an accurate prediction of SOC in case of unknown initial SOC and presence of current sensor noise. The OCV method requires disconnection of the load followed by a long rest period to determine the OCV of a battery. Hence, this approach is not preferred for real-time applications such as EVs. The data driven methods are known for their high accuracy in SOC estimation without detailed knowledge of the battery. However, substantial sample training data is needed for precise execution of these algorithms. In filter based methods such as Kalman filter, SOC can be optimally estimated in the presence of a broadband noise contained within the system bandwidth. However, they are computationally complex, need a highly accurate battery model, require the knowledge of statistical properties of noise, and only valid for Gaussian distribution of the noise. Unlike KF based methods, PF algorithm considers non-Gaussian distribution of noise for estimating the system states. This method has higher efficiency compared to KF based methods but at the cost of more complexity and memory consumption.

In general, the observer based algorithms, such as Luenberger observer, PI observer, and SMO, provide improved computation complexity than KF based methods. Among the observer based methods, the sliding mode algorithm based methods are most widely used for SOC estimation due to their simplicity, low computational cost and strong robustness property against modelling uncertainties and external disturbances. For SOC estimation application, the superiority of SMO in terms of computational time, code complexity, and memory usage over KF based methods is also shown in [130]. Unlike KF based methods, the SMO based methods need a moderately accurate model and valid for both Gaussian and non Gaussian noise. However, these methods suffer from some serious disadvantages such as chattering, discontinuous control injection, and need for low pass filters. Some of the methods such as higher order SMOs also need information of the derivatives of sliding variable and require more number of sensors. To resolve the shortcomings of these methods and provide improved results, new SOC estimation algorithms are required. Therefore, in the next chapter, we present a new SOC estimation approach using conventional super twisting algorithm which strives to resolve the above mentioned issues.

3

Development of SOC Estimation Algorithm Based on Relay Feedback Approach and Conventional Super Twisting Observer

3.1 Introduction

In literature, several SOC estimation techniques have been presented with each having its own advantages and drawbacks. The sliding mode algorithm based observers have been proven to be one of the most useful techniques for battery SOC estimation due to their strong robustness property, simplicity, and low computational cost. The limitations associated with various sliding mode based observers recently used for battery SOC estimation such as first order sliding mode observer, adaptive gain sliding mode observer, and second order sliding mode observer have been discussed in Chapter 2. The main disadvantage with sliding mode methods is chattering phenomenon due to the discontinuous control injection and finite switching frequency, which reduces its accuracy. Moreover, there is a need for low pass filters to extract the estimated signals from these methods, which incurs phase lag and further affects the estimation accuracy [136]. In general, the second order sliding mode methods also require the knowledge of derivative of the sliding variable and necessitate additional sensors resulting in higher cost of the estimation process. Further, the derivative of sliding variable is difficult to obtain accurately due to the significant amplification of the system noise by the derivative term [137, 138]. There are very limited related works that have investigated the problem of battery SOC estimation discussing the above issues. So, the challenge to the research community is to improve these issues while keeping the other advantages of conventional SMO, which motivates the research work of this chapter.

To deal with the above problems, this chapter focuses on development of a new model based SOC estimation approach for the LIB which employs conventional STA based observer. The conventional STA is a special kind of second order sliding mode algorithm that significantly reduces chattering, provides continuous control injection, and ensures convergence of the observer states to the actual states in finite time. It also eliminates the need for low pass filters to extract the estimated signals. Unlike other second order sliding mode algorithms, the STA does not require the information of derivative of the sliding variable, which eventually reduces the need for additional sensors and thus cost of the observer. Since the proposed approach is model based, a second order RC equivalent circuit model of the LIB is simplified to obtain the state equations of the model. In order to identify the battery model parameters required in designing the observer, a state-space based relay feedback approach is employed. This simple closed loop approach provides a good accuracy in identifying the battery model parameters. The efficacy of the proposed method is validated using numerical

simulations.

3.2 LIB modelling

The proposed SOC estimation approach is primarily a model based approach which requires LIB model for developing the SOC estimation algorithm. For estimation and control, the equivalent circuit models are preferred as they can be analysed mathematically without having knowledge of the electrochemistry of the battery. Different equivalent circuit models proposed in literature are presented in Chapter 2.

In this work, the second order RC model [62, 63, 129, 139], as presented in Section 2.2, is utilized to model the LIB due to its excellent balance between simplicity and accuracy. For consistency of the nomenclature and better understanding of the readers, it is displayed here again in Figure 3.1. In this

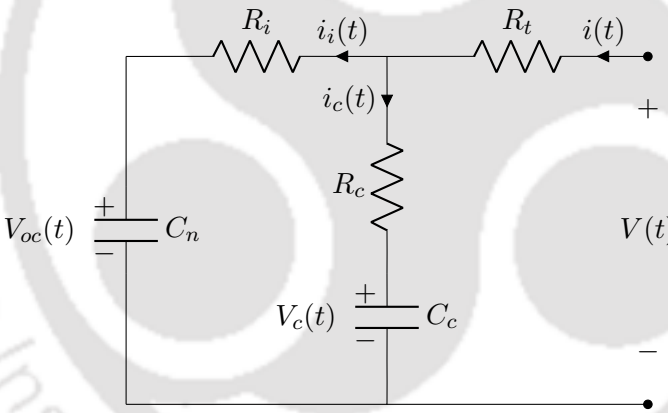

Figure 3.1: Second order RC equivalent circuit model of the LIB.

figure, C_n = bulk capacitance representing the ability of a battery to store the charge, C_c = diffusion capacitance used to model diffusion and surface effects in the battery, R_c = diffusion resistance, R_t = battery terminal resistance, R_i = end resistance, $V_{oc}(t)$ = voltages across C_n, also known as OCV, $V_c(t)$ =voltages across C_c, $V(t)$ = battery terminal voltage, and $i(t)$ = battery terminal current. The terminal current of the battery is considered to be positive while charging the battery and negative while it is discharging. The following equations illustrate the dynamics of the battery equivalent circuit model:

$$V(t) = i(t)R_t + i_c(t)R_c + V_c(t) \tag{3.1}$$

$$V(t) = i(t)R_t + i_i(t)R_i + V_{oc}(t) \tag{3.2}$$

$$\dot{V}_{oc}(t) = i_i(t)/C_n \tag{3.3}$$

$$\dot{V}_c(t) = i_c(t)/C_c \tag{3.4}$$

$$i(t) = i_c(t) + i_i(t) \tag{3.5}$$

Equating (3.1) and (3.2) yields

$$i_i(t) = \frac{i_c(t)R_c + V_c(t) - V_{oc}(t)}{R_i} \tag{3.6}$$

$$i_c(t) = \frac{i_i(t)R_i + V_{oc}(t) - V_c(t)}{R_c} \tag{3.7}$$

For simplicity, based on [62,63,129,139], it is assumed that R_i and R_c are equivalent. Using Kirchhoff's law (3.5), we get from (3.6) and (3.7) as:

$$i_i(t) = \frac{i(t)R_i + V_c(t) - V_{oc}(t)}{2R_i} \tag{3.8}$$

$$i_c(t) = \frac{i(t)R_i - V_c(t) + V_{oc}(t)}{2R_i} \tag{3.9}$$

Using (3.8) and (3.9), (3.3) and (3.4) can be rewritten as:

$$\dot{V}_{oc}(t) = \frac{i(t)R_i + V_c(t) - V_{oc}(t)}{2R_iC_n} \tag{3.10}$$

$$\dot{V}_c(t) = \frac{i(t)R_i - V_c(t) + V_{oc}(t)}{2R_iC_c} \tag{3.11}$$

The output terminal voltage $V(t)$ can be written in different form by substituting (3.8) into (3.2) as:

$$V(t) = 0.5V_{oc}(t) + 0.5V_c(t) + (R_t + R_i/2)i(t) \tag{3.12}$$

Substituting $V_c(t)$ from (3.12) in (3.10) and (3.11), we get

$$\dot{V}_{oc}(t) = \frac{V(t) - V_{oc}(t) - i(t)R_t}{R_iC_n} \tag{3.13}$$

$$\dot{V}_c(t) = \frac{V_{oc}(t) - V(t) + i(t)(R_t + R_i)}{R_i C_c} \tag{3.14}$$

The time derivative of terminal voltage $V(t)$ is derived by differentiating both sides in (3.12) and then substituting (3.13) and (3.14) as:

$$\dot{V}(t) = \left(\frac{C_c - C_n}{2R_i C_n C_c}\right)V(t) + \left(\frac{C_n - C_c}{2R_i C_n C_c}\right)V_{oc}(t) + \left(\frac{C_n R_i + C_n R_t - C_c R_t}{2R_i C_n C_c}\right)i(t) + \left(R_t + R_i/2\right)\dot{i}(t) \tag{3.15}$$

The dynamics of open-circuit voltage $V_{oc}(t)$ is rewritten from (3.13) as:

$$\dot{V}_{oc}(t) = \left(\frac{1}{R_i C_n}\right)V(t) - \left(\frac{1}{R_i C_n}\right)V_{oc}(t) - \left(\frac{R_t}{R_i C_n}\right)i(t) \tag{3.16}$$

It is assumed that the rate of change of terminal current is negligible, and hence $\dot{i}(t)$ in (3.15) can be ignored. This assumption is valid since the current is almost constant between two sampling instants [62,63,139]. Considering $x_1(t) = -V(t)/a_1$, $x_2(t) = V_{oc}(t)$, $y(t) = -V(t)/a_1$, and $u_1(t) = i(t)$, the expression for the state-space representation of the above system is derived from (3.15) and (3.16) as:

$$\underbrace{\begin{bmatrix}\dot{x_1}(t)\\ \dot{x_2}(t)\end{bmatrix}}_{\dot{X}(t)} = \underbrace{\begin{bmatrix}a_1 & 1\\ c_1 & c_2\end{bmatrix}}_{A}\underbrace{\begin{bmatrix}x_1(t)\\ x_2(t)\end{bmatrix}}_{X(t)} + \underbrace{\begin{bmatrix}q_1\\ q_2\end{bmatrix}}_{B}u_1(t) + \begin{bmatrix}0\\ \zeta\end{bmatrix} \tag{3.17}$$

$$y(t) = \underbrace{\begin{bmatrix}1 & 0\end{bmatrix}}_{C}\begin{bmatrix}x_1(t)\\ x_2(t)\end{bmatrix} \tag{3.18}$$

where

$$a_1 = \frac{1}{2R_i}\left(\frac{1}{C_n} - \frac{1}{C_c}\right), \quad c_1 = -\frac{1}{2{R_i}^2 C_n}\left(\frac{1}{C_n} - \frac{1}{C_c}\right)$$

$$c_2 = -\frac{1}{R_i C_n}, \quad q_1 = \frac{C_n R_i + C_n R_t - C_c R_t}{C_n - C_c}, \quad q_2 = -\frac{R_t}{R_i C_n} \tag{3.19}$$

$\zeta(x, t, u)$ is the uncertainties due to modelling errors, sensor inaccuracy, and other external distur-

bances. The transfer function of the system in (3.17)-(3.18) can be found using the following equation:

$$\frac{Y(s)}{U_1(s)} = C(sI - A)^{-1}B \tag{3.20}$$

as

$$\frac{Y(s)}{U_1(s)} = \frac{bs + c}{s^2 + as} \tag{3.21}$$

where

$$a = -(a_1 + c_2) = \frac{C_n + C_c}{2R_iC_nC_c}$$

$$b = q_1 = \frac{C_nR_i + C_nR_t - C_cR_t}{C_n - C_c}$$

$$c = q_2 - c_2q_1 = \frac{1}{C_n - C_c} \tag{3.22}$$

and $Y(s)$ and $U_1(s)$ are the Laplace transformation of $y(t)$ and $u_1(t)$, respectively.

.

3.2.1 Observability test

Before designing a state observer for battery model, it is necessary to check whether it is possible to design the state observer or not for this particular system. For that, we need to perform the observability test of the battery system. The general form of observability matrix is given as [140]:

$$O = \begin{bmatrix} C & CA & CA^2 & ..... & CA^{n-1} \end{bmatrix}^T \tag{3.23}$$

where n is the dimension of matrix A. If the observability matrix O has full rank, then the system is said to be observable. For battery system in (3.17)-(3.18), the dimension $n = 2$. Hence, the observability matrix is obtained as:

$$O = \begin{bmatrix} 1 & 0 \\ a_1 & 1 \end{bmatrix} \tag{3.24}$$

Clearly, the matrix O has the full rank and hence, the system in (3.17)-(3.18) is observable.

3.3 Identification technique for battery model system

System identification corresponds to finding the parameters of the model of an unknown process using the measurements of system's input and output signals [141]. It plays a significant role in analysing a system's operation and the design of controllers and observers. In order to design the state observer for estimating SOC, it is important to first identify the battery model parameters, i.e., the resistances and the capacitances present in the battery model. Alternatively, it is equivalent to identify the coefficients present in the transfer function or the state equations obtained after simplifying the battery model. In case of battery model system, a good identification method is characterized by its simplicity, high accuracy, low memory requirement, and low computational burden on the online state estimation algorithm where the identified parameters are used. In literature, there are several methods used for identification of the battery model. They can be broadly categorized as offline and online methods [142]. In offline identification methods, usually all the input/output data are collected first, and then the model parameters are identified using them. Since the parameters are identified offline, they add very less computational burden on the SOC estimation algorithm compared to the online identification methods. Hence, in this chapter, an offline method is proposed to identify the battery model parameters.

In literature, a few offline methods have been proposed for identification of battery model parameters such as pulse charging-discharging approach [129, 139, 143, 144] and hybrid pulse power characterization approach [145]. They are open loop approaches and require the knowledge of the relationships between the battery model parameters and various electrochemical phenomena such as polarization and diffusion taking place inside the battery. These relationships are different for different battery models and hence need human expertise. In recent years, relay based system identification approach got popular in several applications due to its simplicity and ease of implementation [146–148]. Being a closed-loop scheme, the accuracy is high and the system does not drift away from the nominal operating point [149]. It does not require knowledge of any electrochemical phenomena of the battery and can be applied to any battery model. It requires only the system input, output, and the transfer function obtained after simplifying the battery model for its implementation. Compared to describing function based relay feedback approaches [150, 151], the state-space based relay feedback approaches [152, 153] are more accurate. Therefore, in this chapter, state-space based relay feedback approach is used for development of identification technique for battery model parameters. For sim-

plification, the impact of operating conditions on the battery model parameters is ignored. The slow variation in the model parameters due to changes in operating conditions are assumed as modelling uncertainties to be compensated by the robust observer during state estimation.

3.3.1 Introduction to relay feedback approach

A relay is an on-off nonlinearity which works as a switch. In context to the amplitude of the relay output, relays can be categorized as symmetrical relays and asymmetrical relays. In symmetrical relays, the magnitudes of positive and the negative amplitudes of the relay output are equal and generally used where less number of transfer function parameters need to be identified. Whereas, in asymmetrical relays, the magnitudes of the positive and the negative amplitudes of the relay output are not equal and generally used where more number of transfer function parameters need to be identified. The characteristics of symmetrical and asymmetrical relays are shown in Figure 3.2(a) and 3.2(b),

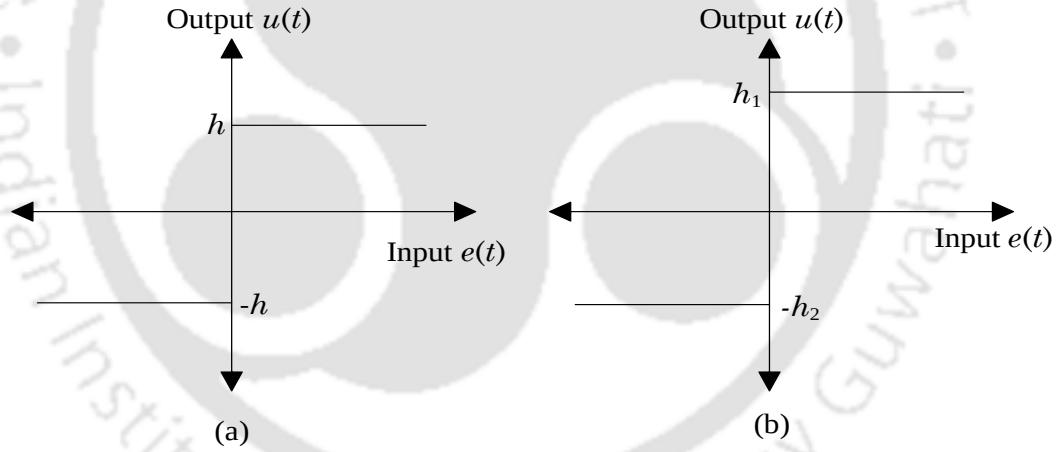

Figure 3.2: (a) Symmetrical relay characteristics and (b) asymmetrical relay characteristics.

respectively, where $e(t)$ = input to the relay, $u(t)$ = output of the relay, and h = magnitude of both positive and negative amplitude of the symmetrical relay output, h_1 = magnitude of positive amplitude of the asymmetrical relay output, and h_2 = magnitude of negative amplitude of the asymmetrical relay output.

For system identification, the basic block diagram of relay feedback approach is shown in Figure 3.3, where $r(t)$ = reference signal, $e(t)$ = input to the relay (error signal), $u(t)$ = output of relay, $u_1(t)$ = input to the process (battery), and $y(t)$ = output of the process. The main property which makes a relay suitable for system identification is that it ensures limit cycle (sustained oscillation) in output. After a certain time, the process reaches its ultimate frequency (the frequency where the

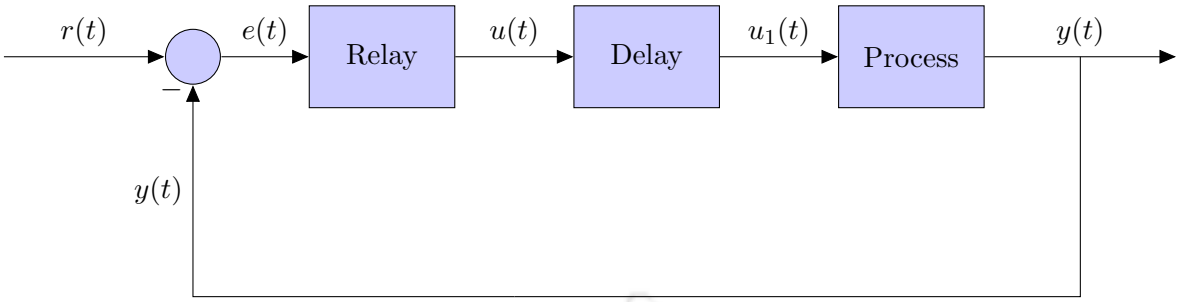

Figure 3.3: Block diagram of relay feedback approach.

phase angle corresponds to -180°) and starts providing sustained oscillatory output. At that time, the closed loop gain in Figure 3.3 becomes -1, which can be regarded as the condition to achieve the sustained oscillatory output. Mathematically, it can be given as:

$$G(s)G_r(s) = -1 \tag{3.25}$$

where $G(s)$ is the transfer function of the process (battery) and $G_r(s)$ is the transfer function obtained after multiplying the transfer functions of relay and delay blocks in Figure 3.3. Being a closed-loop scheme, the accuracy is high and the system does not drift away from the nominal operating point. The time for which the experiment is required to be performed for input/output data is also generally very less.

3.3.2 Parameter identification using relay feedback approach

In this subsection, a parameter identification scheme using state-space based relay feedback approach is developed for type 1 second order minimum phase system and utilized for BECM transfer function given in (3.21). In order to utilize the relay for system identification, a time delay having magnitude θ s is introduced, as shown in Figure 3.3. Hence, the transfer function of the process with delay becomes:

$$\frac{Y(s)}{U(s)} = \frac{bs + c}{s^2 + as} e^{-\theta s} \tag{3.26}$$

where $U(s)$ is the Laplace transformation of $u(t)$ (input to the delay block in Figure 3.3).

Diagonalizing (3.26), we get

$$\frac{Y(s)}{U(s)} = \left(\frac{k_1}{s} + \frac{k_2}{s + a}\right) e^{-\theta s} \tag{3.27}$$

where

$$k_1 = \frac{c}{a}, \quad k_2 = \frac{b-c}{a}$$

Equation (3.27) can be rewritten as:

$$Y(s) = k_1 Y_1(s) + k_2 Y_2(s) \tag{3.28}$$

where

$$Y_1(s) = \frac{1}{s} U(s) e^{-\theta s} \tag{3.29a}$$

$$Y_2(s) = \frac{1}{s+a} U(s) e^{-\theta s} \tag{3.29b}$$

Taking inverse Laplace transform of (3.29), we get

$$\dot{y_1}(t) = u(t-\theta) \tag{3.30a}$$

$$\dot{y_2}(t) = -a y_2(t) + u(t-\theta) \tag{3.30b}$$

Assuming $p_1(t) = y_1(t)$, $p_2(t) = y_2(t)$, and $P(t) = [p_1(t) \quad p_2(t)]^T$, (3.30) can be converted into:

$$\dot{P}(t) = MP(t) + Nu(t-\theta) \tag{3.31a}$$

$$y(t) = RP(t) \tag{3.31b}$$

where

$$M = \begin{bmatrix} 0 & 0 \\ 0 & -a \end{bmatrix}, \quad N = \begin{bmatrix} 1 \\ 1 \end{bmatrix}, \quad R = \begin{bmatrix} \frac{c}{a} & \frac{b-c}{a} \end{bmatrix}$$

In this work, we use asymmetrical relay which is helpful in identification of more number of transfer function parameters. A typical limit cycle output of type 1, second order, and minimum phase system is shown in Figure 3.4.

For $t_0 \leq t \leq t_1$, where $u(t-\theta) = h_1$, $t_0 = 0$, and $t_1 = \theta$

$$P(t) = e^{Mt} P(t_0) + h_1 \int_0^t e^{M(t-\tau)} N d\tau \tag{3.32}$$

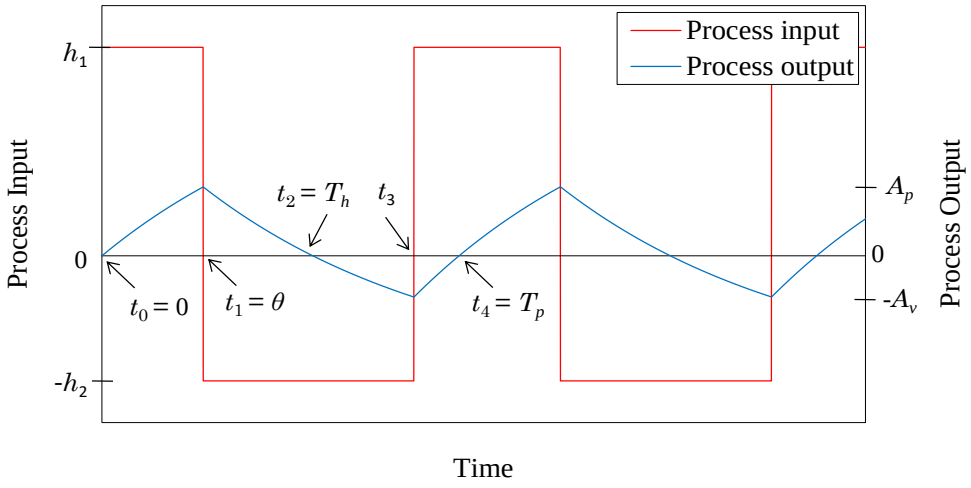

Figure 3.4: Typical process input and output signals.

At $t = t_1 = \theta$,

$$P(t_1) = \begin{bmatrix} 1 & 0 \\ 0 & e^{-a\theta} \end{bmatrix} P(t_0) + \begin{bmatrix} \theta \\ \frac{1-e^{-a\theta}}{a} \end{bmatrix} h_1 \tag{3.33}$$

For $t_1 \leq t \leq t_2$, where $u(t-\theta) = -h_2$ and $t_2 = T_h$

$$P(t) = e^{M(t-\theta)} P(t_1) - h_2 \int_{\theta}^{t} e^{M(t-\tau)} N d\tau \tag{3.34}$$

At $t = t_2 = T_h$,

$$P(T_h) = \begin{bmatrix} 1 & 0 \\ 0 & e^{-a(T_h-\theta)} \end{bmatrix} P(t_1) - \begin{bmatrix} T_h - \theta \\ \frac{1-e^{-a(T_h-\theta)}}{a} \end{bmatrix} h_2 \tag{3.35}$$

For $t_2 \leq t \leq t_3$, where $u(t-\theta) = -h_2$ and $t_3 - t_2 = \theta$

$$P(t) = e^{M(t-t_2)} P(t_2) - h_2 \int_{t_2}^{t} e^{M(t-\tau)} N d\tau \tag{3.36}$$

At $t = t_3$,

$$P(t_3) = \begin{bmatrix} 1 & 0 \\ 0 & e^{-a\theta} \end{bmatrix} P(T_h) - \begin{bmatrix} \theta \\ \frac{1-e^{-a\theta}}{a} \end{bmatrix} h_2 \tag{3.37}$$

For $t_3 \leq t \leq t_4$, where $u(t-\theta) = h_1$

$$P(t) = e^{M(t-t_3)}P(t_3) + h_1 \int_{t_3}^{t} e^{M(t-\tau)} N d\tau \tag{3.38}$$

At $t = t_4 = T_p$,

$$P(T_p) = \begin{bmatrix} 1 & 0 \\ 0 & e^{-a(T_p - T_h - \theta)} \end{bmatrix} P(t_3) + \begin{bmatrix} T_p - T_h - \theta \\ \frac{1-e^{-a(T_p - T_h - \theta)}}{a} \end{bmatrix} h_1 \tag{3.39}$$

Putting the values of $P(t_3)$, $P(T_h)$ and $P(t_1)$ from (3.33), (3.35), (3.37) in (3.39), we get

$$P(T_p) = \begin{bmatrix} 1 & 0 \\ 0 & e^{-aT_p} \end{bmatrix} P(t_0) + \gamma_1 \tag{3.40}$$

where

$$\gamma_1 = \begin{bmatrix} T_p h_1 - T_h(h_1 + h_2) \\ \frac{(h_1+h_2)(1-e^{aT_h})e^{-a(T_p-\theta)} + h_1(1-e^{aT_p})}{a} \end{bmatrix}$$

For sustained oscillations,

$$P(t_0) = P(T_p) \tag{3.41}$$

From (3.40) and (3.41), we get

$$T_p h_1 - T_h h_1 - T_h h_2 = 0 \tag{3.42a}$$

$$P(t_0) = \begin{bmatrix} (\frac{c-ab}{ac})[h_1 + (h_1 + h_2)(\frac{1-e^{aT_h}}{1-e^{aT_p}})e^{-a(T_p-\theta)}] \\ \frac{1}{a}[h_1 + (h_1 + h_2)(\frac{1-e^{aT_h}}{1-e^{aT_p}})e^{-a(T_p-\theta)}] \end{bmatrix} \tag{3.42b}$$

From (3.33) and (3.42), we get

$$P(t_1) = \begin{bmatrix} (\frac{c-ab}{ac})[h_1 + (h_1 + h_2)(\frac{1-e^{aT_h}}{1-e^{aT_p}})e^{-a(T_p-\theta)}] + \theta h_1 \\ \frac{1}{a}[h_1 + (h_1 + h_2)(\frac{1-e^{aT_h}}{1-e^{aT_p}})e^{-aT_p}] \end{bmatrix} \tag{3.43}$$

From (3.35) and (3.43), we get

$$P(T_h) = \begin{bmatrix} (\frac{c-ab}{ac})[h_1 + (h_1+h_2)(\frac{1-e^{aT_h}}{1-e^{aT_p}})e^{-a(T_p-\theta)}] + \theta h_1 + (\theta - T_h)h_2 \\ \frac{1}{a}[(h_1+h_2)(\frac{1-e^{a(T_p+T_h)}}{1-e^{aT_p}})e^{-(aT_h-\theta)} - h_2] \end{bmatrix} \tag{3.44}$$

From (3.37) and (3.44), we get

$$P(t_3) = \begin{bmatrix} (\frac{c-ab}{ac})[h_1 + (h_1+h_2)(\frac{1-e^{aT_h}}{1-e^{aT_p}})e^{-a(T_p-\theta)}] + \theta h_1 - T_h h_2 \\ \frac{1}{a}[(h_1+h_2)(\frac{1-e^{a(T_p+T_h)}}{1-e^{aT_p}})e^{-aT_h} - h_2] \end{bmatrix} \tag{3.45}$$

Subsequently from (3.31)

$$y(\theta) = RP(\theta) \tag{3.46a}$$

$$y(T_h) = RP(T_h) \tag{3.46b}$$

$$y(t_3) = RP(t_3) \tag{3.46c}$$

Now putting the value of $y(\theta)$, $y(T_h)$, and $y(t_3)$ from the limit cycle output shown in Figure 3.4 and R from (3.31), we get

$$A_p = f_1(a, b, c, \theta, T_h, T_p) \tag{3.47a}$$

$$0 = f_2(a, b, c, \theta, T_h, T_p) \tag{3.47b}$$

$$-A_v = f_3(a, b, c, \theta, T_h, T_p) \tag{3.47c}$$

where A_p = magnitude of positive peak amplitude of the limit cycle output occurring at time t_1 and A_v = magnitude of negative peak amplitude of the limit cycle output occurring at time t_3. Solving the equations in (3.47), the value of a, b, and c can be obtained. These values can be further utilized along with (3.22) to find the BECM resistances and capacitances.

3.4 Robust observer design for estimation of battery states

To predict the unknown states of the battery system, there is need for a robust observer which can accurately estimate the battery states under various uncertain conditions with low computational effort. These uncertainties should be carefully handled since they can deteriorate the performance or even lead to instability of the observer. Recently, sliding mode observers have been proven to be one

of the most useful methods for SOC estimation because of their high robustness against modelling uncertainties and external disturbances [129]. However, the sliding mode methods utilized for SOC estimation suffer from various issues such as chattering, discontinuous control injection, and need for low pass filters. In this chapter, the theory of conventional super twisting algorithm (CSTA) has been utilized to design the required observer, which estimates the unknown states of the second order battery equivalent system given in (3.17)-(3.18). CSTA is a special type of second order sliding mode algorithm with various added advantages. In order to design the CSTA based observer and establish its advantages, it is essential to have knowledge of the sliding mode theory.

3.4.1 Basic introduction of sliding mode theory

The sliding mode theory is originated from the concept of variable structure control system (VSCS) [154]. Similar to VSCS, it utilizes discontinuous control laws for driving the state trajectories for performing specific tasks. It was first proposed in Russian language by Emelyanov in 1960s [155], but became popular worldwide in late 1970s after a few works by Itkis [156] and Utkin [157] were published in English. The main highlight of sliding mode approach which makes it very popular among researchers and industries is its inherent robustness property against matched disturbances and parametric uncertainties [158]. Another advantage is that it makes the system act as a reduced order system compared to the original system. In literature, sliding mode techniques have been widely used in designing robust controllers, observers, and exact differentiators for several different types of systems [128].

The objective of the sliding mode control (SMC) is to force the system states to reach a specified surface and then slide along this surface towards the equilibrium [158]. Hence, this specified surface is known as sliding surface. The designing of sliding mode controller consists of two key steps [158]. First, we need to choose an appropriate sliding surface. The choice of sliding surface should be such that the closed loop system can perform the desired task and satisfies all the required specifications when the state trajectory is at the sliding surface. The second step is to design a suitable control action that can force the state trajectory to reach the sliding surface and then stay there afterwards even in the presence of various uncertainties and disturbances present in the system. This phase is known as the sliding phase. When confined to sliding surface, the system dynamics is represented as an ideal sliding motion and shows the controlled system behaviour. The initial phase of control before

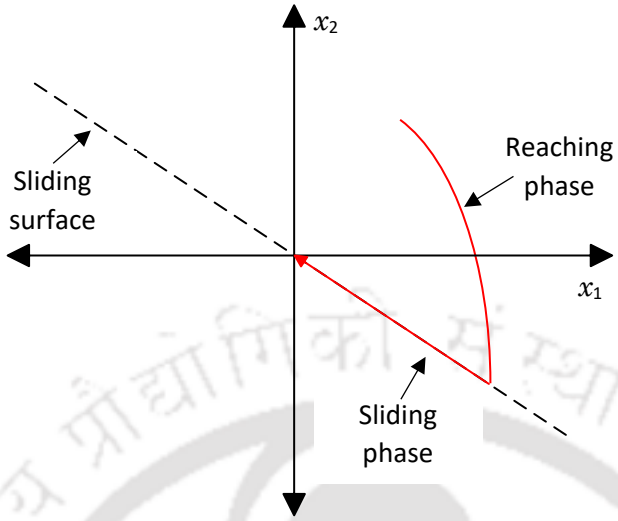

Figure 3.5: Sliding mode control.

reaching the sliding surface is known as reaching phase. At this phase, the state trajectory is directed towards the sliding surface. The various advantages of sliding mode approach are only applicable after establishing the sliding motion. The overall process of SMC is shown in Figure 3.5 [159].

In spite of the robustness and order reduction, the sliding mode methods suffer from a serious problem known as chattering, as shown in Figure 3.6 [131, 160]. It is high frequency vibration of the control action which arises due to the finite switching frequency of the discounting control. The

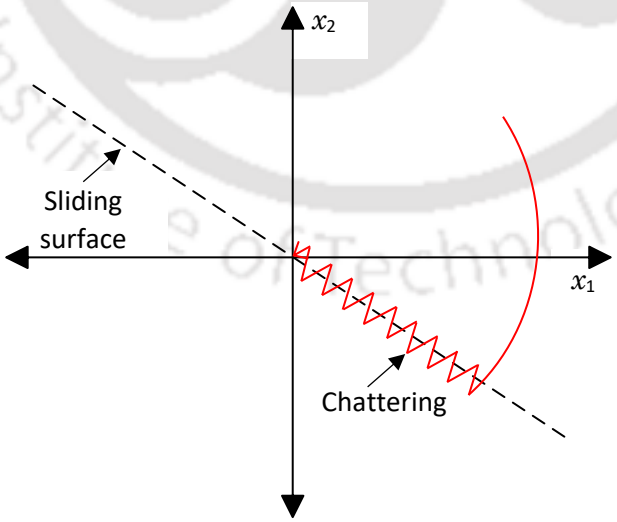

Figure 3.6: Chattering phenomenon.

switching frequency in an ideal sliding mode is considered infinite. However, in physical systems, it is impossible to achieve infinite switching frequency due to various factors such as inertia, nonlinearity,

delay, etc. The switching of control can occur at very high but finite frequency. Consequently, the sliding does not occur precisely at the sliding surface, but within a small vicinity of the sliding surface. It means that the states of the system switch around the sliding surface rather than staying there. The size of the small neighbourhood is inversely proportional to switching frequency. The chattering phenomenon deteriorates the performance of the system and sometimes may even induce instability. In mechanical systems, it can cause stress and even breakdown of the mechanical parts.

In recent years, several efforts have been made to suggest different techniques for alleviating the effect of chattering. The simplest way to get rid of chattering is to replace the discontinuous control action with continuous one without compromising the robustness, accuracy, and other advantages of ideal SMC. For this purpose, in literature, researchers have replaced the discontinuous sign function with the saturation function or sigmoid function [132]. The saturation and sigmoid functions are good continuous approximations of sign function. Hence, they make the control action continuous and eliminate chattering. However, it is found that the invariance property of sliding surface is lost and the sliding of state trajectory is not constrained to the sliding surface anymore, but within its small neighbourhood [132]. Eventually, it degrades the accuracy and robustness of the closed loop system against disturbances.

Another interesting strategy developed in recent years to reduce chattering is the higher order sliding mode (HOSM) approach. The key idea behind the HOSM approach is to generalize the concept of sliding mode on the higher order time derivatives of sliding variable, rather than only the first time derivative as in standard sliding mode [133]. It not only keeps the main advantages of the standard sliding mode approach, but also reduces the chattering significantly and provides even better accuracy than the standard sliding mode approach. There are several HOSM techniques presented in literature. The order of sliding mode is defined as the number of continuous time derivatives of the sliding variable, including the zeroth one, whose vanishing describes the dynamics of the sliding manifold [133]. In other words, we can say that the m^{th} order sliding mode approach not only drives the sliding variable but also its all higher order derivatives upto $(m\text{-}1)^{th}$ order to zero. The discontinuous control terms generally appear in the m^{th} order time derivative of sliding variable. The main criticism in implementing the HOSM techniques is the additional information demand of higher order time derivatives of sliding variable. An m^{th} order sliding mode approach demands the information of all time derivatives of sling variable upto $(m\text{-}1)^{th}$ order. In practice, the second order

sliding mode technique is the most widely used HOSM technique due to its good trade-off between the various advantages, simplicity, and amount of information demand [161]. In second order sliding mode technique, the control action directly affects the second time derivative of the sliding variable. The design of control action uses the information of sliding variable and its first time derivative. An appropriate control action can ensure the finite-time convergence of the state trajectory of the system to the sliding manifold.

3.4.2 Design of state observer using conventional STA

The conventional STA is a special kind of second order sliding mode algorithm first proposed in [162]. It provides continuous control input and reduces chattering significantly [163]. Unlike other second order sliding mode algorithms, the STA does not require the information of the derivative of the sliding variable, which eventually reduces the need for additional sensors and thus cost of the operation. In STA, the trajectory on the phase plane is repeated rotations around the origin. The absolute values of the intersection of the state trajectory with the axes as well as the time of each rotation reduce in geometric progression [164]. The STA was originally developed for designing a controller. In recent years, due to its various advantages, it is also implemented for developing observers [164–166] and robust exact differentiators [128, 167]. The key idea behind the development of any sliding mode observer is to generate a sliding motion on the error between the actual plant output and the estimated output of the observer to ensure that the estimated states precisely resemble with the actual states of the system. Hence, conventional sliding mode observer (CSTO) posses all the advantages associated with the CSTA. Unlike other sliding mode based observers, CSTO does not require low pass filters to extract the estimated signals which generally cause delay and affect the estimation accuracy. In order to design any control strategy using the estimated states from the observer, it is desired to have finite-time convergence of the observer states to the actual states [164]. The CSTO provides finite-time convergence of the states and satisfy the separation principle. In case of battery state estimation, this observer will also compensate the modelling uncertainties which may arise due to ageing of battery, noise while performing relay feedback test, and nonlinear behaviour of the battery. The observer designed for the LIB system to estimate the states is as follows:

$$\dot{\hat{x}}_1 = a_1 x_1 + \hat{x}_2 + q_1 u_1 + \gamma |\tilde{x}_1|^{1/2} sign(\tilde{x}_1) \tag{3.48a}$$

$$\dot{\hat{x}}_2 = c_1 x_1 + c_2 \hat{x}_2 + q_2 u_1 + \beta sign(\tilde{x}_1) \tag{3.48b}$$

where $\tilde{x}_1 = x_1 - \hat{x}_1$ and

$$sign(\tilde{x}) = \begin{cases} 1, & \text{if } \tilde{x} > 0 \\ -1, & \text{if } \tilde{x} < 0 \\ \in [-1, 1], & \text{if } \tilde{x} = 0 \end{cases}$$

The estimated parameters of the battery model using relay feedback approach are used here. Using (3.17) and (3.48), the battery state error dynamics is obtained as:

$$\dot{\tilde{x}}_1 = \tilde{x}_2 - \gamma |\tilde{x}_1|^{1/2} sign(\tilde{x}_1) \tag{3.49a}$$

$$\dot{\tilde{x}}_2 = F(x_1, x_2, \hat{x}_2, t) - \beta sign(\tilde{x}_1) \tag{3.49b}$$

where $\tilde{x}_2 = x_2 - \hat{x}_2$ and

$$F(x_1, x_2, \hat{x}_2, t) = c_2 \tilde{x}_2 + \zeta(x_1, x_2, t, u_1)$$

For a physical system such as a battery, the terminal voltage, OCV, and their derivatives are always bounded for the bounded input current. The control input injection of the observer is also continuous. Assuming $\zeta(x_1, x_2, t, u_1)$ to be bounded, it can be ensured that there exists a f^+ for which the following inequality is satisfied [168]:

$$|F(x_1, x_2, \hat{x}_2, t)| \leq f^+ \tag{3.50}$$

Then, the finite-time convergence of battery state observer can be ensured by the following choice of γ and β:

$$\beta \geq f^+ \tag{3.51a}$$

$$\gamma \geq \sqrt{\frac{2}{\beta - f^+}} \frac{(\beta + f^+)(1 + r)}{1 - r} \tag{3.51b}$$

where r is a constant, $0 < r < 1$.

Proof: A geometric approach similar to that given in [164] is used to prove the finite-time convergence of the proposed battery state observer given in (3.48). It can be easily seen from (3.49) that the convergence of the observer states to the actual states is equivalent to the convergence of $\tilde{x}_1$ and $\dot{\tilde{x}}_1$

to zero.

From (3.49) and (3.50), the differential inclusion satisfied by $\tilde{x}_2$ can be obtained as:

$$\dot{\tilde{x}}_2 \in [-f^+, f^+] - \beta sign(\tilde{x}_1) \tag{3.52}$$

The differential inclusion in this thesis is understood in the Filippov sense [169]. Taking derivative of the first equation of (3.49) in both sides with $\tilde{x}_1 \neq 0$ and using (3.52), we get

$$\ddot{\tilde{x}}_1 \in [-f^+, f^+] - \left(\frac{0.5\gamma}{|\tilde{x}_1|^{\frac{1}{2}}}\dot{\tilde{x}}_1 + \beta sign(\tilde{x}_1)\right) \tag{3.53}$$

Now, the differential inclusion in (3.53) will be utilized to explain the majorant curve shown in Figure 3.7. Consider the initial values as $\tilde{x}_1 = 0$ and $\tilde{x}_2 = x_2$. It is to be noted that if the initial value of x_2 is positive, then the trajectory will enter the half-plane where $\tilde{x}_1 > 0$. Similarly, if initial value of x_2 is negative, then the trajectory will enter the half plane where $\tilde{x}_1 < 0$. Suppose $\tilde{x}_1 > 0$ with $\dot{\tilde{x}}_1 > 0$, then the trajectory is confined between the axes $\tilde{x}_1 = 0$, $\dot{\tilde{x}}_1 = 0$ and the trajectory of the following equation:

$$\ddot{\tilde{x}}_1 = -(\beta - f^+) \tag{3.54}$$

The trajectory of (3.54) is shown by line (a) in Figure 3.7. Consider the point where the curve intersects the axis $\dot{\tilde{x}}_1 = 0$ be $\tilde{x}_{1M}$. Integrating both sides of (3.54), we can obtain

$$2(\beta - f^+)\tilde{x}_{1M} = \dot{\tilde{x}}_{10}^2 \tag{3.55}$$

where $\dot{\tilde{x}}_{10} > 0$ is the value of $\dot{\tilde{x}}_1$ with $\tilde{x}_1 = 0$. For $\tilde{x}_1 > 0$, $\dot{\tilde{x}}_1 > 0$, the following inequality is satisfied:

$$\ddot{\tilde{x}}_1 \leq f^+ - \beta sign(\tilde{x}_1) - \frac{0.5\gamma}{|\tilde{x}_1|^{\frac{1}{2}}}\dot{\tilde{x}}_1 < 0. \tag{3.56}$$

Hence, the trajectory is directed towards the axis $\dot{\tilde{x}}_1 = 0$. In Figure 3.7, the majorant curve for $\tilde{x}_1 > 0$, $\dot{\tilde{x}}_1 \geq 0$ is described by the following equation:

$$\dot{\tilde{x}}_1^2 = 2(\beta - f^+)(\tilde{x}_{1M} - \tilde{x}_1) \tag{3.57}$$

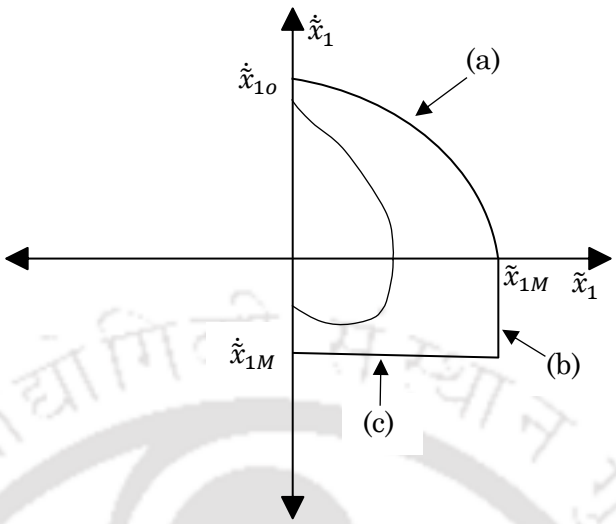

Figure 3.7: Majorant curve.

For $\tilde{x}_1 > 0$, $\dot{\tilde{x}}_1 \leq 0$, there are two parts in the majorant curve. In the first part, the point $(\tilde{x}_{1M}, 0)$ goes down instantly to $(\tilde{x}_{1M}, \dot{\tilde{x}}_{1M})$ in the worst case when the right hand side of (3.53) is zero. The term $\dot{\tilde{x}}_{1M}$ is given as:

$$\dot{\tilde{x}}_{1M} = -\frac{2}{\gamma}(\beta + f^+)\tilde{x}_{1M}^{\frac{1}{2}} \tag{3.58}$$

The first part is presented by line (b) in Figure 3.7. The second part is represented by line (c) in Figure 3.7 which is a straight line obtained by connecting $(\tilde{x}_{1M}, \dot{\tilde{x}}_{1M})$ and $(0, \dot{\tilde{x}}_{1M})$. From (3.51), (3.55) and (3.58), we get

$$\frac{|\dot{\tilde{x}}_{1M}|}{|\dot{\tilde{x}}_{10}|} < \frac{1-r}{1+r} < 1. \tag{3.59}$$

Suppose $\dot{\tilde{x}}_{10}, \dot{\tilde{x}}_{1M} = \dot{\tilde{x}}_{11}, \dot{\tilde{x}}_{12}, ..., \dot{\tilde{x}}_{1j}, ...$ are denoted as the consequent crossing points of the trajectory of the system given in (3.49) with the axis $\tilde{x}_1 = 0$, starting from the point $(0, \dot{\tilde{x}}_{10})$. The last quantity guarantees the convergence of $(0, \dot{\tilde{x}}_{1j})$ to $\tilde{x}_1 = \dot{\tilde{x}}_1 = 0$ as well as the convergence of $\sum_{j=0}^{\infty} |\dot{\tilde{x}}_{1j}|$.

Now, in order to prove finite-time convergence, we will consider the dynamics of $\tilde{x}_2$ given in (3.49). The following inequality can be obtained using (3.49):

$$0 < \beta - f^+ \leq |\dot{\tilde{x}}_2| \leq \beta + f^+ \tag{3.60}$$

From the dynamics of $\tilde{x}_1$ in (3.49), it is clear that when $\tilde{x}_1 = 0$, $\tilde{x}_2 = \dot{\tilde{x}}_1$ and holds for small

neighbourhood of the origin. Taking this into account and using (3.60), we obtain

$$|\dot{\tilde{x}}_{1j}| \geq (\beta - f^{+})t_j \tag{3.61}$$

where t_j are the time intervals between the successive intersection of the trajectory with the axis $\tilde{x}_1 = 0$. From (3.61), we get

$$t_j \leq \frac{|\dot{\tilde{x}}_{1j}|}{\beta - f^{+}} \tag{3.62}$$

The total convergence time is obtained by summing all t_j given as:

$$T_f \leq \sum \frac{|\dot{\tilde{x}}_{1j}|}{\beta - f^{+}} \tag{3.63}$$

Hence, the finite-time convergence of the battery observers states to the actual states is ensured.

3.5 Numerical simulation results

The battery considered for performing numerical simulations in this chapter comprises of a $LiMn_2O_4$ cathode, an artificial graphite anode, and has a nominal capacity (N_{cap}) of 5 Ah [129]. The nominal, full charge (V_{fc}), and cut-off (V_{co}) voltages are 3.8V, 4.2V, and 3.04 V, respectively. The dimension of the battery is 250 mm × 125 mm× 5 mm and it weighs 120 g. The bulk capacitance of the battery can be obtained by investigating the amount of energy stored using the following expression [129]:

$$C_n = \frac{3600 N_{cap} V_{fc}}{0.5({V_{fc}}^2 - {V_{co}}^2)} \tag{3.64}$$

In (3.64), multiplying the nominal capcity (N_{cap}) with 3600 converts its unit from Ah to Ampere-second. Using the values of N_{cap}, V_{fc}, and V_{co}, the value of C_n is calculated as 18000 F. The actual value of the unknown parameters of the battery model are given as follows: $R_t = 1\ m\Omega$, $R_i = 3\ m\Omega$, $R_c = 3\ m\Omega$, and $C_c = 200$ F. The specifications of the battery are taken from [129].

Relay feedback test with asymmetrical relay settings is carried out to identify the battery model parameters. Relay settings are taken as $h_1 = 5$ and $h_2 = 3$. A time delay of 0.5 s is introduced. The relay output and obtained limit cycle output of the process are shown in Figure 3.8 and 3.9, respectively. The information contained in the limit cycle output such as positive and negative

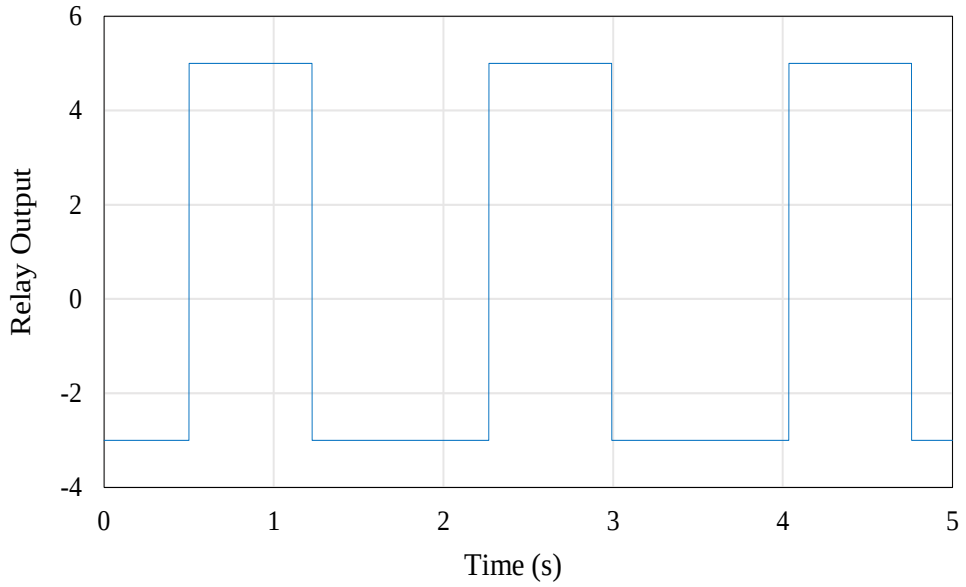

Figure 3.8: Output signal of the relay.

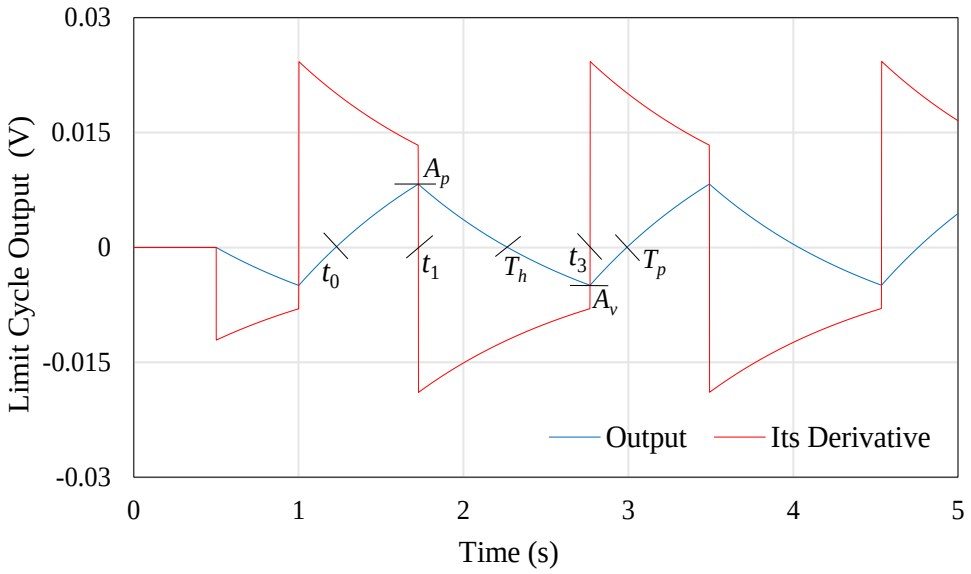

Figure 3.9: Limit cycle output of the process and its derivative.

peak amplitudes, t_0, t_1, T_h, t_3, and T_p are used to estimate the parameters of the transfer function (a, b, c) using (3.47). The values of identified transfer function parameters are as follows: $a = 0.843$, $b = 3.99 \times 10^{-3}$, and $c = 5.62 \times 10^{-5}$. Using the values of a, b, c, C_n, and (3.22), $R_i = 2.91\ m\Omega$, $C_c =$ 206.4 F, $R_c = 2.91\ m\Omega$, and $R_t = 1.05\ m\Omega$ are calculated. The value of a_1 = -0.824, $c_1 = 1.53 \times 10^{-2}$, $c_2 = -1.85 \times 10^{-2}$, $q_1 = 4.03 \times 10^{-3}$, and q_2 = -1.85 $\times 10^{-5}$ are found subsequently using (3.19). It is found that the maximum error in parameter identification using this technique is within 5%.

Next, with the help of estimated battery model parameters, the CSTA based observer is designed.

Using (3.51), for finite-time convergence of the states $\beta = 7.7 \times 10^{-2}$ and $\gamma = 4.6$ are considered. To verify the effectiveness of the proposed observer, discharging test is carried out on LIB by injecting a discharge pulse, as shown in Figure 3.10, to the battery. The magnitude of discharge pulse is 5 A

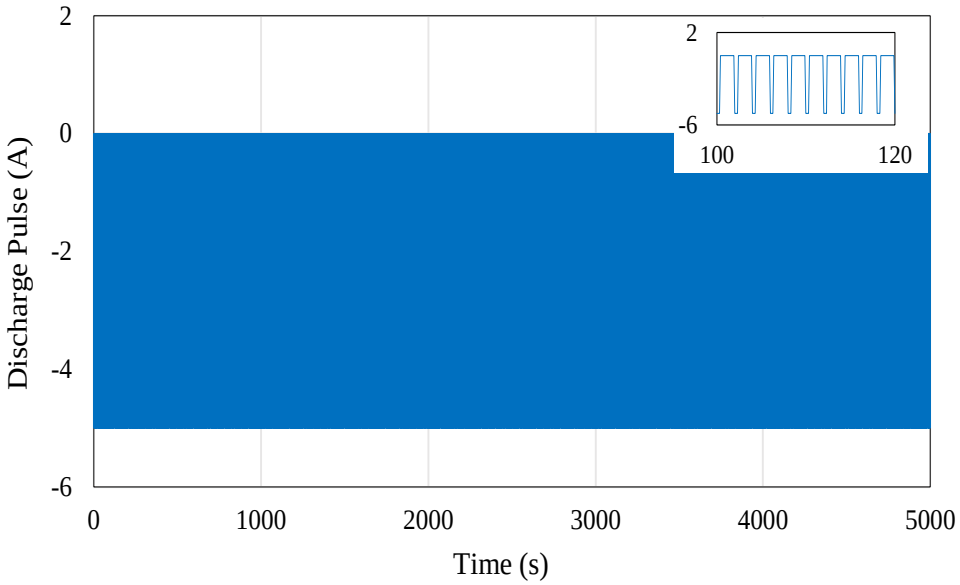

Figure 3.10: Discharge pulse.

and its discharge duration is 0.4 s in a cycle. It is provided at a regular interval of 1.6 s. The actual voltage and estimated terminal voltage from the proposed approach are shown in Figure 3.11. The

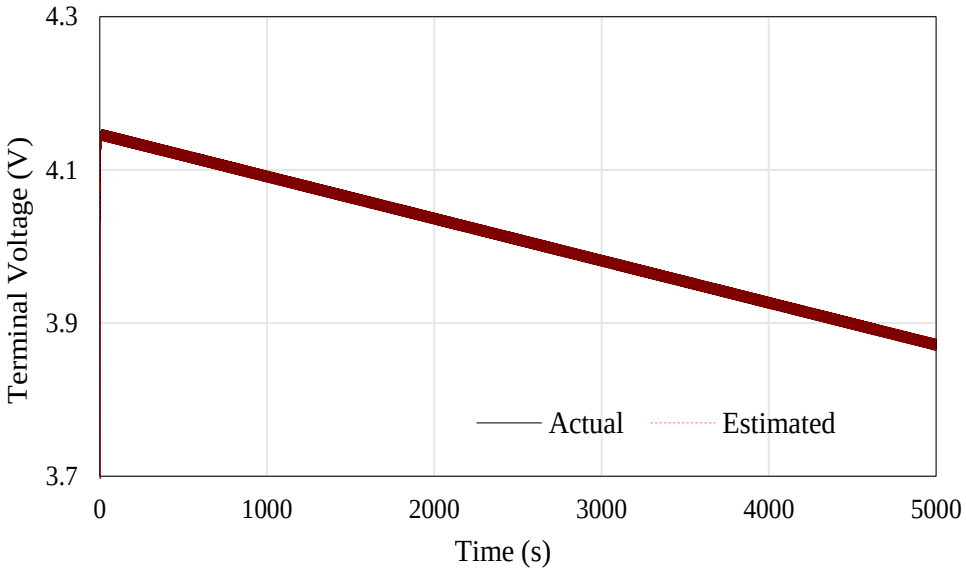

Figure 3.11: Terminal voltage comparison.

error between them is shown in Figure 3.12. It is found that the maximum absolute error (MAE) in estimating the terminal voltage of the battery is 0.0125 V (after convergence) and the root-mean-

square error (RMSE) is 0.004 V. To establish the superiority of the proposed approach, the estimated

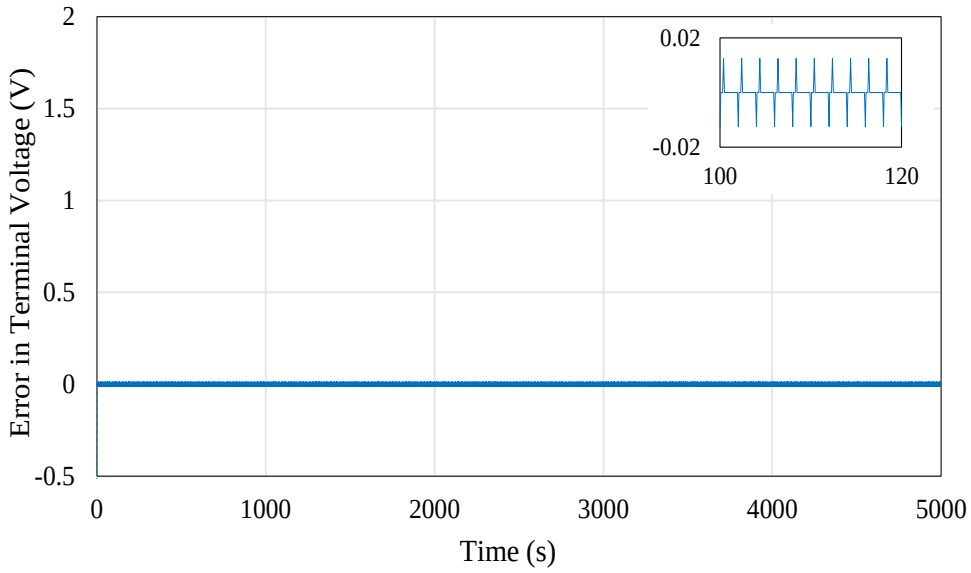

Figure 3.12: Error in terminal voltage.

OCV from the proposed approach is compared with that of SOSMO. The actual and the estimated OCV for each method are shown in Figure 3.13. Figure 3.14 demonstrates the corresponding errors

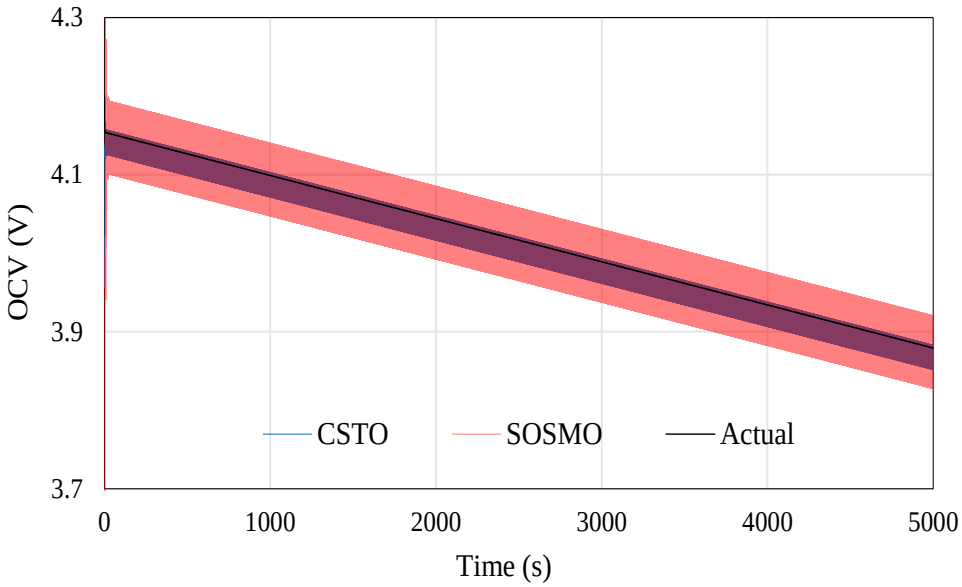

Figure 3.13: Open circuit voltage comparison.

between the estimated and the actual OCV for each method. The MAEs in OCV estimation for CSTO and SOSMO are found to be 0.03% and 0.05%, respectively. The RMSEs for CSTO and SOSMO are also caclulated as 0.01% and 0.03%, respectively. From Figure 3.14, it is found that the chattering

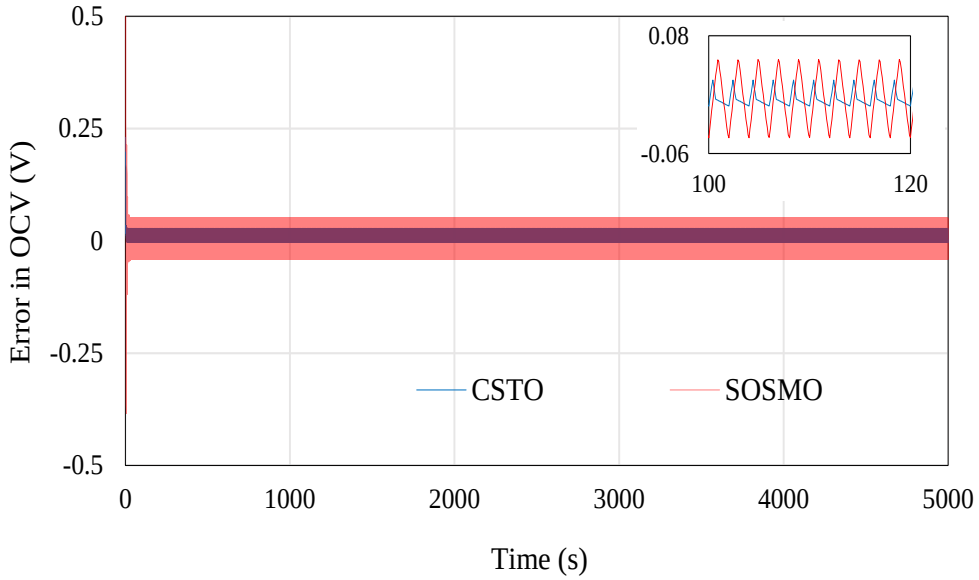

Figure 3.14: Error in estimated OCV.

is significantly reduced for CSTO compared to SOSMO. Between 500-600 s, the chattering width for CSTO and SOSMO are 0.03 and 0.09, respectively. From the estimated OCV, SOC of the battery can be predicted using the relationship given in [129]. Higher accuracy in OCV estimation ensures higher accuracy of the SOC. Therefore, it can be said that the proposed approach provides better accuracy and reduced chattering than SOSMO in estimating the SOC of the battery.

3.6 Summary

In this chapter, a new SOC estimation approach based on conventional STA is proposed. The STA reduces chattering significantly and sorts out various issues associated with the different sliding mode based SOC observers such as discontinuous control, need for more number of sensors, and need for low pass filters. The battery state equations have been derived and observability of the system has been established. In order to design the observer, the required battery model parameters are estimated by the relay feedback approach. This is a closed loop approach and provides good identification accuracy. A geometrical approach using majorant curve is presented for establishing the finite-time convergence of the battery SOC observer. Numerical simulations are performed to verify the efficacy of the proposed method. The OCV obtained from CSTO is compared with that of SOSMO and it is found that the proposed approach provides better estimation accuracy and lower chattering compared to SOSMO.

The work presented in this chapter acts as the foundation of this thesis and has scope for further improvement in several aspects. Although this chapter uses numerical simulation to establish the efficacy of the proposed method, experimental results with an actual physical battery and a real-time driving cycle will establish the efficacy of the method better in actual EVs. The strict Lyapunov super twisting algorithm based SOC estimation approach is presented in the next chapter to further improve the estimation of SOC of a battery under various dynamical conditions.

Note: A part of work presented in this chapter has been published with title "Estimation of state of charge of Li-ion battery in EVs using relay feedback approach and super twisting sliding mode observer" in 56th IEEE Conference on Decision and Control (CDC), 2017.

4

Development of Strict Lyapunov Super Twisting Observer for SOC Estimation Based on Real-Time Identification of Battery Model Parameters

4.1 Introduction

In Chapter 3, CSTO, along with relay feedback approach, is employed for developing the SOC estimation algorithm. Compared to the existing sliding mode based SOC observers, the various advantages of CSTO are detailed in that chapter. However, it is also associated with a few shortcomings. In CSTO, the robustness of the observer can be ensured for a very limited range of uncertainties. It can be seen that the uncertainties in the state equation (3.17) of the battery model in Chapter 3 are considered only for its second equation. The disturbance in the first state equation of (3.17) is assumed to be zero. However, in a physical system, the modelling uncertainties, sensor inaccuracy, and other external disturbances also cause the uncertainties in the first state equation of (3.17). Hence, this assumption needs to be reconsidered for the application of real-time battery system. Recently, in another paper by Huangfu et al. [170], CSTO has been utilized for SOC estimation, but that considers uncertainties only in its first state equation of battery model. It also fails to ensure convergence of the unknown states in finite time. Moreover, in both Chapter 3 and [170], the BECM parameters are assumed to be fixed, which is not the case in real-time battery system due to the variation of these parameters with C-rate, SOC, temperature, and ageing. The offline identification technique used in Chapter 3 also needs an additional setup to perform the identification test and additional memory in BMS to store the battery model parameters data for their further use. Hence, there is need for an SOC estimation method that not only can provide the various advantages associated with CSTO, but also can ensure finite-time convergence and robustness for a more comprehensive class of uncertainties with real-time identification of the battery model parameters.

In this chapter, we propose a new approach for SOC estimation using SLSTA based observer which tries to resolve the above mentioned issues. In addition to various advantages associated with CSTO, the SLSTA based observer can also ensure the robust stability for a class of uncertainties much wider than that used in the conventional STA based observer. It also provides finite-time stability for all the states. The robust finite-time convergence of the proposed SOC observer is proven using a strict Lyapunov function. In this chapter, the derivation of state equations from battery model also incorporates the relationship between SOC and OCV in it. The nonlinearity present in this relationship is considered as uncertainty and will be taken care of by the robust observer. Instead of OCV, directly SOC is considered as a state of the system. In order to design the observer, the required battery model parameters are identified using recursive least square with forgetting (RLSF)

approach. It is a standard online identification scheme and can track the changes in the battery model parameters with various factors such as C-rate, SOC, temperature, and ageing. Hence, their effect can be avoided in battery modelling which provides an opportunity to use a simple battery model. The SLSTA based observer, in combination with the RLSF approach, attenuates the influence of the various uncertainties and provides a significant improvement in estimating SOC compared to the other existing sliding mode observer based SOC estimation approaches. The proposed method is implemented on an actual battery setup by using a real-time driving cycle current profile. The results demonstrate that the proposed approach performs better than the various well-known approaches in terms of accuracy, robustness, computational time, and convergence speed.

4.2 Simplified battery model

The second order RC equivalent circuit model used in Chapter 3 is also utilized for battery modelling in this chapter. Unlike Chapter 3, SOC is directly considered as a state of the system instead of OCV in this chapter. For this purpose, the relationship between SOC and OCV is incorporated in deriving the state equations. This will also provide an opportunity to the observer to compensate any uncertainty present in this relationship. The steps to derive the state equations for the battery model will remain same from (3.1)-(3.16) as presented in Section 3.2. We will directly use the relationships established in (3.15) and (3.16) to carry out the further derivation. For convenience, these equations are rewritten here as follows:

$$\dot{V}(t) = \left(\frac{C_c - C_n}{2R_iC_nC_c}\right)V(t) + \left(\frac{C_n - C_c}{2R_iC_nC_c}\right)V_{oc}(t) + \left(\frac{C_nR_i + C_nR_t - C_cR_t}{2R_iC_nC_c}\right)i(t) + \left(R_t + R_i/2\right)\dot{i}(t) \tag{4.1}$$

$$\dot{V}_{oc}(t) = \left(\frac{1}{R_iC_n}\right)V(t) - \left(\frac{1}{R_iC_n}\right)V_{oc}(t) - \left(\frac{R_t}{R_iC_n}\right)i(t) \tag{4.2}$$

In general, the relationship between OCV and SOC is nonlinear and can be approximated with a very high order polynomial. However, such relationship will make the SOC observer design very complex. Hence, in this thesis, the SOC-OCV curve is considered to be piecewise linear due to its linear behaviour for a small interval of SOC [125, 134]. Since the curve is slowly varying with various factors such as ageing and temperature, the relationship between OCV and SOC is assumed to be

fixed. The SOC-OCV relationship is approximated as:

$$V_{oc}(t) = pZ(t) + q + \Delta f_1 \tag{4.3}$$

where $Z(t)$ is the SOC at time t, Δf_1 is the nonlinearity present in SOC-OCV relationship, p and q are distinct constants corresponding to distinct SOC intervals, which can be determined by fitting of (4.3) in SOC-OCV curve. For a battery system, it can be inferred from the existing literature that p and q are positive [125, 134]. In this chapter, the derivation of SOC-OCV curve is explained for the test battery in subsection 4.5.2.

Using (4.3), (4.1) can be rewritten as:

$$\dot{V}(t) = -a_1 V(t) + a_2 Z(t) + q_1 i(t) + q_2 \dot{i}(t) + a_1 q + \Delta f_2 \tag{4.4}$$

where

$$a_1 = \frac{C_n - C_c}{2R_i C_n C_c}, \quad a_2 = a_1 p$$

$$q_1 = \frac{C_n R_i + C_n R_t - C_c R_t}{2R_i C_n C_c}, \quad q_2 = R_t + \frac{R_i}{2} \tag{4.5}$$

and Δf_2 is the small error due to the approximation of the relationship between p and q as given in (4.3).

Using (4.3) in (4.2), we get

$$\dot{Z}(t) = b_2 V(t) - b_1 Z(t) - b_2 q + q_3 i(t) + \Delta f_3 \tag{4.6}$$

where

$$b_1 = \frac{1}{R_i C_n}, \quad b_2 = \frac{b_1}{p}, \quad q_3 = \frac{q_4}{p}, \quad q_4 = -\frac{R_t}{R_i C_n} \tag{4.7}$$

and Δf_3 is the small error due to the approximation of relationship between p and q as given in (4.3).

Considering $x_1(t) = V(t)$, $x_2(t) = Z(t)$, $y(t) = V(t)$, $u_1(t) = i(t)$ and $u_2(t) = \dot{i}(t)$, (4.4) and (4.6) can be rewritten as:

$$\dot{x}_1(t) = -a_1 x_1(t) + a_2 x_2(t) + q_1 u_1(t) + q_2 u_2(t) + a_1 q + \zeta_1 \tag{4.8}$$

$$\dot{x}_2(t) = b_2 x_1(t) - b_1 x_2(t) - b_2 q + q_3 u_1(t) + \zeta_2 \tag{4.9}$$

$$y(t) = x_1(t) + \Delta f_4 \tag{4.10}$$

where $\zeta_1(x,t,u) = \Delta f_2 + \Delta f_5$, $\zeta_2(x,t,u) = \Delta f_3 + \Delta f_6$, Δf_4, Δf_5, and Δf_6 are the uncertainties due to measurement noise, modelling inaccuracy, and external disturbances. From the observability test described in Section 3.2, it is easy to conclude that if $C_n \neq C_c$, the system considered above is observable. In a practical battery $C_n \gg C_c$, hence the system is always observable.

The transfer function of the battery model is obtained from (4.1) and (4.2) is as follows:

$$\frac{Y(s)}{U_1(s)} = \frac{bs^2 + cs + d}{s^2 + as} \tag{4.11}$$

where

$$a = \frac{C_n + C_c}{2R_i C_n C_c}, \quad b = R_t + R_i/2$$

$$c = \frac{(C_n + C_c)(R_i + R_t)}{2R_i C_n C_c}, \quad d = \frac{1}{2R_i C_n C_c} \tag{4.12}$$

$Y(s)$ and $U_1(s)$ are the transformation of $y(t)$ and $u_1(t)$ in complex frequency domain.

4.3 Identification of battery model system

In Chapter 3, the parameters of the battery model are identified using state-space based relay feedback approach. It is assumed that the battery model parameters are constant with respect to the various operating conditions. However, the battery model parameters vary with several factors such as C-rate, SOC, temperature, and ageing [171]. The offline methods give erroneous identification results under such conditions and may induce significant error in SOC estimation. Moreover, the offline methods need an additional setup to perform the identification test and additional memory in BMS to store the BECM parameters data for their further use. The online estimation methods can overcome the above shortcomings and update the battery model parameters during its operation according to the changes in the operating conditions. A good online identification method should track the changes in the parameters for high accuracy and have a low computational complexity such

that it can be easily implemented on a low cost micro-controller utilized for BMS.

In literature, various online approaches are presented for identification of battery model parameters. In [172], the joint estimation of battery model parameters and SOC is proposed, where the BECM parameters are assumed as additional state variables. Two inpendent Kalman filters are used in dual EKF [173] and dual UKF [174] methods to estimate BECM parameters and SOC separately. the performance of the EKF-based method greatly depends on the accuracy of the model However, the performance of KF based methods higly rely on the accuracy of the battery model and knowledge of the noise statistics. They also have high computational burden due to recursive complex computation of various matrices. Heuristic algorithms such as genetic algorithm (GA) [175] and particle swarm optimization (PSO) [176] are also employed for identification of BECM parameters. In [177], it is established that the PSO has better accuracy and faster convergence than the other heuristic approaches. In BMS applications, the recursive least square algorithms are most widely used due to their simplicity, high accuracy, and low computational cost. For the purpose of battery model parameter identification, ordinary recursive least square (ORLS) is being used extensively by many researchers [178] till date. In [179], the performance of EKF, PSO, and ORLS have been compared and it is found that the ORLS has better accuracy, robustness, and computational time under dymanic conditions. However, the problem with ORLS is that the covariance becomes zero with time after which the parameters will not get updated further. To further improve the identification accuracy of ORLS, its variants have been used recently for battery parameter identification such as weighted RLS [180], recursive extended least square [181], moving window RLS [182], etc. All the methods are primarily differentiated by the way they assign weight to the data samples. In this chapter, we use standard RLSF approach [78, 105] for identification of the time-variant battery model parameters. Introduction of forgetting factor slows down the fading of the covariance matrix and improves the shortcoming of ORLS to a large extent. Since RLSF approach constantly updates the battery model parameters as per the current operating conditions, the effect of ageing and other factors can be considered as the simple recursive change in the BECM parameters.

4.3.1 Introduction to recursive least square with forgetting approach

The least square technique is an identification approach that estimates the unknown time-invariant parameters in such a way that the sum of squares of the difference between the actual values and the

estimated values is minimized [183]. It is mathematically presented below. Consider a system in linear parametric form as:

$$y(k) = \theta^T(k)\phi \tag{4.13}$$

where y = actual output of the system, θ = regressor vector, and ϕ = actual parameter vector.

The expression of the cost function to be minimized is represented by:

$$J(k) = \frac{1}{2}\sum_{m=1}^{k}\left(y(m) - \theta^T(m)\hat{\phi}\right)^2 \tag{4.14}$$

where $\hat{\phi}$ is the estimated value of ϕ. More details and derivation of this method can be found in [184].

The parameter vector $\hat{\phi}$ can be obtained by minimizing the cost function as follows :

$$\hat{\phi} = \left(\sum_{m=1}^{k}\theta(m)\theta^T(m)\right)^{-1}\left(\sum_{m=1}^{k}\theta(m)y(m)\right) \tag{4.15}$$

For real-time parameter identification, it is not a good idea to repeatedly use (4.15) to calculate the parameter vector with the availability of new data. Since (4.15) involves the matrix inversion, repeated execution of (4.15) will lead to very high computational cost. The ORLS approach solves this issue and is given by

$$\hat{\phi}(k) = \hat{\phi}(k-1) + H(k)[y(k) - \theta^T(k)\hat{\phi}(k-1)]$$

$$H(k) = \frac{G(k-1)\theta(k)}{1 + \theta^T(k)G(k-1)\theta(k)}$$

$$G(k) = G(k-1) - H(k)\theta^T(k)G(k-1) \tag{4.16}$$

where $H(k)$ is the gain that determines the effect of the current prediction error on the update of the parameter estimate and $G(k)$ is the covariance matrix of the estimated parameters.

It can be seen from (4.16) that the present parameters are estimated by updating the previous parameters which do not require complex calculation such as matrix inversion. The disadvantage of ORLS is that it gives equal weights to all previous data. However, in real-time battery, the most recent current and voltage samples reflect more accurate battery behaviour than older samples. Hence, a forgetting factor is introduced in which more weight is assigned to recent data than the older data [78, 105]. The main difference with the ORLS approach is how the covariance matrix $G(k)$ is

updated. In ORLS, the covariance vanishes to zero with time, losing its capability to keep track the changes in BECM parameters. Introduction of forgetting factor slows down the fading of the covariance matrix and improves the shortcoming of ORLS to a large extent. The cost function to be minimized for RLSF approach is given as:

$$J(k) = \frac{1}{2}\sum_{m=1}^{k} \lambda^{k-m}(y(m) - \theta^T(m)\hat{\phi})^2 \tag{4.17}$$

where λ is the forgetting factor which generally lies in the range of $[0.9, 1]$ for most of the applications. The following set of equations, which govern the RLSF algorithm [105], are used to estimate the parameter vector $\phi(k)$:

$$\begin{aligned} \hat{\phi}(k) &= \hat{\phi}(k-1) + H(k)[y(k) - \theta^T(k)\hat{\phi}(k-1)] \\ H(k) &= \frac{G(k-1)\theta(k)}{\lambda + \theta^T(k)G(k-1)\theta(k)} \\ G(k) &= \frac{1}{\lambda}[G(k-1) - H(k)\theta^T(k)G(k-1)] \end{aligned} \tag{4.18}$$

It can be seen from (4.18), the expression of covariance matrix is divided by the forgetting factor λ at each update. This eventually slows down fading of the covariance matrix and keep the ability of the identification scheme to track changes in the parameters.

4.3.2 Implementation of RLSF for battery model parameter identification

In order to implement the RLSF algorithm for parameter identification of utilized battery model, the transfer function in (4.11) is first discretized using the bilinear transformation

$$s = \frac{2}{T_s}\frac{1 - z^{-1}}{1 + z^{-1}} \tag{4.19}$$

where T_s is the sampling time and z^{-1} is the unit backward shift operator.

The discretized transfer function obtained is as follows:

$$\frac{Y(z^{-1})}{U_1(z^{-1})} = \frac{d_0 + d_1 z^{-1} + d_2 z^{-2}}{1 + c_1 z^{-1} + c_2 z^{-2}} \tag{4.20}$$

where

$$c_1 = \frac{-4}{2 + aT_s}, \quad c_2 = \frac{2 - aT_s}{2 + aT_s},$$

$$d_0 = \frac{4b + 2cT_s + dT_s{}^2}{2(2 + aT_s)}, \quad d_1 = \frac{dT_s{}^2 - 4b}{2 + aT_s}, \quad d_2 = \frac{4b - 2cT_s + dT_s{}^2}{2(2 + aT_s)} \tag{4.21}$$

The difference equation of the battery model from (4.20) is obtained as follows:

$$y(k) = \theta^T(k)\phi(k) + \Delta N \tag{4.22}$$

where ΔN is the white noise present in the system.

The regressor vector $\theta(k)$ and the parameter vector $\phi(k)$ are given as:

$$\theta(k) = \begin{bmatrix} y(k-1) & y(k-2) & u_1(k) & u_1(k-1) & u_1(k-2) \end{bmatrix}^T$$

$$\phi(k) = \begin{bmatrix} -c_1 & -c_2 & d_0 & d_1 & d_2 \end{bmatrix}^T$$

The relationship between $\phi(k)$ and a, b, c, d are obtained using (4.21) as follows:

$$a = \frac{2(1 - c_2)}{T_s(1 + c_2)}, \quad b = \frac{d_0 + d_2 - d_1}{2(1 + c_2)}$$

$$c = \frac{2(d_0 - d_2)}{T_s(1 + c_2)}, \quad d = \frac{2(d_0 + d_1 + d_2)}{T_s{}^2(1 + c_2)} \tag{4.23}$$

The set of equations presented in (4.18) are used to estimate the parameter vector $\phi(k)$. From the estimated $\phi(k)$ and (4.23), the estimated values of a, b, c, and d are obtained. The estimated resistances and capacitances in the battery model are derived using (4.12) as follows:

$$\hat{R}_t = 2\hat{b} - \frac{\hat{c}}{\hat{a}}, \quad \hat{R}_i = \hat{R}_c = 2\left(\frac{\hat{c}}{\hat{a}} - \hat{b}\right)$$

$$\hat{C}_n = \frac{1}{2}\left[\frac{\hat{a}}{\hat{d}} + \left(\frac{\hat{a}^2}{\hat{d}^2} - \frac{\hat{a}}{(\hat{c} - \hat{a}\hat{b})\hat{d}}\right)^{1/2}\right]$$

$$\hat{C}_c = \frac{1}{2}\left[\frac{\hat{a}}{\hat{d}} - \left(\frac{\hat{a}^2}{\hat{d}^2} - \frac{\hat{a}}{(\hat{c} - \hat{a}\hat{b})\hat{d}}\right)^{1/2}\right] \tag{4.24}$$

where '$\hat{*}$' denotes the estimated value of '$*$'. Finally, the estimated values of parameters a_1, b_1, q_1, q_2, and q_4 defined in (4.5) and (4.7) are calculated using (4.24).

4.4 Design of state observer using SLSTA

In this section, the design procedure of SLSTA based observer for estimation of battery states is presented. In addition to the several advantages of conventional STA, the SLSTA based observer provides robustness against a more comprehensive class of uncertainties than the conventional STA [185]. Conventional STA does not explain how the convergence is affected if both ζ_1 and ζ_2 in (4.8) and (4.9) are non-zero together. The proposed observer overcomes this limitation. In order to design the observer, it is assumed that the rate of change of terminal current is negligible. This assumption is valid since the current is almost constant between two sampling instants [62,63]. The strict Lyapunov super twisting observer (SLSTO) designed to estimate the battery states is as follows:

$$\dot{\hat{x}}_1(t) = -\hat{a}_1 y(t) + \hat{a}_2 \hat{x}_2(t) + \hat{q}_1 u_1(t) + \hat{a}_1 q + \gamma |\tilde{x}_1|^{1/2} sign(\tilde{x}_1) \tag{4.25}$$

$$\dot{\hat{x}}_2(t) = \hat{b}_2 y(t) - \hat{b}_1 \hat{x}_2(t) - \hat{b}_2 q + \hat{q}_3 u_1(t) + \beta sign(\tilde{x}_1) \tag{4.26}$$

where '$\hat{*}$' denotes the identified value of battery model parameter '$*$', $\hat{x}_1$ and $\hat{x}_2$ are the state estimates of the system states x_1 and x_2 given in (4.8)-(4.9), $\gamma = \gamma_1 \sqrt{\hat{a}_2}$, and $\tilde{x}_1 = x_1 - \hat{x}_1$. The error dynamics using (4.8)-(4.10) and (4.25)-(4.26) is as follows:

$$\dot{\tilde{x}}_1 = \hat{a}_2 \tilde{x}_2 - \gamma |\tilde{x}_1|^{1/2} sign(\tilde{x}_1) + F_1(x, \hat{x}, t, u)$$

$$\dot{\tilde{x}}_2 = -\beta sign(\tilde{x}_1) + F_2(x, \hat{x}, t, u) \tag{4.27}$$

where

$$F_1(x, t, u) = a_1 \Delta f_4 - \Delta a_1 y + \Delta a_2 x_2 + \Delta q_1 u_1 + \Delta a_1 q + \zeta_1(x, t, u)$$

$$F_2(x, t, u) = -b_2 \Delta f_4 + \Delta b_2 y - b_1 x_2 + b_1 \hat{x}_2 - \Delta b_1 \hat{x}_2 - \Delta b_2 q - \Delta q_3 u_1 + \zeta_2(x, t, u) \tag{4.28}$$

$\tilde{x}_2 = x_2 - \hat{x}_2$, $\Delta a_1 = a_1 - \hat{a}_1$, $\Delta b_1 = b_1 - \hat{b}_1$, $\Delta q_1 = q_1 - \hat{q}_1$, and $\Delta q_3 = q_3 - \hat{q}_3$.

Considering the continuous control injection of the observer and boundedness of $V, \dot{V}, i, Z, \zeta_1, \zeta_2$, and

Δf_4, it can also be considered that the following inequalities are satisfied [168]:

$$|F_1(x,t,u)| \leq \varrho_1 + \varrho_2(|\tilde{x}_1| + \hat{a}_2^2\tilde{x}_2^2)^{1/2}$$

$$|F_2(x,t,u)| \leq f^+ \tag{4.29}$$

where f^+, ϱ_1, and ϱ_2 are positive constants.

Suppose the perturbations to the system (4.27) is bounded by (4.29). Then, the following choice of β and γ_1 guarantee the finite-time convergence or global ultimate boundedness of the states:

$$\gamma_1 = \Psi\sqrt{\frac{2k_2 f^+}{(1-k_1)\sigma}} \tag{4.30}$$

$$\beta = \frac{(1+k_1)f^+}{(1-k_1)} \tag{4.31}$$

provided the following inequality is satisfied

$$\Psi - \frac{2}{k_2}\sigma > \sigma^2 - k_1(1+\Psi)\sigma + \frac{1}{4}(1+\Psi)^2 \tag{4.32}$$

where $0 < k_1 < 1$, $k_2 > 1$, Ψ and σ are positive constants. Convergence or ultimate boundedness depends on the value of ϱ_1 and ϱ_2. When $\varrho_1 = 0$ and ϱ_2 is small enough, the convergence of estimated states to the actual states is ensured. In case, when $\varrho_1 \neq 0$, the estimated states converge to certain small bound around the actual states.

Proof: Suppose $e_1 = \tilde{x}_1$ and $e_2 = \hat{a}_2\tilde{x}_2$, (4.27) can be rewritten as:

$$\dot{e}_1 = e_2 - \gamma|e_1|^{1/2}sign(e_1) + F_1(x,t,u)$$

$$\dot{e}_2 = -\beta_1 sign(e_1) + F_3(x,t,u) \tag{4.33}$$

where $\beta_1 = \hat{a}_2\beta$ and $F_3(x,t,u) = \hat{a}_2 F_2(x,t,u)$.

Since $\hat{a}_2$ is positive and bounded, we have

$$|F_3(x,t,u)| \leq \hat{a}_2 f^+ = f_1^+ \tag{4.34}$$

In order to show the convergence or ultimate boundedness of states in (4.33), the strict Lyapunov function candidate is considered as:

$$\nu(e) = \Phi^T P \Phi \tag{4.35}$$

where $\Phi^T = [\Phi_1 \;\; \Phi_2] = \left[|e_1|^{\frac{1}{2}} sign(e_1) \;\; e_2\right]$ and $P = [p_{ij}]$ is a constant symmetric positive definite matrix. It can be observed that, $\Phi = 0$ ensures $e_1 = e_2 = 0$. It is well known from geometric/Lyapunov methods that if $\gamma > 0$ and $\beta_1 > 0$, then the trajectories will converge to the equilibrium point $e_1 = e_2 = 0$ for $F_1 = F_3 = 0$ [164, 185].

The derivative of Φ can be obtained as:

$$\dot{\Phi} = \frac{1}{|\Phi_1|} A_1 \Phi \tag{4.36}$$

where

$$A_1 = \begin{bmatrix} -0.5\gamma & 0.5 \\ -\beta_1 & 0 \end{bmatrix}$$

is Hurwitz. Hence, there always exists a symmetric positive matrix $Q_1 = [q_{ij}]$ such that the following Algebraic Riccati equation is satisfied:

$$A_1^T P + P A_1 = -Q_1 \tag{4.37}$$

The derivative of $\nu(e)$ using (4.35) and (4.36) is obtained as:

$$\dot{\nu}(e) = -|e_1|^{-\frac{1}{2}} \Phi^T Q_1 \Phi + \frac{2}{|e_1|^{\frac{1}{2}}} \left[\frac{F_1}{2} \;\; |e_1|^{\frac{1}{2}} F_3\right] P \Phi \tag{4.38}$$

Using (4.29) and (4.34), $\dot{\nu}(e)$ is rewritten as:

$$\dot{\nu}(e) = |e_1|^{-\frac{1}{2}} \left\{ \Phi^T \left[A_2^T(t,e) P + P A_2(t,e)\right] \Phi + [F_1 \;\; 0] P \Phi \right\} \tag{4.39}$$

where

$$A_2(t,e) = \begin{bmatrix} -\frac{1}{2}\gamma & \frac{1}{2} \\ F_3 sign(e_1) - \beta_1 & 0 \end{bmatrix}$$

From (4.35) and (4.39), it can be seen that $\nu(e)$ is positive definite and $A_2^T(t,e)P + PA_2(t,e)$ is negative definite if the following inequalities are satisfied:

$$\begin{gathered} p_{22} > p_{12}^2, \quad p_{12} < 0, \\ \gamma p_{12} + 0.25(1-\gamma p_{12})^2 + 2p_{12}^2(\beta_1 - F_3 sign(e_1)) - (1 - \gamma p_{12} p_{22}(\beta_1 - F_3 sign(e_1))) \\ + (\beta_1 - F_3 sign(e_1))^2 p_{22}^2 < 0 \end{gathered} \tag{4.40}$$

From (4.33), it is clear that if $\beta_1 < f_1^+$, then the equilibrium point will be unstable for the disturbance F_3. Using this fact, it follows that (4.40) will be satisfied if (4.32) is true, where

$$\Psi = -\gamma p_{12}, \;\; k_2 = \frac{p_{22}}{p_{12}^2}, \;\; \sigma = p_{22}(\beta_1 + f_1^+), \;\; k_1 = \frac{\beta_1 - f_1^+}{\beta_1 + f_1^+} \tag{4.41}$$

Hence,

$$\dot{\nu}(e) \leq -|e_1|^{-\frac{1}{2}} \Phi^T Q_2 \Phi + |e_1|^{-\frac{1}{2}} [F_1 \;\; 0] P \Phi \tag{4.42}$$

where the elements of P and Q_2 are obtained from (4.41) as:

$$p_{11} = 1, \quad p_{22} = \frac{(1-k_1)\sigma}{2f_1^+}, \quad p_{12} = -\sqrt{\frac{p_{22}}{k_2}}$$

$$q_{11} = \gamma + 2p_{12}(\beta_1 + f_1^+) + 2f_1^+(1 - \gamma p_{12})\frac{p_{22}}{p_{12}}$$

$$q_{12} = -\frac{1}{2}(1 - \gamma p_{12}) + (\beta_1 + f_1^+)p_{22}, \quad q_{22} = -p_{12} \tag{4.43}$$

Using the fact

$$\lambda_{min}\{Q_2\}\|\Phi\|_2^2 \leq \Phi^T Q_2 \Phi \leq \lambda_{max}\{Q_2\}\|\Phi\|_2^2$$

we obtain

$$\dot{\nu}(e) \leq -|e_1|^{-\frac{1}{2}} \left[\lambda_{min}\{Q_2\}\|\Phi\|_2^2 - (\varrho_1 + \varrho_2\|\Phi\|_2)\varepsilon\|\Phi\|_2 \right]$$

$$\leq -\Big[\lambda_{min}\{Q_2\} - \varrho_2\varepsilon\Big]\|\Phi\|_2 + \varrho_1\varepsilon$$

where $\varepsilon = (1 + p_{12})^{1/2}$. When ϱ_2 is small (i.e., $\varrho_2 < \lambda_{max}\{Q_2\}/\varepsilon$), the following holds for every ϱ_1:

$$\dot{\nu}(e) \leq -\Big[\lambda_{min}\{Q_2\} - \varrho_2\varepsilon\Big]\Big[d\|\Phi\|_2 + (1-d)\|\Phi\|_2\Big] + \varrho_1\varepsilon$$

$$\leq -\frac{d\Big[\lambda_{min}\{Q_2\} - \varrho_2\varepsilon\Big]}{\lambda_{max}^{1/2}\{P\}}\nu^{1/2}(e), \ \forall \ \|\Phi\|_2 \geq \mu \tag{4.44}$$

where $0 < d < 1$ is a constant and

$$\mu = \frac{\varrho_1\varepsilon}{(1-d)(\lambda_{min}\{Q_2\} - \varrho_2\varepsilon)}$$

Since

$$\lambda_{min}\{P\}\|\Phi\|_2^2 \leq \nu(e) \leq \lambda_{max}\{P\}\|\Phi\|_2^2 \tag{4.45}$$

we can write

$$||\Phi|| \leq \frac{\nu^{1/2}(e)}{\lambda_{min}^{1/2}\{P\}} \tag{4.46}$$

Therefore, the trajectory which enters

$$\Gamma = \{e \epsilon \mathbb{R}^2 | \nu(e) \leq \lambda_{max}\{P\}\mu^2\} \tag{4.47}$$

in finite time, stays there for all future time such that

$$||\Phi|| \leq \frac{\lambda_{max}^{1/2}\{P\}}{\lambda_{min}^{1/2}\{P\}}\mu \tag{4.48}$$

Eq. (4.48) guarantees that after convergence, the error trajectories will always remain bounded by a small region around equilibrium even in the presence of various uncertainties. It can be seen that if $\varrho_1 = 0$, the error dynamics converge to the origin. This completes the proof of robust stability of the observer.

4.5 Experimental results

In this section, the experimental results of the proposed approach for SOC estimation are demonstrated in seven separate subsections. Subsection 4.5.1 presents the setup used to perform all the required tests. In Subsection 4.5.2, the relationship between SOC and OCV for the test battery is established. The implementation of the RLSF approach for battery model identification and design of SLSTA based observer are demonstrated in Subsection 4.5.3. Subsection 4.5.4 discusses the results of the estimated SOC by the proposed method considering erroneous initial SOC condition and provides comparative study with other existing approaches in terms of various aspects such as accuracy, computational time, convergence time, and chattering width. The effect of current and voltage sensor noise is investigated in Subsection 4.5.5. The robustness of the proposed observer against the model identification errors is studied in Subsection 4.5.6. In Subsection 4.5.7, the measurement noise and identification errors are considered together to verify the effectiveness of the proposed method. Figure 4.1 shows the structure of the proposed approach.

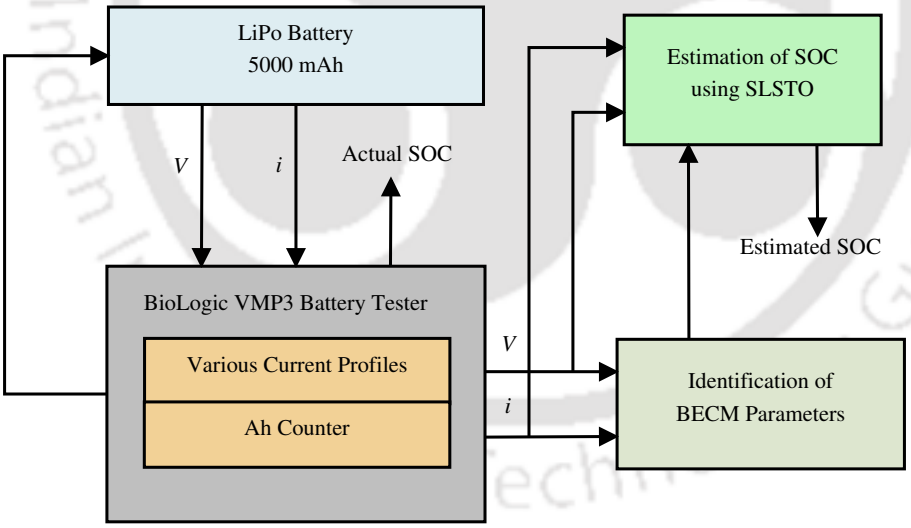

Figure 4.1: Structure of the proposed method.

4.5.1 Experimental setup

To evaluate the performance and efficacy of the proposed approach, a lithium polymer (LiPo) battery (BDE6S73104P), as shown in Figure 4.2(a), with nominal capacity 5000 mAh is utilized. The dimension of the battery is 90 mm × 60 mm× 5 mm and, it weighs 110 g. The full charge, nominal, and cut-off voltages are 4.2 V, 3.7 V, and 3.25 V, respectively. The experiments are performed using a

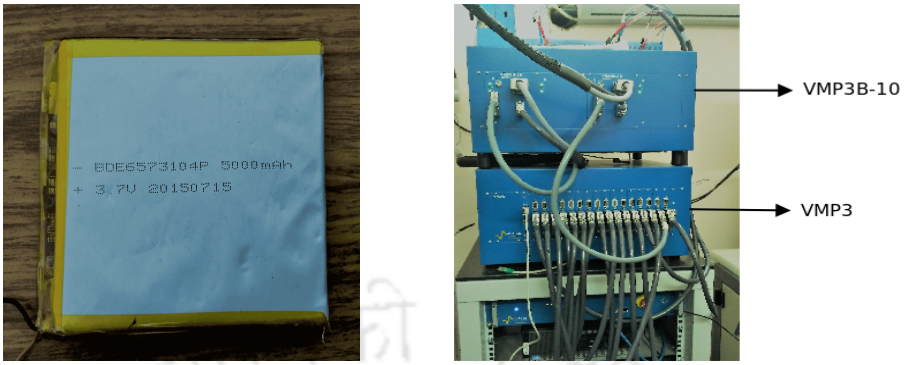

(a) (b)

Figure 4.2: (a) Lithium polymer battery and (b) BioLogic VMP3 and VMP3B-10.

battery testing equipment (BioLogic VMP3) having 16 independent channels. It has a voltage range of ±20 V and the current range of 10 μA-400 mA. The maximum current is enhanced to 10 A using an external booster VMP3B-10 along with BioLogic VMP3 for making it ideal for the experiments. The accuracy of the voltage and the current sensors are very high with resolutions of 5 μV and 760 pA, respectively. The battery testing equipment, as well as the external booster, is shown in Figure 4.2(b). The setup provides the necessary current and voltage to control the charging and the discharging process through a software known as EC-Lab.

4.5.2 Relationship between OCV and SOC

In this work, the relationship between OCV and SOC for the utilized battery is obtained by first discharging it from its fully charged state to the fully discharged state and then charging it back to the initial state. Instead of a unidirectional current test, both charge and discharge tests are performed to consider the effect of hysteresis phenomena taking place inside the battery [61]. Before starting the discharge test, the battery is ensured to be fully charged, i.e., 4.2 V. A constant discharge current with C/40 rate is then applied to the battery until the battery voltage becomes equal to the cut-off voltage, i.e., 3.25 V. This sufficiently small C-rate makes battery terminal voltage and OCV almost equal. After that, a constant voltage discharging is done until the current becomes very small (C/80). Similarly, the battery is again charged with C/40 rate upto the peak voltage, followed by a constant voltage charging until the current reduced to C/80. The terminal voltage vs. time data is recorded in the host computer during the process. The SOC is also computed at each sampling instant using coulomb counting method. Figure 4.3 shows the SOC vs. OCV characteristics for the concerned LiPo

battery for both charging and discharging process. Finally, the average of both curves is considered

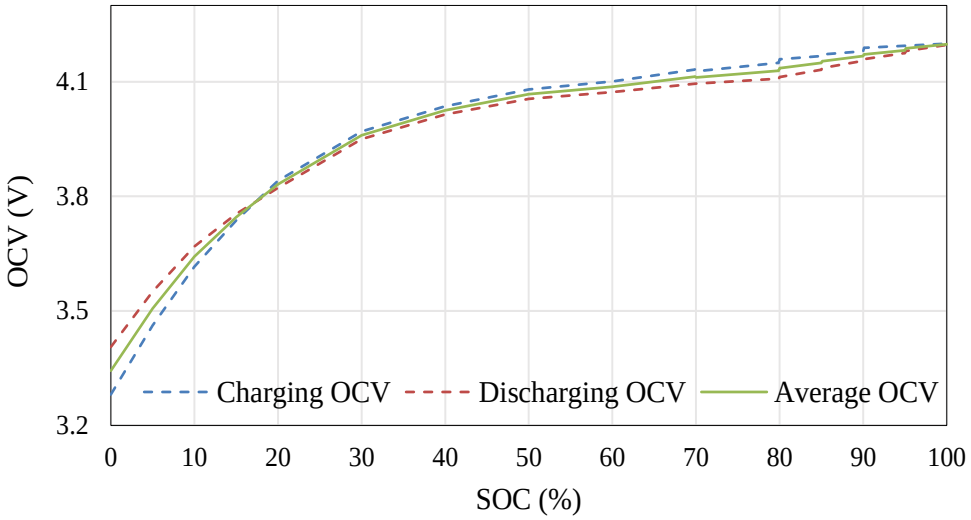

Figure 4.3: Variation of OCV with SOC of the LiPo battery.

as the true OCV. Since the OCV-SOC curve is almost linear for a small SOC range, the values of p and q in (4.3) for a few SOC range are approximated and shown in Table 4.1.

Table 4.1: Parameters for SOC-OCV relationship

SOC (%)	**0-5**	**5-10**	**10-15**	**15-20**	**20-25**	**25-30**	**30-35**
p	3.26	2.72	2.06	1.72	1.28	1.17	0.65
q	3.34	3.37	3.44	3.49	3.57	3.65	3.76
SOC (%)	**35-40**	**40-50**	**50-60**	**60-70**	**70-80**	**80-90**	**90-100**
p	0.61	0.42	0.19	0.24	0.28	0.32	0.31
q	3.79	3.85	3.97	3.94	3.92	3.88	3.89

4.5.3 Battery model parameter identification and design of proposed observer

To identify the battery model parameters, dynamic stress test is conducted by loading the current profile of a chassis dynamometer drive schedule (CDDS) [186], as shown in Figure 4.4, to the LiPo battery. CDDS is the driving schedule that provides a real-time profile of withdrawal/supply of current from/to the battery when the vehicle runs at city traffic conditions. The battery terminal voltage is recorded at every sampling instant and is shown in Figure 4.5 as 'Actual'. The present and the previous

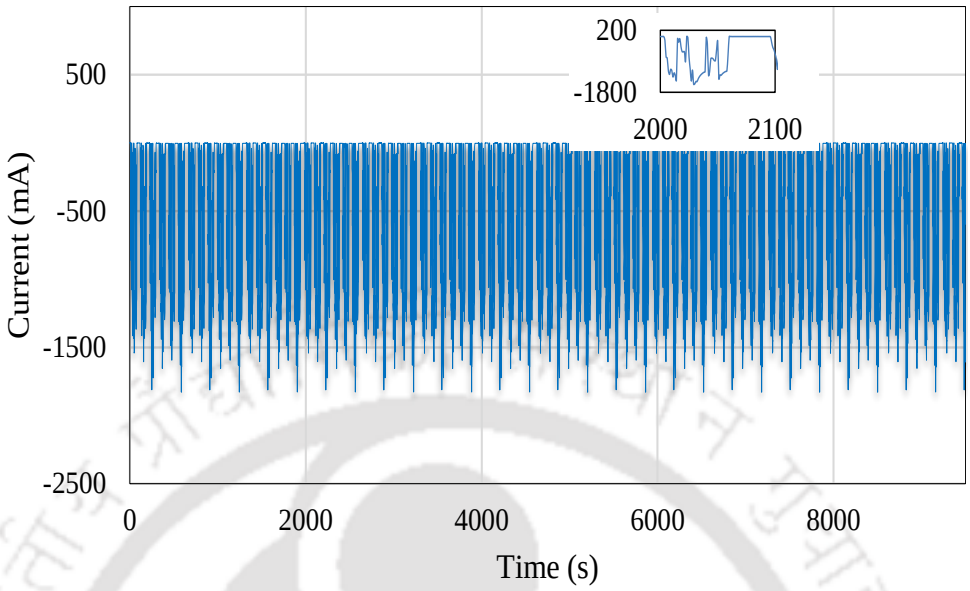

Figure 4.4: CDDS current profile.

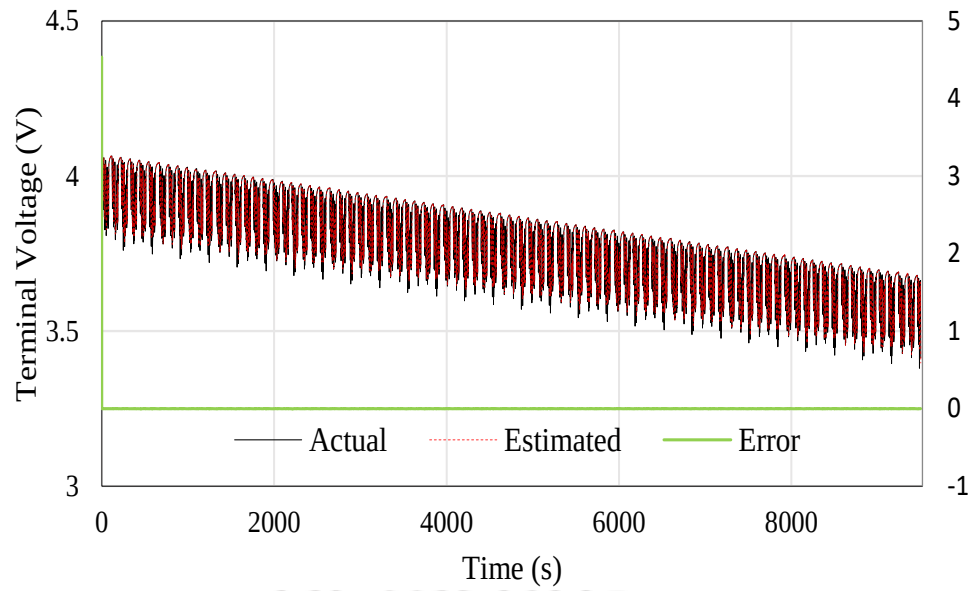

Figure 4.5: Terminal voltages and the error between them.

terminal voltage and current data are utilized to identify $\phi(k)$ at every sampling instant using (4.18), as explained in Section 4.3. The sampling time 1 s and forgetting factor 0.95 are used for this purpose. Then, the relationship, as given in (4.23), is used to obtain the unknown transfer function parameters a, b, c, and d, whose values are updated dynamically. These values are further utilized to obtain the time-variant battery model resistances and capacitances using (4.24). The identified results of R_t, R_i, C_n, and C_c are shown in Figure 4.6. It can be seen from Figure 4.6 that the parameters vary significantly with C-rate and SOC. BECM parameters are closely related to the terminal voltage and

current, which are fluctuating within specific ranges in response to the dynamics of the LiPo battery corresponding to the CDDS profile. The fluctuations reflect the complex characteristics of real-time variation of BECM parameters with the change of discharging and charging current. Hence, the online identification reduces the modelling error. Finally, the SLSTA based observer parameters are updated using (4.5) and (4.7).

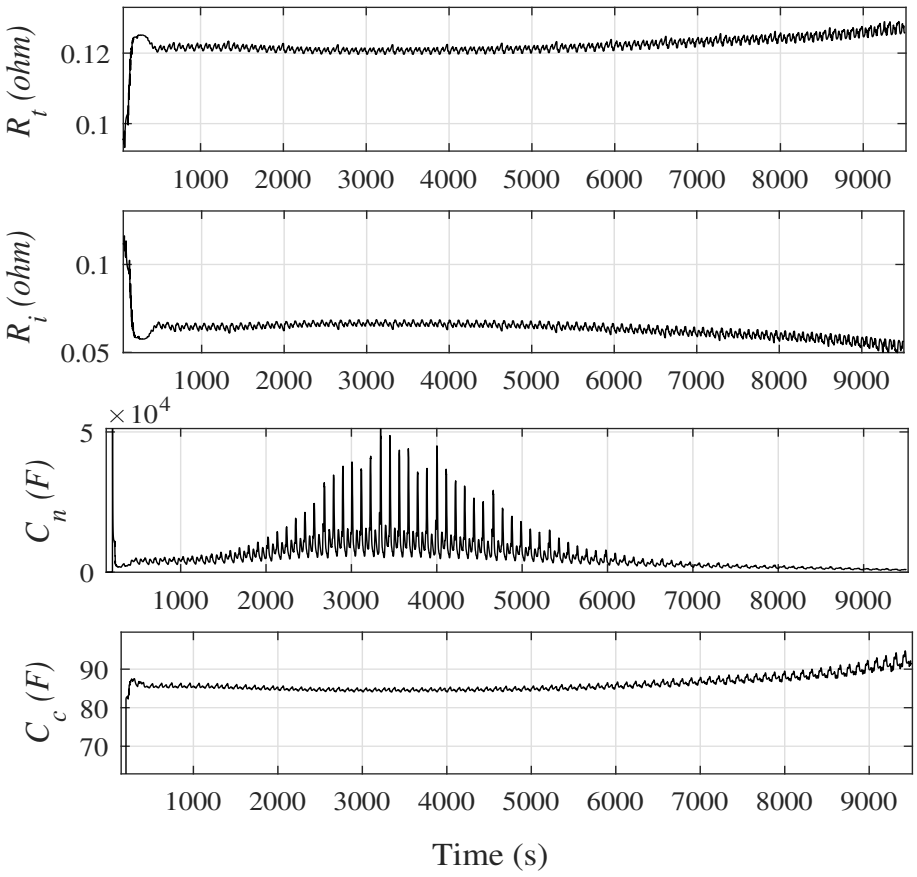

Figure 4.6: Variation of battery model parameters.

Keeping the inequality (4.32) in mind, we consider $k_1 = 7.83 \times 10^{-1}$, $k_2 = 12.83$, $\psi = 10.07 \times 10^{-1}$ and $\sigma = 3.6 \times 10^{-4}$. Using (4.30) and (4.31), the observer gains are obtained as $\beta = 4.68 \times 10^{-4}$ and $\gamma_1 = 5.6$. The same current profile loaded to the battery is injected as input to the observer to verify its efficacy. The actual and the estimated terminal voltage from the proposed observer are compared and is shown in Figure 4.5. It is observed from the figure that the maximum error (after convergence) between them is within 0.2 V, which ensures effective performance of the proposed method.

4.5.4 Estimated SOC from the proposed approach and its comparative study

In literature, the efficacy of AGSMO is verified extensively compared to SMO and other well-known approaches for battery SOC estimation [134, 135]. The effectiveness of PI observer to estimate SOC is also shown in [125]. Hence, in this chapter, to demonstrate the superiority in terms of accuracy, computational time, convergence time, and robustness, the proposed approach is compared with AGSMO and PI observer designed for SOC estimation. For each method, efforts have been made to tune the parameters such that the best results are obtained. The initial SOC condition with a 60% error is considered for each experiment. The battery tester BioLogic VMP3 has an inbuilt Ampere-hour counter from which the reference SOC is obtained.

The estimated SOC for various methods without adding any external noise are presented in Figure 4.7, and their corresponding % errors are shown in Figure 4.8. The uncertainties in this case are

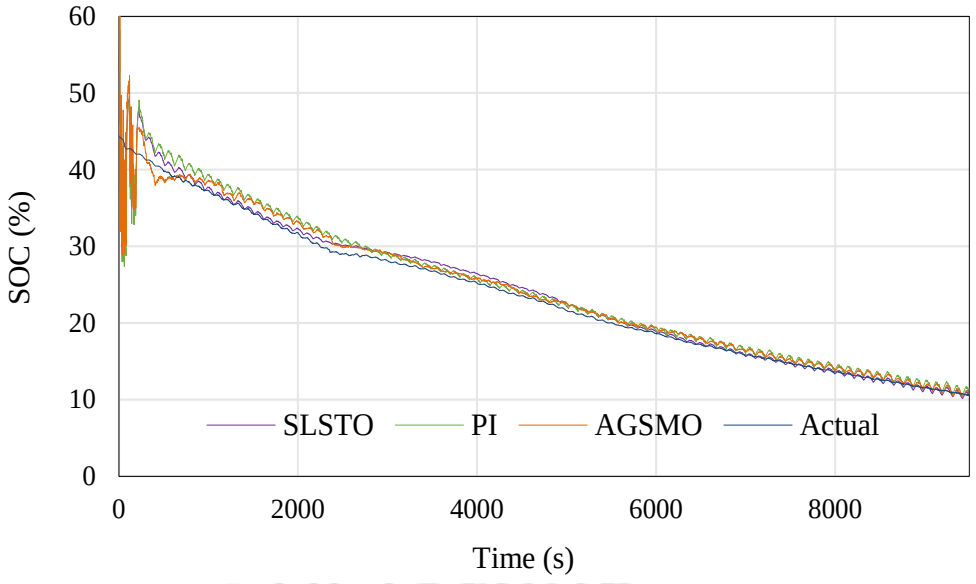

Figure 4.7: Comparison of actual and estimated SOC without added noise.

due to the internal system noise and modelling errors. Since the battery testing equipment used in laboratory is very accurate, the measurement noise in current and voltage are negligible. It is inferred from Figure 4.8 that the chattering is reduced in SLSTO compared to AGSMO. Between 5000-5100 s, the chattering width for SLSTO and AGSMO are 0.19% and 0.33%, respectively. The MAE and RMSE for each method are given in Table 4.2, which establishes the supremacy of the proposed method over others. The MAE also demonstrates the region of convergence (ROC) of the SOC estimation error. From the table, it is seen that AGSMO converges to its ROC faster than SLSTO. However,

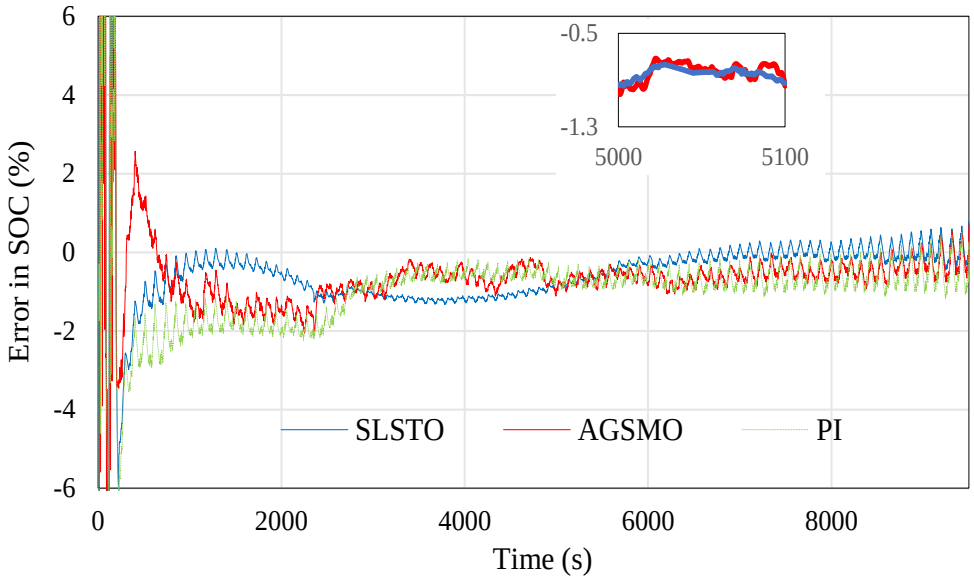

Figure 4.8: Error between actual and estimated SOC.

Table 4.2: Comparison of SOC estimation without added noise

Method	MAE (%)	RMSE (%)	Computational time (s)	Convergence time (s)
SLSTO (Proposed)	1.38	0.70	2.52	589
AGSMO	2.05	0.88	24.45	429
PI	2.58	1.06	2.01	713

the ROC is much greater for AGSMO. The computational time is also found for each method. The computational time of SLSTO is higher than the PI observer, but the difference between them is very small. Since the proposed approach performs better than PI observer in all the other aspects, this difference can be ignored. In the following subsections, the effectiveness of the proposed approach under various working conditions are discussed.

4.5.5 Effect of current and voltage measurement noise

To verify the robustness of the proposed method against the external disturbances such as current and voltage measurement noise, a high amount of white noise with standard deviation of 0.08 and 0.04 are added to the current and voltage channels, respectively. Under such condition, the SOC is estimated for each method, as shown in Figure 4.9. Figure 4.10 shows the errors in SOC estimation

for each method. The chattering width for SLSTO and AGSMO for 5000-5100 s are found to be 0.62% and 1.05%, respectively. It shows that the chattering in SLSTO is significantly lower than

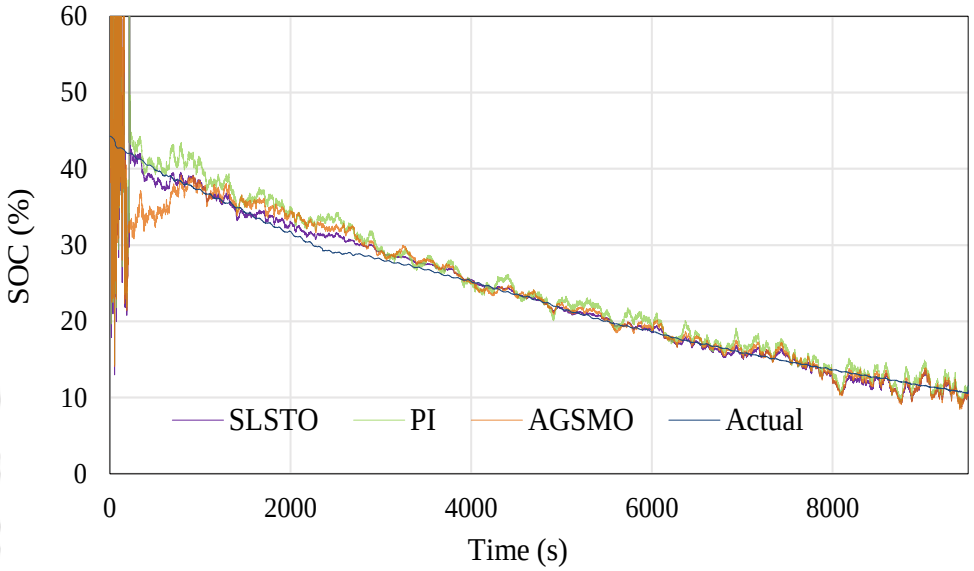

Figure 4.9: Comparison of actual and estimated SOC with added noise.

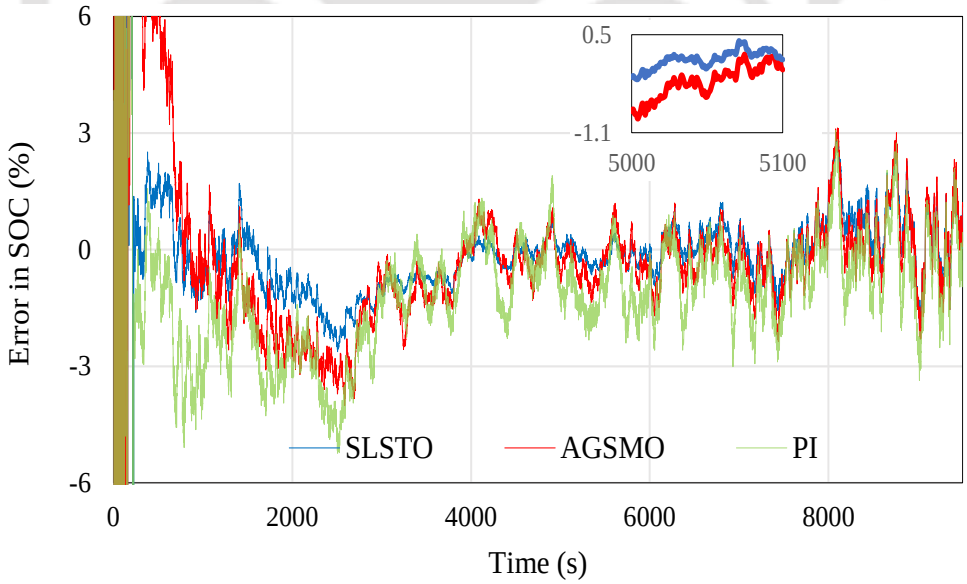

Figure 4.10: Error between actual and estimated SOC.

AGSMO. The MAE/ROC, RMSE, computational time, and convergence time for each method are shown in Table 4.3. It is observed from the table that SLSTO has better accuracy than AGSMO and PI observer even under noisy conditions which establishes the superiority of the proposed approach.

Table 4.3: Comparison of SOC estimation with added noise

Method	MAE (%)	RMSE (%)	Computational time (s)	Convergence time (s)
SLSTO (Proposed)	2.97	0.93	2.57	622
AGSMO	4.01	1.30	25.8	662
PI	5.24	1.77	2.06	790

4.5.6 Robustness study against identification error for the proposed observer

The proposed approach is also robust against the modelling errors. To verify it, 10% error is added to all the resistances and capacitances of the battery model. To show the effect of ageing, we increase the resistances and reduce the capacitances by 10%. Figure 4.11 an 4.12 show the estimated SOC from each method and their corresponding errors. It is seen from Figure 4.12 that the SOC estimated

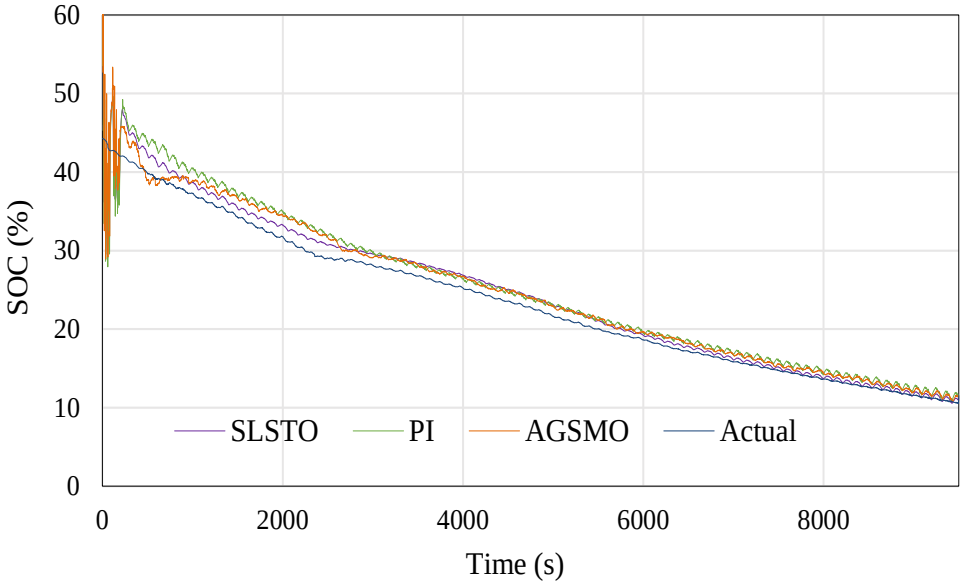

Figure 4.11: Comparison of actual and estimated SOC with added model identification error.

by the proposed approach is more accurate than others, even after adding the model identification errors. For SLSTO, AGSMO and PI, the MAEs are 2.23%, 3.58% and 3.87%, and the RMSEs are 1.15%, 1.47% and 1.81%, respectively. The important conclusion from these experiments is that even if the BECM identification approach fails to provide a very good parameter estimation sometimes due to ageing and other external factors, the proposed observer can still provide good SOC estimation accuracy.

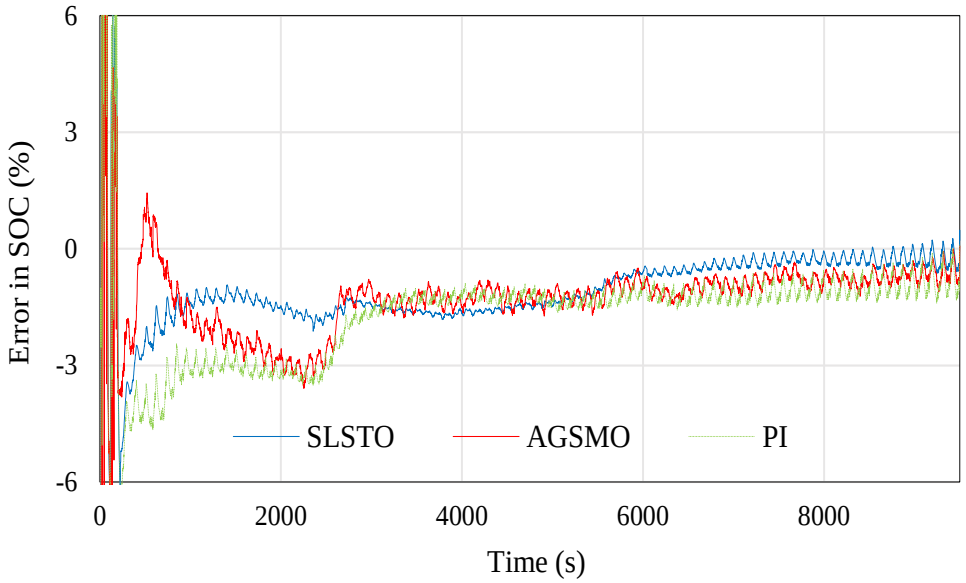

Figure 4.12: Error between actual and estimated SOC.

4.5.7 Study of combined effect of measurement noise and identification error

Another situation is analysed where both identification errors and noises are considered together. The estimated SOC for each method are shown in Figure 4.13 and their corresponding errors are demonstrated in Figure 4.14. The MAEs for SLSTO, AGSMO and PI are obtained as 3.14%, 5.01%,

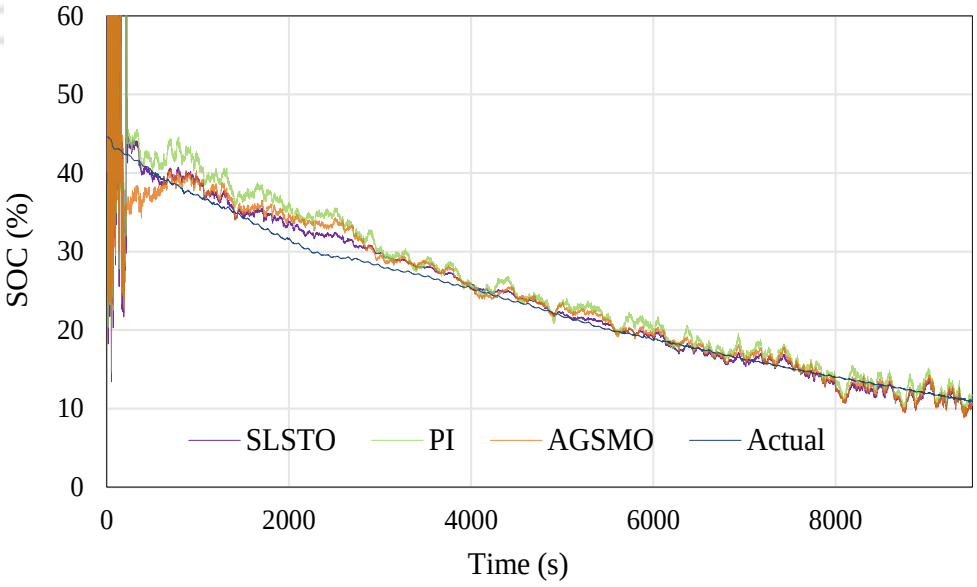

Figure 4.13: Comparison of actual and estimated SOC with added noise and identification errors together.

6.24%, and the RMSEs are 1.21%, 1.60% and 2.36%, respectively. Hence, in the presence of modelling uncertainties and various noises, the proposed approach outperforms the existing approaches in terms

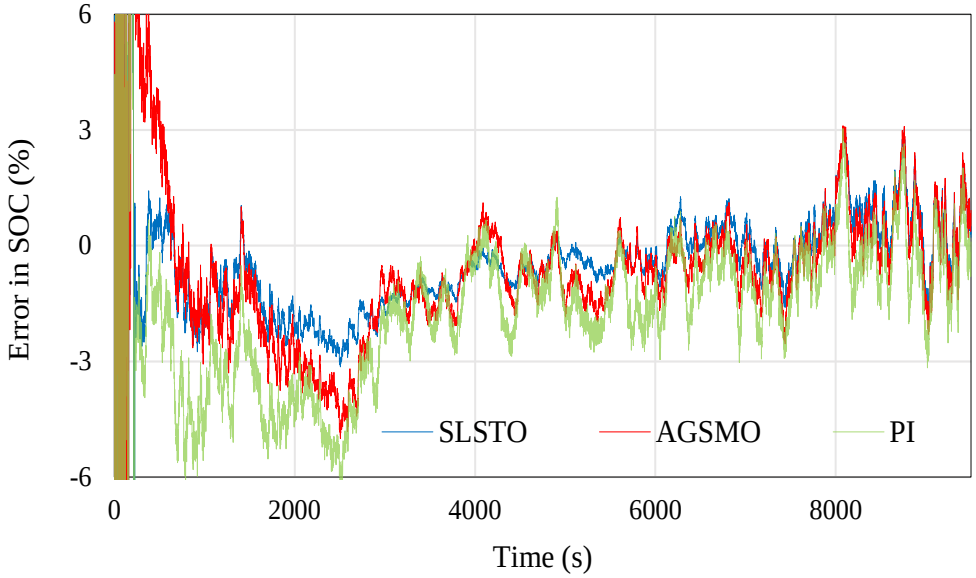

Figure 4.14: Error between actual and estimated SOC.

of accuracy, robustness against noise, and sensitivity to the identification errors.

It can be inferred from the above results that the proposed method estimates SOC efficiently for unknown initial conditions due to the robust convergence of the observer. Due to continuous control injection, the chattering is significantly improved compared to AGSMO. The convergence time of the proposed observer is higher than that of AGSMO but lower than the PI observer. The computational time is slightly greater than PI observer but much lower than AGSMO. Hence, the proposed observer provides a balance between convergence time and computational time. The experimental results indicate that the accuracy and robustness of the proposed observer are higher than the other methods under both normal and noisy conditions, due to various advantages offered by SLSTO. The effect of model identification error is analysed, and it is found that the proposed method performs better than the other methods in case of an inaccurate battery model. Moreover, in the presence of both identification errors and noises together, the proposed approach also outperforms the existing approaches in terms of accuracy and robustness. The above discussed parameters are vital in designing a high quality SOC observer.

4.6 Summary

In this chapter, a new robust SOC estimation algorithm based on SLSTO is proposed. Besides enjoying the various advantages associated with CSTO, the proposed SOC observer guarantees the

robustness for a more comprehensive class of uncertainties than CSTO. Lyapunov stability theory has been used to prove the robust finite-time stability of the SOC observer. The derivation of state equations also incorporates the relationship between SOC and OCV in it. Instead of OCV, directly SOC is considered as a state of the system. In order to design the observer, the required battery model parameters are identified using recursive least square with forgetting approach. To verify the efficacy of the proposed method, the experiments are performed on a LiPo battery with a real-time driving cycle (CDDS) current profile. The proposed method is compared with AGSMO and PI observer for SOC estimation in various work environments. The reduction of the chattering for SLSTO compared to the AGSMO is also demonstrated. The robustness against measurement noise, computational time, and the convergence speed are also compared which establishes the overall effectiveness of the proposed method. The proposed approach also efficiently deals with identification errors enabling it to provide satisfactory results under the impact of external factors such as ageing, which may influence the identification parameters.

Despite the several advantages, the proposed observer in this chapter requires the information of the upper bounds of uncertainties. In a complex physical system such as battery, it is not always possible to have exact knowledge of these bounds which may cause overestimation of the observer gains. Next chapter focuses on overcoming this limitation and proposes a further improved adaptive SOC estimation approach.

Note: The work in this chapter has been published with title "Strict Lyapunov super twisting observer design for state of charge prediction of lithium-ion batteries" in IET Renewable Power Generation, 2021.

5

Development of SOC Observer Based on Adaptive Lyapunov Super Twisting Algorithm

5.1 Introduction

In previous chapters, two new SOC estimation algorithms based on CSTO and SLSTO have been proposed. Compared to the existing sliding mode based SOC observers, the CSTO has several advantages which are detailed in Chapter 3. However, the CSTO is proven to be robust only for a very limited class of uncertainties. The SLSTO overcomes this problem and provides a good estimation accuracy and robustness under a much wider class of uncertainties than that of CSTO. Nevertheless, both the methods demand the knowledge of upper bounds of the uncertainties to design the observer gains. In a complex physical system such as battery, it is not always possible to have exact knowledge of these bounds. In absence of the knowledge of these bounds, it is required to guess them with the experience of the system for designing the observer gains. In such cases, overestimation or underestimation of these bounds can take place. Underestimation may cause the loss of stability and divergence of the observer states. Hence in most cases, these bounds are overestimated. Overestimation of the bounds results in larger gains than necessary (overestimation of observer gains), which eventually increases the chattering and severely affects the accuracy of the observer. Hence, we need an algorithm that not only preserves the various advantages associated with conventional STA, but also can ensure robust estimation for a comprehensive class of uncertainties without demanding the information of the upper bounds of the uncertainties for its implementation.

In this chapter, we propose a new approach for SOC estimation based on ALSTO. The proposed SOC observer is an improved version of conventional STO and preserves the various advantages associated with it. It can also deal with a more comprehensive class of uncertainties compared to CSTO. The main advantage of the proposed method is that unlike the CSTO and SLSTO, it does not demand any information on boundaries of the uncertainties and their derivatives except for their existence. The ALSTO adaptively minimizes the associated gains in such a way that the sliding is maintained and no overestimation of the observer gains take place [187, 188]. This further helps to reduce the chattering significantly. Lyapunov stability theory is used to prove the robust finite-time convergence of the proposed SOC observer. In order to design the observer, we use the same set of battery model parameters obtained using RLSF approach in Chapter 4. The proposed technique is implemented on the battery setup used in Chapter 4 and the obtained results demonstrate that the proposed approach performs better than SLSTO based approach and various other well-established approaches.

5.2 Battery modelling and its parameter identification

The battery model, derivation of its state equations, and model parameter identification technique described in Chapter 4 are utilized for developing SOC estimation algorithm in this chapter. For convenience of the readers, the state equations and identification steps which will be used further in this chapter are summarized here. The state and the output equations of the battery model given in (4.8)-(4.10) are rewritten here as follows:

$$\dot{x}_1(t) = -a_1 x_1(t) + a_2 x_2(t) + q_1 u_1(t) + q_2 u_2(t) + a_1 q + \zeta_1 \tag{5.1}$$

$$\dot{x}_2(t) = b_2 x_1(t) - b_1 x_2(t) - b_2 q + q_3 u_1(t) + \zeta_2 \tag{5.2}$$

$$y(t) = x_1(t) + \Delta f_4 \tag{5.3}$$

where $x_1(t) = V(t)$ and $x_2(t) = Z(t)$ are the states, $y(t) = V(t)$ is the output, $u_1(t) = i(t)$ and $u_2(t) = \dot{i}(t)$ are the inputs of the battery model system. $Z(t)$ is SOC of the battery at time t, $\zeta_1(x,t,u)$, $\zeta_2(x,t,u)$, and Δf_4 are the uncertainties due to measurement noise, modelling inaccuracy, and external disturbances. The coefficients of the state equations $(a_1, a_2, b_1, b_2, q_1, q_2, q_3)$ are related to the battery model resistances (R_i, R_t, R_c), capacitances (C_n, C_c), and the coefficients relating the OCV and SOC (p, q). The relationships are given as follows:

$$a_1 = \frac{C_n - C_c}{2R_i C_n C_c}, \quad a_2 = a_1 p, \quad b_1 = \frac{1}{R_i C_n}, \quad b_2 = \frac{b_1}{p}$$

$$q_1 = \frac{C_n R_i + C_n R_t - C_c R_t}{2R_i C_n C_c}, \quad q_2 = R_t + \frac{R_i}{2}, \quad q_3 = \frac{q_4}{p}, \quad q_4 = -\frac{R_t}{R_i C_n} \tag{5.4}$$

It is worth noting that $a_1, a_2, b_1, b_2, q_1, q_2$ are positive and q_3, q_4 are negative. The governing equations of RLSF approach, given in Section 4.3, used for identification of BECM parameters are as follows:

$$\hat{\phi}(k) = \hat{\phi}(k-1) + H(k)[y(k) - \theta^T(k)\hat{\phi}(k-1)]$$

$$H(k) = \frac{G(k-1)\theta(k)}{\lambda + \theta^T(k)G(k-1)\theta(k)}$$

$$G(k) = \frac{1}{\lambda}[G(k-1) - H(k)\theta^T(k)G(k-1)] \tag{5.5}$$

where

$$\theta(k) = \begin{bmatrix} y(k-1) & y(k-2) & u_1(k) & u_1(k-1) & u_1(k-2) \end{bmatrix}^T$$

is the regressor vector, and

$$\hat{\phi}(k) = \begin{bmatrix} -\hat{c}_1 & -\hat{c}_2 & \hat{d}_0 & \hat{d}_1 & \hat{d}_2 \end{bmatrix}^T$$

is the vector containing estimated parameters related to battery model parameters, λ is the forgetting factor which generally lies in the range of $[0.9, 1]$, $H(k)$ is the gain which determines the effect of the current prediction error on the update of the parameter estimate, $G(k)$ is the covariance matrix of the estimated parameters, and '$\hat{*}$' denotes the estimated value of '$*$'. The sampling time used for discretization is denoted by T_s. The estimated resistances and capacitances in the battery model are derived using the following equations:

$$\begin{aligned} \hat{R}_t &= 2\hat{b} - \frac{\hat{c}}{\hat{a}}, \quad \hat{R}_i = \hat{R}_c = 2\left(\frac{\hat{c}}{\hat{a}} - \hat{b}\right) \\ \hat{C}_n &= \frac{1}{2}\left[\frac{\hat{a}}{\hat{d}} + \left(\frac{\hat{a}^2}{\hat{d}^2} - \frac{\hat{a}}{(\hat{c} - \hat{a}\hat{b})\hat{d}}\right)^{1/2}\right] \\ \hat{C}_c &= \frac{1}{2}\left[\frac{\hat{a}}{\hat{d}} - \left(\frac{\hat{a}^2}{\hat{d}^2} - \frac{\hat{a}}{(\hat{c} - \hat{a}\hat{b})\hat{d}}\right)^{1/2}\right] \end{aligned} \tag{5.6}$$

with

$$\begin{aligned} \hat{a} &= \frac{2(1-\hat{c}_2)}{T_s(1+\hat{c}_2)}, \quad \hat{b} = \frac{\hat{d}_0 + \hat{d}_2 - \hat{d}_1}{2(1+\hat{c}_2)} \\ \hat{c} &= \frac{2(\hat{d}_0 - \hat{d}_2)}{T_s(1+\hat{c}_2)}, \quad \hat{d} = \frac{2(\hat{d}_0 + \hat{d}_1 + \hat{d}_2)}{T_s^2(1+\hat{c}_2)} \end{aligned} \tag{5.7}$$

5.3 Design of proposed adaptive observer

In this section, the design procedure of adaptive Lyapunov super twisting algorithm (ALSTA) based observer is explained for estimating states of the uncertain system given in (5.1)-(5.3). The proposed SOC observer is an improved version of conventional STO and preserves the various advantages associated with it. It deals with a more comprehensive class of uncertainties compared to CSTO.

Unlike CSTO and SLSTO, the proposed observer does not demand any information on boundaries of the various uncertainties except for their existence [164, 187]. It avoids underestimation and overestimation of the observer gains and thus reduces chattering while ensuring convergence. In ALSTO, the control gains are increased dynamically until the sliding mode is established. Subsequently, reduction of gains starts taking place and is reversed once there is any drift of the sliding variable or its gradient from the equilibrium point. Based on the assumption on derivative of terminal current considered in Chapter 4, the proposed observer is designed to estimate the battery states as follows:

$$\dot{\hat{x}}_1(t) = -\hat{a}_1 y(t) + \hat{a}_2 \hat{x}_2(t) + \hat{q}_1 u_1(t) + \hat{a}_1 q + k_1(t)|x_1 - \hat{x}_1|^{1/2} sign(x_1 - \hat{x}_1) \tag{5.8}$$

$$\dot{\hat{x}}_2(t) = \hat{b}_2 y(t) - \hat{b}_1 \hat{x}_2(t) - \hat{b}_2 q + \hat{q}_3 u_1(t) + k_2(t) sign(x_1 - \hat{x}_1) \tag{5.9}$$

where '$\hat{*}$' denotes the estimated values of '$*$'. The error dynamics using (5.1)-(5.3) and (5.8)-(5.9) are obtained as follows:

$$\begin{aligned} \dot{\tilde{x}}_1 &= \hat{a}_2 \tilde{x}_2 - k_1(t)|\tilde{x}_1|^{1/2} sign(\tilde{x}_1) + F_1(x, \hat{x}, t, u) \\ \dot{\tilde{x}}_2 &= -k_2(t) sign(\tilde{x}_1) + F_2(x, \hat{x}, t, u) \end{aligned} \tag{5.10}$$

where

$$F_1(x, t, u) = a_1 \Delta f_4 - \Delta a_1 y + \Delta a_2 x_2 + \Delta q_1 u_1 + \Delta a_1 q + \zeta_1(x, t, u)$$

$$F_2(x, t, u) = -b_2 \Delta f_4 + \Delta b_2 y - b_1 x_2 + b_1 \hat{x}_2 - \Delta b_1 \hat{x}_2 - \Delta b_2 q - \Delta q_3 u_1 + \zeta_2(x, t, u) \tag{5.11}$$

$\tilde{x}_1 = x_1 - \hat{x}_1$, $\tilde{x}_2 = x_2 - \hat{x}_2$, $\Delta a_1 = a_1 - \hat{a}_1$, $\Delta b_1 = b_1 - \hat{b}_1$, $\Delta q_1 = q_1 - \hat{q}_1$, and $\Delta q_3 = q_3 - \hat{q}_3$.

Considering the continuous control injection of the observer and boundedness of $V, \dot{V}, i, Z, \zeta_1, \zeta_2$, and Δf_4, it can also be considered that the following inequalities are satisfied [168]:

$$\begin{aligned} |\ F_1(x, \hat{x}, t, u)\ | &\leq \delta_1 |\tilde{x}_1|^{1/2} \\ |\ F_2(x, \hat{x}, t, u)\ | &\leq \delta_2 \end{aligned} \tag{5.12}$$

where $\delta 1$ and δ_2 are positive constants [188].

Suppose the perturbations to the system (5.10) are bounded by (5.12). Then, there exists a finite time such that convergence of (5.10) is guaranteed for any initial condition of the states if the dynamics of $k_1(t)$ and $k_2(t)$ are chosen as follows:

$$\dot{k}_1(t) = \begin{cases} \mu_1\sqrt{\frac{\beta_1}{2}}sign(|\tilde{x}_1|-\sigma), & \text{if } k_1 > k_0 \\ \alpha, & \text{otherwise} \end{cases}$$

$$k_2(t) = \frac{1}{2}\left(\frac{\omega k_1}{\hat{a}_2}\right) \tag{5.13}$$

where $|\tilde{x}_1(0)|> \sigma$ and k_0 is a small positive constant with $|k_1(0)|> k_0$. ω, β_1, α, and μ_1 are arbitrary positive constants.

Proof: Suppose $e_1 = \tilde{x}_1$ and $e_2 = \hat{a}_2\tilde{x}_2$, (5.10) can be rewritten as:

$$\dot{e}_1 = e_2 - k_1(t)|e_1|^{1/2}sign(e_1) + F_1(x,\hat{x},t,u)$$

$$\dot{e}_2 = -k_t sign(e_1) + F_t(x,\hat{x},t,u) \tag{5.14}$$

where $k_t(t) = \hat{a}_2 k_2(t)$ and $F_t(x,\hat{x},t,u) = \hat{a}_2 F_2(x,\hat{x},t,u)$.

Since $\hat{a}_2$ is positive and bounded, we have

$$|F_t(x,\hat{x},t,u)| \leq \delta_t \tag{5.15}$$

Consider

$$S = [s_1 \;\; s_2]^T = [|e_1|^{1/2}sign(e_1) \;\; e_2]^T \tag{5.16}$$

where $|S| = \sqrt{|e_1|+e_2^2}$ and $|s_1| = |e_1|^{1/2}$

In view of (5.16), (5.14) can be represented in state matrix form as:

$$\begin{bmatrix} \dot{s}_1 \\ \dot{s}_2 \end{bmatrix} = \frac{1}{2|s_1|}\begin{bmatrix} -k_1(t) & 1 \\ -2k_t(t) & 0 \end{bmatrix}\begin{bmatrix} s_1 \\ s_2 \end{bmatrix} + \frac{1}{2|s_1|}\begin{bmatrix} 1 & 0 \\ 0 & 2|s_1| \end{bmatrix}\begin{bmatrix} F_1 \\ F_t \end{bmatrix} \tag{5.17}$$

Considering (5.12) and (5.15), it can be said that there always exists $0 < \delta_3(x, \hat{x}, t) \leq \delta_1$ and $0 < \delta_4(x, \hat{x}, \hat{a}_2, t) \leq \delta_t$ such that

$$F_1 = \delta_3 |e_1|^{1/2} sign(e_1) = \delta_3 s_1$$

$$F_t = \delta_4 sign(e_1) = \delta_4 \frac{s_1}{|s_1|} \tag{5.18}$$

Using (5.18), (5.17) can be rewritten as:

$$\begin{bmatrix} \dot{s}_1 \\ \dot{s}_2 \end{bmatrix} = \frac{1}{2|s_1|} \begin{bmatrix} -(k_1(t) - \delta_3) & 1 \\ -2(k_t(t) - \delta_4) & 0 \end{bmatrix} \begin{bmatrix} s_1 \\ s_2 \end{bmatrix} = \bar{A}(s_1) \begin{bmatrix} s_1 \\ s_2 \end{bmatrix} \tag{5.19}$$

It can be observed from (5.16) that the finite-time convergences of s_1 and s_2 ensures finite-time convergences of e_1 and e_2, and hence $\tilde{x}_1$ and $\tilde{x}_2$. To analyse the stability of (5.19), consider the Lyapunov function candidate as:

$$\Lambda(S, k_1, k_t) = \Lambda_0(S) + \frac{1}{2\beta_1} k_3^2 + \frac{1}{2\beta_2} k_4^2 \tag{5.20}$$

where

$$k_3 = k_1 - k_1^*, \quad k_4 = k_t - k_t^*,$$

$$\Lambda_0(S) = S^T P S,$$

$$P = \begin{bmatrix} \lambda + \omega^2 & -\omega \\ -\omega & 1 \end{bmatrix},$$

λ, k_1^* and k_t^* are some positive constants [187]. Differentiating (5.20) with respect to time in both sides, we get

$$\dot{\Lambda}(S, k_1, k_t) = S^T [\bar{A}^T P + P\bar{A}] S + \frac{1}{\beta_1} k_3 \dot{k}_1 + \frac{1}{\beta_2} k_4 \dot{k}_t \tag{5.21}$$

Using (5.19) and (5.20), the first term in right hand side (RHS) of (5.21) is computed and is as follows:

$$\dot{\Lambda}_0(S) = S^T [\bar{A}^T P + P\bar{A}] S \leq -\frac{1}{2|s_1|} S^T Q S \tag{5.22}$$

where Q is a symmetric positive definite matrix given as:

$$Q = \begin{bmatrix} q_{11} & q_{12} \\ q_{21} & 2\omega \end{bmatrix}$$

with

$$q_{11} = 2\lambda k_1 + 2\omega(\omega k_1 - 2k_t) - 2(\lambda + \omega^2)\delta_3 + 4\omega\delta_4$$

$$q_{21} = q_{12} = (2k_t - \omega k_1 - \lambda - \omega^2) + \omega\delta_3 - 2\delta_4 \tag{5.23}$$

It is seen that the following relationships ensure positive definiteness of Q with minimum eigenvalue value ω:

$$k_t = \frac{1}{2}\omega k_1 \tag{5.24}$$

and

$$k_1 > \frac{6\delta_1\omega(\lambda + \omega^2) - 3\omega^2(4\delta_t + 1) + (\omega\delta_1 - 2\delta_t - \lambda - \omega^2)^2}{6\omega\lambda} \tag{5.25}$$

In view of $\lambda_{min}(Q) \geq \omega$ and the well-known inequality

$$\lambda_{min}(P)||S||^2 \leq S^T P S \leq \lambda_{max}(P)||S||^2 \tag{5.26}$$

we can write

$$\dot{\Lambda}_0(S) \leq -\frac{1}{2|s_1|} S^T Q S \leq -\frac{\omega}{2|s_1|}||S||^2 \tag{5.27}$$

Using (5.16), (5.20) and (5.26), we have

$$|s_1| = |e_1|^{1/2} \leq ||S|| \leq \frac{\Lambda_0^{1/2}(S)}{\lambda_{min}^{1/2}(P)} \tag{5.28}$$

Using (5.26)-(5.28), we can write

$$\dot{\Lambda}_0(S) \leq -n\Lambda_0^{1/2}(S) \tag{5.29}$$

where

$$n = \frac{\omega\lambda_{min}^{1/2}(P)}{2\lambda_{max}(P)}$$

Now, from (5.21) and (5.29), we have

$$\dot{\Lambda}(S,k_1,k_t) \leq -\frac{1}{2|s_1|}S^TQS + \frac{1}{\beta_1}k_3\dot{k}_1 + \frac{1}{\beta_2}k_4\dot{k}_t$$

$$\begin{aligned} &\leq -n\Lambda_0^{1/2}(S) - \frac{\mu_1}{\sqrt{2\beta_1}}|k_3| - \frac{\mu_2}{\sqrt{2\beta_2}}|k_4| + \frac{1}{\beta_1}k_3\dot{k}_1 \\ &\quad + \frac{1}{\beta_2}k_4\dot{k}_t + \frac{\mu_1}{\sqrt{2\beta_1}}|k_3| + \frac{\mu_2}{\sqrt{2\beta_2}}|k_4| \end{aligned} \tag{5.30}$$

Using the following well-known inequality

$$(v_1^2 + v_2^2 + v_3^2)^{1/2} \leq |v_1| + |v_2| + |v_3| \tag{5.31}$$

we can obtain from (5.20) as

$$-n\Lambda_0^{1/2}(S) - \frac{\mu_1}{\sqrt{2\beta_1}}|k_3| - \frac{\mu_2}{\sqrt{2\beta_2}}|k_4| \leq -m\Lambda^{1/2}(S) \tag{5.32}$$

where $m = min(n, \mu_1, \mu_2)$.

In view of (5.32), (5.30) can be rewritten as:

$$\begin{aligned} \dot{\Lambda}(S,k_1,k_t) &\leq -m\Lambda^{1/2}(S) + \frac{1}{\beta_1}k_3\dot{k}_1 + \frac{1}{\beta_2}k_4\dot{k}_t \\ &\quad + \frac{\mu_1}{\sqrt{2\beta_1}}|k_3| + \frac{\mu_2}{\sqrt{2\beta_2}}|k_4| \end{aligned} \tag{5.33}$$

Assuming $k_1(t)$ and $k_t(t)$ are bounded with bounds k_1^* and k_t^*, respectively (will be proven later in this section), we can rewrite (5.33) as:

$$\dot{\Lambda}(S) \leq -m\Lambda^{1/2}(S) + D \tag{5.34}$$

where

$$D = -|k_3|\left(\frac{1}{\beta_1}\dot{k}_1 - \frac{\mu_1}{\sqrt{2\beta_1}}\right) - |k_4|\left(\frac{1}{\beta_2}\dot{k}_t - \frac{\mu_2}{\sqrt{2\beta_2}}\right) \tag{5.35}$$

Now, when $|e_1| = |\tilde{x}_1| \geq \sigma$ and $k_1(t) > k_0$, $D = 0$ can be ensured if

$$\omega = \frac{2\mu_2}{\mu_1}\sqrt{\frac{\beta_2}{\beta_1}} \tag{5.36}$$

is chosen. Thus, finite-time convergence of s_1 and s_2 and hence e_1 and e_2 is guaranteed.

When $|e_1| \leq \sigma$, D may be positive or negative. The negative value of D ensures finite-time convergence. However, its positive value may lead to e_1 greater than σ due to the decrease in control gains. As soon as e_1 becomes greater than σ, the control gains start increasing, and finite-time convergence is achieved as explained earlier. Hence, (5.13) always ensures finite-time convergence of e_1 and e_2. It is also guaranteed that e_1 always stays in a domain $|e_1| \leq \gamma_1$, $\gamma_1 \geq \sigma$.

Now, we prove the boundedness of $k_1(t)$ and $k_t(t)$ assumed before. For $\sigma < e_1 \leq \gamma_1$, the solution to (5.13) can be obtained as:

$$k_1(t) = k_1(0) + \mu_1\sqrt{\frac{\beta_1}{2}}t, \quad 0 \leq t \leq T_f \tag{5.37}$$

where T_f is the convergence time. For $e_1 \leq \sigma$, $k_1(t)$ can be increasing only till its value reaches k_0, otherwise it is always decreasing. Hence, in view of (5.13), $k_1(t)$ and $k_t(t)$ are always bounded. Due to the boundedness of the RHS of (5.25) and the fact that $k_1(t)$ increases linearly with respect to time, the inequality in (5.25) is established in finite-time. Hence, as soon as the k_1 starts satisfying (5.25), the finite-time convergence of the states is achieved.

5.4 Results and discussion

In order to verify the efficacy of the proposed approach, we conduct the necessary experiments by using the test setup described in Section 4.5. In that section, the SOC-OCV relationship has also been established for the test battery. In the present section, the results of implementation of the proposed SOC estimation algorithm are illustrated and their outcomes are discussed thoroughly. A comparative study of the proposed approach with other existing approaches is performed in terms of various aspects such as accuracy, computational time, convergence speed, and chattering width. The effect of sensor noises on estimation accuracy and the robustness of the proposed observer against the modelling errors are also investigated.

5.4.1 BECM parameter identification and proposed observer design

The battery model parameters are identified in the same way as discussed in Chapter 4. For this purpose, we load the current profile of CDDS, presented in Figure 4.4 of Chapter 4, to the LiPo battery. The battery terminal voltage is recorded at every sampling instant and is shown in Figure 5.1 as 'Actual'. The present and the previous terminal voltage and current data are utilized to identify the real-time $\phi(k)$ using (5.5). The forgetting factor of 0.95 is used for this purpose. The relationships,

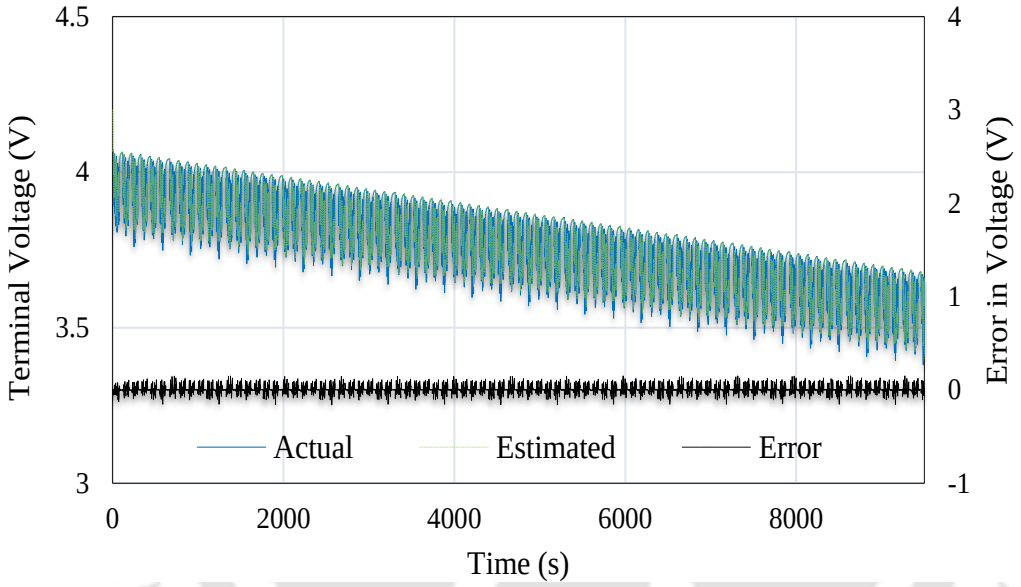

Figure 5.1: Comparison of estimated and measured terminal voltage.

as given in (5.6), are used to obtain the time-variant battery model resistances and capacitances. The variation of real-time identified parameters of BECM can be seen in Figure 5.2.

To design the observer, the battery state-space model parameters a_1, b_1, q_1 and q_4 are estimated and constantly updated for each sampling instant using (5.4). The same current profile loaded to the battery is injected as input to the observer to verify its efficacy. In order to design the dynamics of adaptive gains of the proposed observer, we consider $\mu_1 = 0.05$, $\beta_1 = 0.2$, $\sigma = 0.02$, $\alpha = 0.2$, $\omega = 1 \times 10^{-7}$, and $k_0 = 0.05$. The corresponding terminal voltage profile is estimated and compared with the measured terminal voltage profile, as shown in Figure 5.1. It is observed from the figure that the MAE (after convergence) between them is within 0.15 V and RMSE is 0.03 V, which ensures efficacy of the proposed method.

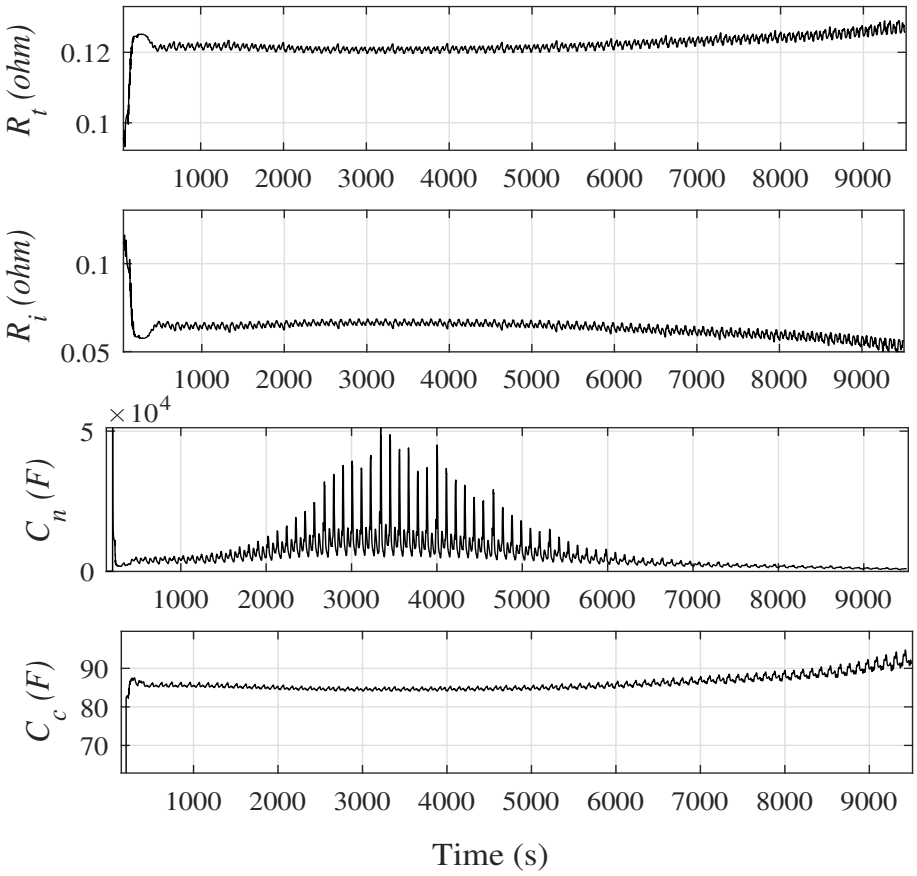

Figure 5.2: Variation of battery model parameters.

5.4.2 SOC estimation using proposed approach and its comparative study

In this chapter, to demonstrate the superiority of the proposed method, we compare it with some well-established SOC estimation approaches such as AGSMO [134], time-varying discrete sliding mode observer (TVDSMO) [189], and PI observer [125]. For each method, efforts have been made to tune the parameters such that the best results are obtained. The initial SOC condition with a 60% error is considered for each experiment. The reference SOC is obtained from the precise battery tester BioLogic VMP3 that has an inbuilt Ampere-hour counter. The estimated SOC for various methods are presented in Figure 5.3 and the corresponding % error in SOC estimation are shown in Figure 5.4. The MAE and RMSE for each method are given in Table 5.1, which establishes the improved accuracy of the proposed method over others. The results obtained in Chapter 4 in identical conditions are also included in this table for comparison. It is inferred from Figure 5.4 and 4.8 (Chapter 4) that the chattering is reduced in ALSTO as compared to SLSTO, AGSMO, and TVDSMO. Between 5000-5100 s, the chattering width for SLSTO, AGSMO, TVDSMO, and ALSTO are 0.19%, 0.33%, 1.27%, and

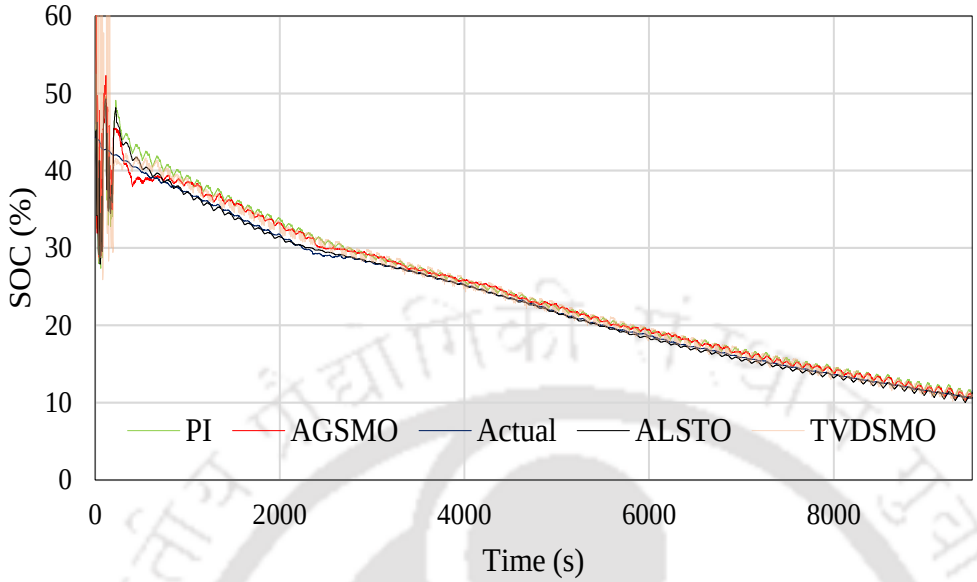

Figure 5.3: Comparative study of SOC estimation results.

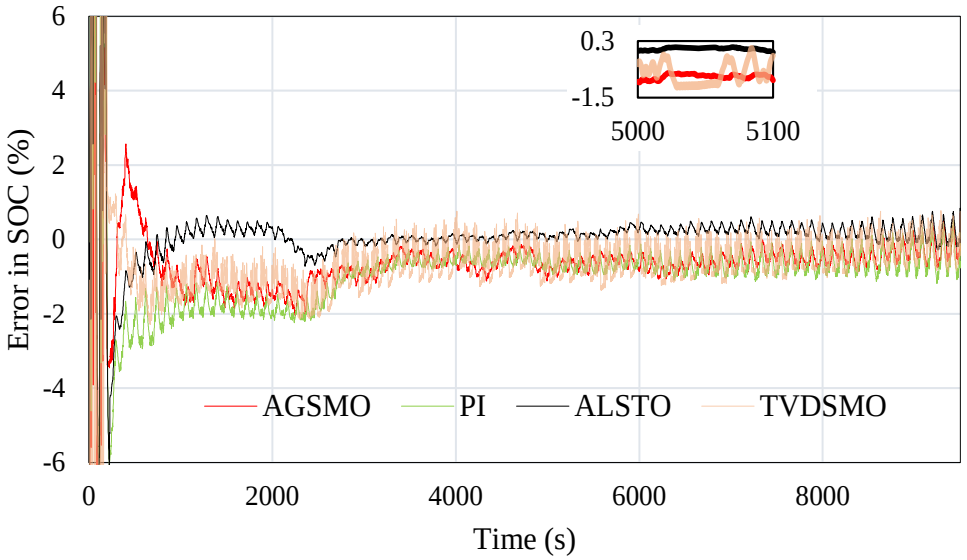

Figure 5.4: Error between actual and estimated SOC.

0.14%, respectively. At the start, the estimated SOC for the proposed observer has large error due to the erroneous initial conditions; but after 392 s, it becomes stable and converges to the true SOC profile. Table 5.1 shows that ALSTO converges faster than SLSTO, AGSMO and PI observer. The computational time to execute the algorithm for each method is also determined. It is seen from Table 5.1 that all the methods except AGSMO incur small computational time. In the following subsections, the effectiveness of the proposed approach under various working conditions are discussed.

Table 5.1: Comparative study of SOC estimation methods

Method	MAE (%)	RMSE (%)	Computational time (s)	Convergence time (s)
ALSTO (Proposed)	1.29	0.44	2.71	392
AGSMO	2.05	0.88	24.45	429
TVDSMO	2.29	0.91	2.23	374
PI	2.58	1.06	2.01	713
SLSTO (Chapter 4)	1.38	0.70	2.52	589

5.4.3 Effect of current and voltage measurement noise

Unlike the battery testing equipment used in laboratory which is very accurate, a significant amount of measurement noise in current and voltage sensors can exist in a real-time system. To verify the robustness of the proposed method against the external disturbances such as current and voltage measurement noise, high amount of white noise with standard deviation of 0.08 and 0.04 are added to the current and voltage channels, respectively. Under such condition, the estimated SOC for

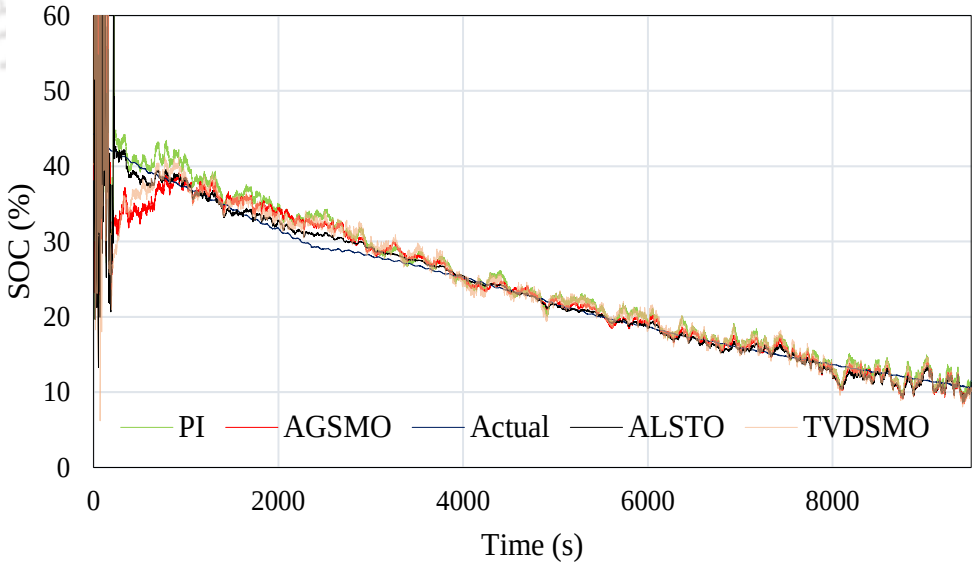

Figure 5.5: Comparative study of SOC estimation results with added noise.

each method and their corresponding errors are shown in Figure 5.5 and 5.6, respectively. The MAE, RMSE, computational time, and convergence time for each method are presented in Table 5.2. The results obtained using SLSTO in Chapter 4 under identical condition are also included in this table for

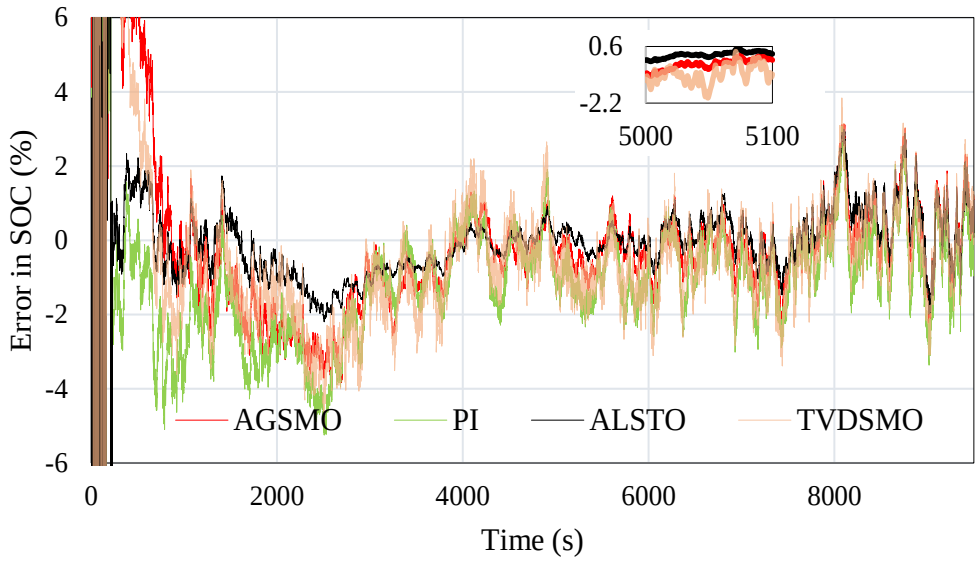

Figure 5.6: Error between actual and estimated SOC for added noise case.

Table 5.2: Comparison of SOC estimation with added noise

Method	MAE (%)	RMSE (%)	Computational time (s)	Convergence time (s)
ALSTO (Proposed)	2.98	0.83	2.75	505
AGSMO	4.01	1.30	25.8	662
TVDSMO	4.96	1.52	2.27	514
PI	5.24	1.77	2.06	790
SLSTO (Chapter 4)	2.97	0.93	2.57	622

comparison. Table 5.2 validates the robustness of the proposed observer under noisy conditions. From Figure 5.6 and 4.10 (Chapter 4), the chattering width for SLSTO, AGSMO, TVDSMO, and ALSTO for 5000-5100 s are found to be 0.62%, 1.05%, 2.24%, and 0.59%, respectively. It shows that even under noisy conditions, the chattering in ALSTO is significantly lower compared to other methods.

5.4.4 Robustness study against identification error for the proposed observer

In this subsection, we study the robustness of the proposed observer in handling the inaccurate identification of BECM parameters. For this purpose, 10% error is added to all the resistances and capacitances of the battery model. To show the effect of ageing, we increase the resistances and reduce the capacitances by 10%. Figure 5.7 and 5.8 show the SOC estimated from each method and their

corresponding errors. It is seen from Figure 5.8 that the SOC estimated by the proposed approach is more accurate than others, even after adding the model identification errors. For ALSTO, AGSMO, TVDSMO and PI, the MAEs are 2.17%, 3.58%, 3.74% and 3.87%, and the RMSEs are 0.59%, 1.47%, 1.61% and 1.81%, respectively. Under identical condition, the MAE and RMSE for SLSTO have been found in Chapter 4 as 2.23% and 1.15%, receptively. The important conclusion from these experiments

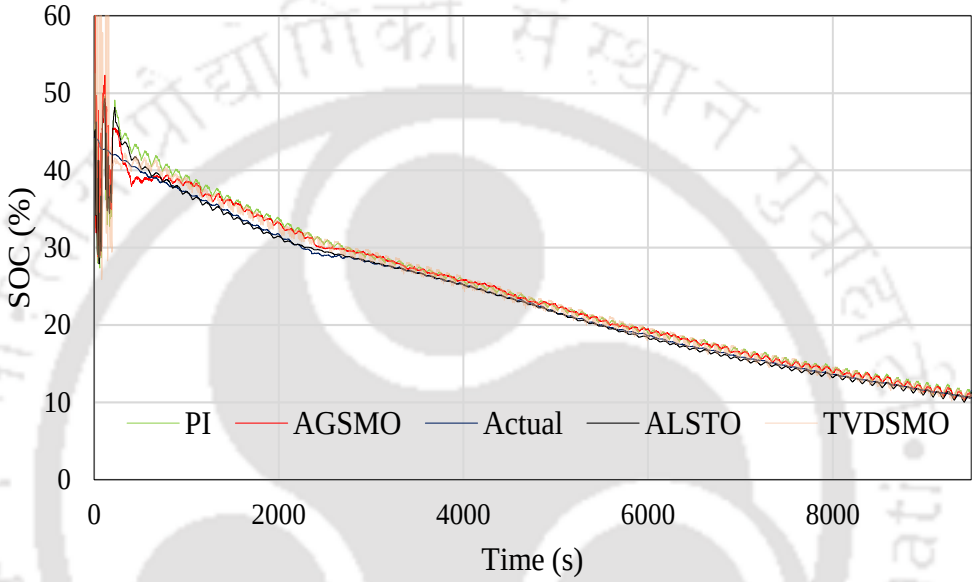

Figure 5.7: Estimated SOC from proposed approach with added identification error.

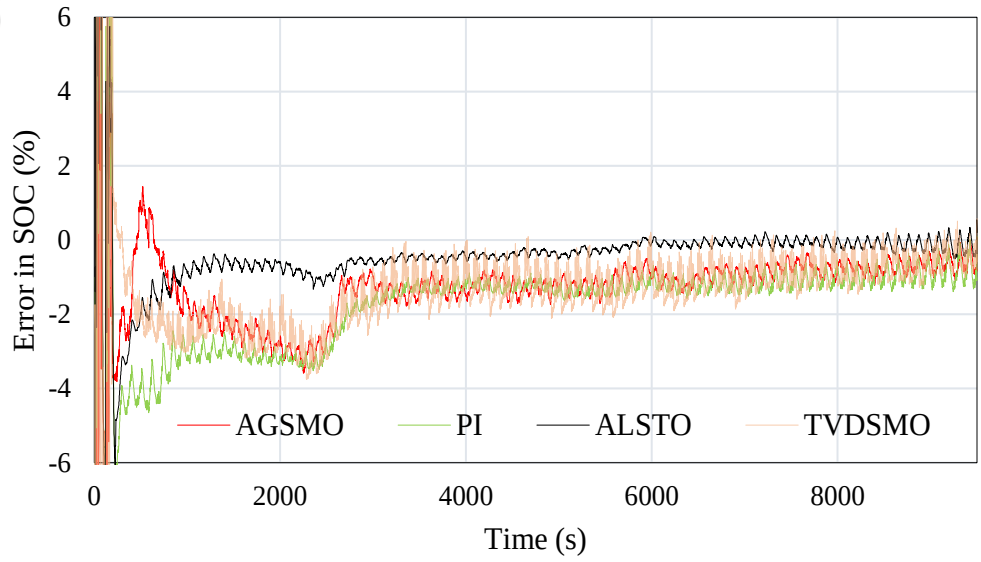

Figure 5.8: Error between actual and estimated SOC for added identification error case.

is that even if the BECM identification approach fails to provide a very good parameter estimation sometimes due to ageing and other external factors, the proposed observer can still provide good SOC

estimation accuracy.

5.4.5 Study of combined effect of measurement noise and identification error

Another situation is analysed where both identification errors and noises stated above are considered together. The estimated SOC for each method are shown in Figure 5.9 and their corresponding

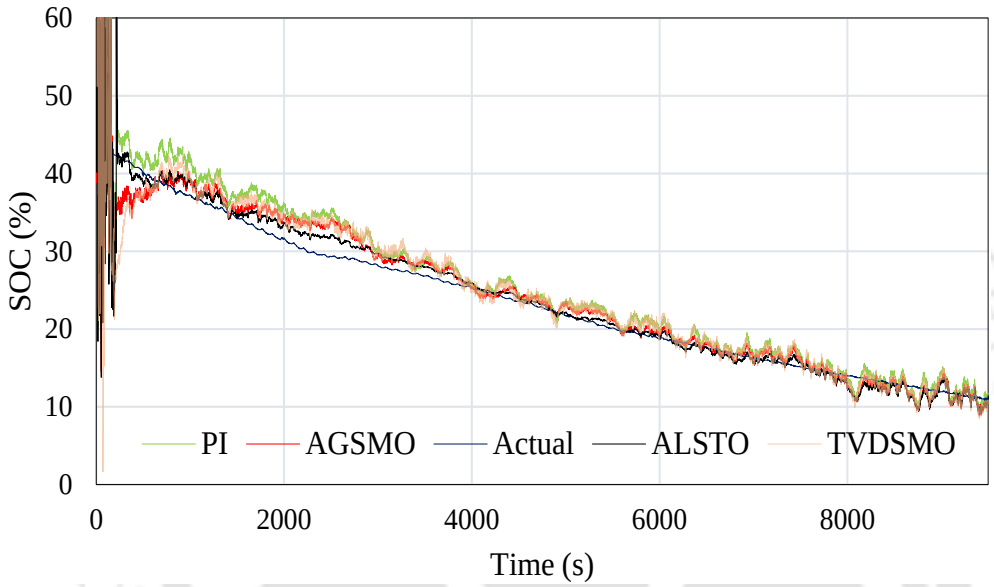

Figure 5.9: Comparison of actual and estimated SOC with added noise and identification errors together.

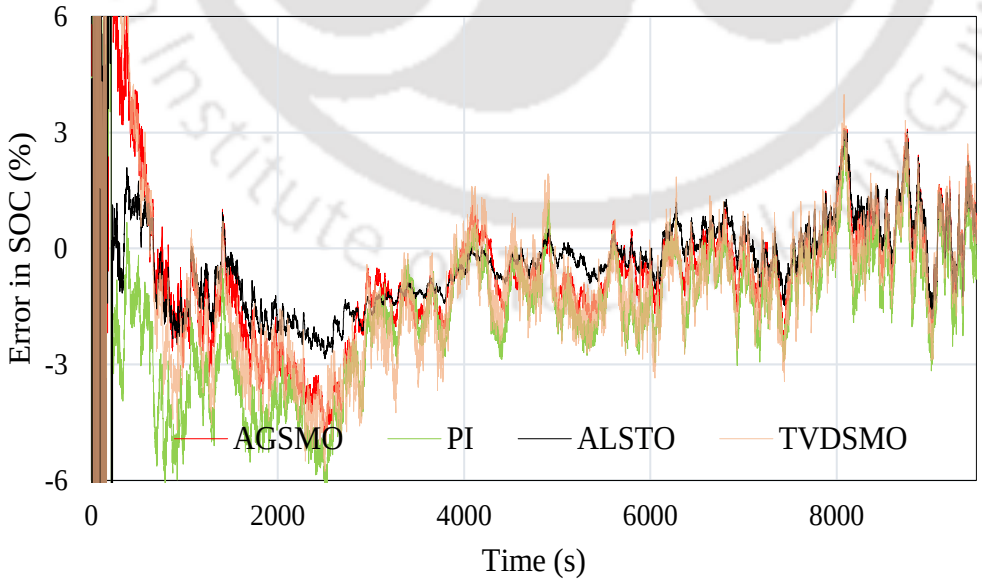

Figure 5.10: Error between actual and estimated SOC for added noise and identification errors together.

errors are demonstrated in Figure 5.10. The MAEs for ALSTO, AGSMO, TVDSMO and PI are obtained as 3.06%, 5.01%, 5.76% and 6.24%, and the RMSEs are 1.13%, 1.60%, 1.96% and 2.36%,

respectively. Under identical condition, the MAE and RMSE for SLSTO presented in Chapter 4 have been found to be 3.14% and 1.21%, receptively. Hence, in the presence of modelling uncertainties and various noises together, the proposed approach outperforms the existing approaches in terms of accuracy, robustness against noise, and sensitivity to the identification errors.

5.5 Summary

In this chapter, a new robust approach based on ALSTO is combined with a standard online BECM parameter identification scheme to predict the SOC of the LIB. The various advantages of the ALSTO compared to the other sliding mode algorithms are discussed extensively. Unlike CSTO and SLSTO, this algorithm can provide robust finite-time stability for a comprehensive class of uncertainties without overestimating the observer gains in the absence of knowledge of the bounds of uncertainties and their derivatives. To verify the efficacy of the proposed method, the experiments are performed on a LiPo battery with a CDDS current profile. The proposed method is compared with SLSTO and various other well-established methods for SOC estimation in various work environments. It is shown that the proposed approach shows high SOC estimation accuracy and performs better than the other methods. The reduction of the chattering for ALSTO compared to the other methods is also demonstrated. The computational time, convergence time, and the robustness against measurement noise are compared which establishes the overall effectiveness of the proposed method. The proposed approach efficiently deals with identification errors enabling it to provide good SOC estimation accuracy under the impact of various external factors such as ageing.

Despite the several advantages of the proposed approach, there are still a few concerns which can be addressed to further improve the performance of SOC estimation method, such as: (i) slow convergence of the observer if the trajectory is far from origin and (ii) use of fixed forgetting factor may lead to poor identification ability, low robustness, and slow convergence of circuit parameters under certain operating conditions. To further improve the performance of the SOC estimation, the next chapter will carefully try to resolve these issues.

Note: The work in this chapter has been published with title "An approach to estimate lithium-ion battery state of charge based on adaptive Lyapunov super twisting observer" in IEEE Transactions on Circuit and Systems I: Regular Papers, 2021.

6

Development of a Fast Convergent SOC Observer with Improved Real-time Parameter Identification

6.1 Introduction

In Chapter 5, ALSTO in combination with RLSF approach has been proposed for estimating SOC of the LIB. In general, super twisting algorithm and its different variants have strong behaviour only against the disturbances around the origin (equilibrium), but weak for the states far from the origin leading to slow convergence [190]. In order to identify the required battery model parameters to design the observer, RLSF approach provides good estimation accuracy and has been used in Chapter 4 and 5. Nevertheless, the convergence speed and ability of dynamic identification of RLSF are affected in the case of poor or interfered excitation and fluctuating signals [183, 191, 192]. It is found that the fixed forgetting factor in RLSF approach fails to provide either high stability, fast convergence, or good tracking ability. Hence, an SOC estimation algorithm is required which can ensure faster convergence of the trajectory and provide good performance in BECM parameter identification under the conditions where RLSF is not effective.

In this chapter, we propose a novel battery SOC observer, known as adaptive generalized integral super twisting observer (AGISTO), by combining the various advantages associated with generalized super twisting algorithm (GSTA), adaptive algorithms, and integral sliding mode algorithm. The proposed observer makes the convergence faster even when the trajectories are far from origin and works efficiently without the knowledge of the upper bounds of various uncertainties for both known and unknown initial conditions. The class of uncertainties for which the finite-time convergence of the system is guaranteed is also wider than the ALSTO. A strong Lyapunov function is utilized to prove the convergence of the proposed observer. In order to identify the required BECM parameters to design the SOC observer, an adaptive forgetting factor based recursive least square (AFFRLS) approach is developed which can provide high stability, fast convergence, and good tracking ability together by varying the forgetting factor with the root-mean-square of the prediction error. The proposed technique is implemented on the battery setup presented in Chapter 4 and the obtained results demonstrate the effectiveness of the proposed approach.

6.2 Battery modelling

The second order RC model shown in Figure 3.1 (Chapter 3) is also utilized in this chapter for designing the battery SOC observer. The assumptions associated with the battery model, the

derivation of the battery state equations, and observability test will remain same as those of Chapter 4. For convenience, the state and the output equations given in (4.8)-(4.10) which will be used further in this chapter are rewritten here as follows:

$$\dot{x}_1(t) = -a_1 x_1(t) + a_2 x_2(t) + q_1 u_1(t) + q_2 u_2(t) + a_1 q + \zeta_1 \tag{6.1}$$

$$\dot{x}_2(t) = b_2 x_1(t) - b_1 x_2(t) - b_2 q + q_3 u_1(t) + \zeta_2 \tag{6.2}$$

$$y(t) = x_1(t) + \Delta f_4 \tag{6.3}$$

where $x_1(t) = V(t)$ and $x_2(t) = Z(t)$ are the states, $y(t) = V(t)$ is the output, $u_1(t) = i(t)$ and $u_2(t) = \dot{i}(t)$ are the inputs of the battery model system. $\zeta_1(x,t,u)$, $\zeta_2(x,t,u)$, and Δf_4 are the uncertainties due to measurement noise, modelling inaccuracy, and external disturbances. The coefficients of the state equations $(a_1, a_2, b_1, b_2, q_1, q_2, q_3)$ are related to the battery model resistances (R_i, R_t, R_c), capacitances (C_n, C_c) and the coefficients relating the OCV and SOC (p, q). They are given as follows:

$$a_1 = \frac{C_n - C_c}{2R_i C_n C_c}, \quad a_2 = a_1 p, \quad b_1 = \frac{1}{R_i C_n}, \quad b_2 = \frac{b_1}{p}$$

$$q_1 = \frac{C_n R_i + C_n R_t - C_c R_t}{2R_i C_n C_c}, \quad q_2 = R_t + \frac{R_i}{2}, \quad q_3 = \frac{q_4}{p}, \quad q_4 = -\frac{R_t}{R_i C_n} \tag{6.4}$$

It is worth noting that $a_1, a_2, b_1, b_2, q_1, q_2$ are positive and q_3 is negative.

As shown in Section 4.3, the difference equation of the battery model in (6.1)-(6.3) can be written as follows:

$$y(k) = \phi^T(k)\theta(k) + \Delta N \tag{6.5}$$

where

$$\theta(k) = \begin{bmatrix} y(k-1) & y(k-2) & u_1(k) & u_1(k-1) & u_1(k-2) \end{bmatrix}^T$$

is the regressor vector,

$$\phi(k) = \begin{bmatrix} -c_1 & -c_2 & d_0 & d_1 & d_2 \end{bmatrix}^T$$

is the vector containing the parameters related to battery model parameters, and ΔN is the white noise present in the system.

The relationship of the discretized parameters with resistances and capacitances in the battery model are given as:

$$R_t = 2b - \frac{c}{a}, \quad R_i = R_c = 2\left(\frac{c}{a} - b\right)$$

$$C_n = \frac{1}{2}\left[\frac{a}{d} + \left(\frac{a^2}{d^2} - \frac{a}{(c-ab)d}\right)^{1/2}\right]$$

$$C_c = \frac{1}{2}\left[\frac{a}{d} - \left(\frac{a^2}{d^2} - \frac{a}{(c-ab)d}\right)^{1/2}\right] \tag{6.6}$$

where

$$a = \frac{2(1-c_2)}{T_s(1+c_2)}, \quad b = \frac{d_0 + d_2 - d_1}{2(1+c_2)},$$

$$c = \frac{2(d_0 - d_2)}{T_s(1+c_2)}, \quad \hat{d} = \frac{2(d_0 + d_1 + d_2)}{T_s^2(1+c_2)},$$

and T_s is the sampling time.

6.3 Identification technique for battery model system

The RLSF approach provides good identification accuracy for time-varying parameters and has been widely applied to many engineering problems including BMS. Unlike the ORLS, in this approach, more weight is assigned to the recent data than the older data. Introduction of forgetting factor slows down the fading of the covariance matrix than that of ORLS, enabling it to keep tracking the changes in parameters efficiently. In general, the forgetting factor lies in the range of $[0.9, 1]$ for most of the applications. The governing equations of the RLSF approach used for parameter identification are as follows:

$$\hat{\phi}(k) = \hat{\phi}(k-1) + H(k)[y(k) - \theta^T(k)\hat{\phi}(k-1)]$$

$$H(k) = \frac{G(k-1)\theta(k)}{\lambda + \theta^T(k)G(k-1)\theta(k)}$$

$$G(k) = \frac{1}{\lambda}[G(k-1) - H(k)\theta^T(k)G(k-1)] \tag{6.7}$$

where λ is the forgetting factor, $\hat{\phi}$ is the estimated parameter vector, θ is the regressor vector, $H(k)$ is the gain which determines the effect of the current prediction error on the update of the parameter estimate, $G(k)$ is the covariance matrix of the estimated parameters, and '$\hat{*}$' denotes the estimated value of '$*$'.

The RLSF approach may not be able to provide best performance and needs further improvement under certain conditions. It fails to provide adequate robustness when the algorithm is poorly excited or interfered, i.e., the old information is forgotten gradually, while there is interfered new information or very little new dynamic information [183,191]. It may lead to covariance windup or blowup problem. Moreover, the convergence speed and dynamic identification ability of RLSF are affected in the case of violent fluctuations or drastic changes in signals [192]. These problems generally arise due to the fixed nature of forgetting factor present in RLSF algorithm. To address the above issues, an adaptive forgetting factor based RLS approach is proposed in this section.

6.3.1 Recursive least square approach with adaptive forgetting factor

In RLSF algorithm, the forgetting factor is a crucial parameter. While selecting the forgetting factor, there is a trade-off between tracking capability, stability, convergence speed, and sensitivity to noise of the algorithm. The higher forgetting factor leads to better stability and convergence speed at the cost of lower tracking capability. Oppositely, the lower forgetting factor causes better tracking capability, but lower stability and convergence speed. In case of very small identification error, the forgetting factor is not required and the introduction of the forgetting factor may even further increase the parameter identification error. In the other case of large identification error, it is needed to have an optimal forgetting factor that may help the identification scheme to convergence faster and improve the identification error. Hence, the fixed variable factor can not provide either high stability, fast convergence, or good tracking ability.

To address the above mentioned problems, Fortescue et al. provide a self-tuning forgetting factor approach in [193]. In [194], it is addressed that the Fortescue's forgetting factor approach and its different variants constrain the forgetting factor to a very small region close to unity. It limits the adaptive ability of RLS approach and cannot solve the covariance wind-up problem efficiently. In [195], a BECM identification approach is proposed where the forgetting factor incorporates adaptiveness feature. However, this method also uses a variant of Fortescue's variable forgetting factor approach. In [196], J.D. Park provided a variable forgetting factor approach while its improved version with similar structure is suggested in [192]. Since this method involves only a few additional simple calculations than RLSF approach, there is no significant difference in computational time with RLSF approach. The forgetting factor in [192] varies according to the current prediction error and

lies between one and a predefined minimum value. However, it is shown in [191] that J.D. Park's identification algorithm cannot track the changes in the parameters when the forgetting factor becomes one and is not competent for identifying the BECM parameters. Moreover, since the forgetting factor in J.D. Park's method is obtained by only one data point, i.e., current prediction error, the stability of this approach is not high. In order to solve these issues with J.D park's method, some modifications to this algorithm are suggested in [191]. Therefore, in this chapter, we propose an improved identification approach which features the advantages of both [192] and [191] by modifying the variable forgetting factor approach presented in [192] with similar modifications suggested in [191]. The adaptive forgetting factor presented in this chapter is given as:

$$\lambda(k) = \lambda_{min} + (\lambda_{max} - \lambda_{min}) h^{L(k)} \tag{6.8a}$$

$$L(k) = round\left(\left(\frac{e_{rms}}{e_{base}}\right)^2\right) \tag{6.8b}$$

$$e_{rms} = \left[\frac{\sum_{i=k-M+1}^{k} e^2(i)}{M}\right]^{1/2} \tag{6.8c}$$

where λ_{min}, λ_{max} are the minimum and maximum value of forgetting factor, respectively, M is the number of data points in the window period, h is sensitivity, and e_{rms} is the root-mean-square (RMS) value of prediction error in the window period, e_{base} is the allowable error reference, and $e(i)$ is the error at i^{th} instant.

In AFFRLS algorithm, when the e_{rms} is very large, the forgetting factor is equal or close to λ_{min}. When it is very small, the forgetting factor is equal or close to λ_{max}. Hence, this method can improve the convergence rate of parameter identification in case of violent fluctuations or drastic changes in signals. This approach can also ensure a good identification accuracy for stable signals. The coefficient h indicating the sensitivity of forgetting factor to the errors may be chosen as any value between 0 and 1. The response speed of parameter identification is slow when h is close to 1. On the contrary, the response speed of parameter identification is too fast when h is close to 0, leading to reduced accuracy of the scheme. Hence, by considering the balance between identification speed and accuracy, the value of h is generally selected as 0.9 [192]. It can be seen from (6.8) that when e_{rms} exceeds e_{base}, the identification parameters are considered unstable and the forgetting factor decreases rapidly to a smaller value. In contrast, when e_{rms} is less than e_{base}, the identification parameters are considered accurate and stable. In such a situation, the forgetting factor increases to a larger value.

As the RMS error value gets larger, the forgetting factor becomes smaller and vice versa. Hence, the forgetting factor is adaptively changed with change of identification error. Finally, (6.7) along with (6.8) completes the design of AFFRLS approach.

6.4 Design of proposed SOC observer

In this section, we propose an observer to estimate battery states by combining the features of integral sliding mode [197], GSTA [190], and adaptive algorithms [187], called as AGISTO. The main feature of integral sliding mode is that it forces system trajectory to start at the sliding surface in case of known initial conditions. It eliminates the reaching phase where the system is generally affected by the disturbances [197, 198]. In case of any unknown initial condition, it is known that the STA forces the state trajectories to the sliding surface in finite time. However, the convergence is slow in case the trajectories are far from the origin [190, 199]. The GSTA includes additional linear terms apart from the standard nonlinear ones present in STA and makes the convergence faster even when the trajectories are far away from origin. The range of uncertainties for which the finite-time convergence of the system is guaranteed is much wider than ALSTO. In general, the knowledge of disturbance bounds is essential to design a GSTA based observer. In physical systems, it is not always possible to have adequate knowledge of these bounds. The adaptive algorithms sort out this issue and do not demand the information of these bounds except for their existence [187]. Based on the assumption on the derivative of terminal current considered in Chapter 4, the proposed observer is designed to estimate the battery states as follows:

$$\dot{\hat{x}}_1(t) = -\hat{a}_1 y(t) + \hat{a}_2 \hat{x}_2(t) + \hat{q}_1 u_1(t) + \hat{a}_1 q + L_1 \tilde{x}_1 + k_1(t)|\sigma|^{1/2} sign(\sigma) + k_2(t)\sigma \tag{6.9}$$

$$\dot{\hat{x}}_2(t) = \hat{b}_2 y(t) - \hat{b}_1 \hat{x}_2(t) - \hat{b}_2 q + \hat{q}_3 u_1(t) + k_3(t) sign(\sigma) + k_4(t)|\sigma|^{1/2} sign(\sigma) + k_5(t)\sigma \tag{6.10}$$

where

$$k_1(t) = p_1 k_p(t), \;\; k_2(t) = p_2 k_p(t),$$

$$k_3(t) = 0.5 p_1^2 k_q(t), \;\; k_4(t) = 1.5 p_1 p_2 k_q(t), \;\; k_5(t) = p_2^2 k_q(t) \tag{6.11}$$

$k_p(t), k_q(t)$ are dynamic gains, p_1, p_2 are positive constants, $\sigma(t)$ is the sliding surface, $\tilde{x}_1 = x_1 - \hat{x}_1$, and $\hat{*}$ is estimated value of $*$.

The error dynamics using (6.1)-(6.2) and (6.9)-(6.10) is as follows:

$$\dot{\tilde{x}}_1 = \hat{a}_2\tilde{x}_2 - L_1\tilde{x}_1 - k_1(t)|\sigma|^{1/2}sign(\sigma) - k_2(t)\sigma + F_1(x,t,u) \tag{6.12}$$

$$\dot{\tilde{x}}_2 = -k_3(t)sign(\sigma) - k_4(t)|\sigma|^{1/2}sign(\sigma) - k_5(t)\sigma + F_2(x,t,u) \tag{6.13}$$

where

$$F_1(x,t,u) = a_1\Delta f_4 - \Delta a_1 y + \Delta a_2 x_2 + \Delta q_1 u_1 + \Delta a_1 q + \zeta_1(x,t,u)$$

$$F_2(x,t,u) = -b_2\Delta f_4 + \Delta b_2 y - b_1 x_2 + b_1\hat{x}_2 - \Delta b_1\hat{x}_2 - \Delta b_2 q - \Delta q_3 u_1 + \zeta_2(x,t,u) \tag{6.14}$$

$\tilde{x}_2 = x_2 - \hat{x}_2$, $\Delta a_1 = a_1 - \hat{a}_1$, $\Delta b_1 = b_1 - \hat{b}_1$, $\Delta q_1 = q_1 - \hat{q}_1$, and $\Delta q_3 = q_3 - \hat{q}_3$.

Considering the continuous control injection of the observer and boundedness of $V, \dot{V}, i, Z, \zeta_1, \zeta_2$, and Δf_4, it can also be considered that the following inequalities are satisfied:

$$|F_1| \leq \delta_1|\sigma|^{1/2}, \quad |F_2| \leq \delta_2 \tag{6.15}$$

where δ_1 and δ_2 are positive constants. Suppose $\delta_1 = \delta_3 p_1$, where δ_3 is another positive constant, then we have

$$|F_1| \leq \delta_3 p_1|\sigma|^{1/2} \leq \delta_3(p_1|\sigma|^{1/2} + p_2|\sigma|) \tag{6.16}$$

If $|F_2| \leq \delta_2$, then F_2 will also satisfy the following wider uncertainty bound:

$$|F_2| \leq \delta_2\left(1 + \frac{3p_2}{p_1}|\sigma|^{1/2} + \frac{2p_2^2}{p_1^2}|\sigma|\right) = \delta_4(0.5p_1^2 + 1.5p_1p_2|\sigma|^{1/2} + p_2^2|\sigma|) \tag{6.17}$$

where $\delta_4 = 2\delta_2/p_1^2$. It can be seen that (6.16) considers a much wider class of uncertainties compared to the ALSTO where the uncertainty bound consists of only the square root term. The real-time uncertainties can be mathematically better represented by the combination of two different powers of magnitude of sliding variable rather than single one. Similarly, the uncertainty considered in (6.17) is also much wider than that of ALSTO.

In general, $\tilde{x}_1$ is considered as the sliding variable in designing sliding mode observers. Motivated

from [197, 198], in this work, the sliding surface σ with integral term is considered as:

$$\sigma(t) = \tilde{x}_1(t) + \int_0^t L_1 \tilde{x}_1(\tau)\, d\tau - \tilde{x}_1(0) \tag{6.18}$$

Taking the derivative of $\sigma(t)$ in (6.18), we get

$$\dot{\sigma}(t) = \dot{\tilde{x}}_1(t) + L_1 \tilde{x}_1(t) \tag{6.19}$$

Substituting $\dot{\tilde{x}}_1(t)$ from (6.12)-(6.13) in (6.19), we get

$$\dot{\sigma}(t) = \hat{a}_2 \tilde{x}_2 - k_1(t)|\sigma|^{1/2} sign(\sigma) - k_2(t)\sigma + F_1(x,t,u) \tag{6.20}$$

The system represented by (6.20) and (6.13) is a modified version of super twisting observer having some additional linear terms apart from the standard nonlinear ones present in CSTO. This modified structure of STA is generally known as GSTA. GSTA includes additional linear terms which are more powerful than the nonlinear terms in stabilizing the system when the trajectory is far from the origin. It can be observed that when $p_1 = 0$ and $p_2 > 0$, system behaves as standard the linear algorithm. If $p_2 = 0$ and $p_1 > 0$, then the GSTA works as standard STA.

Consider the boundedness given in (6.16) and (6.17). Then for any initial condition of the states, the finite-time convergence of the system represented by (6.20) and (6.13) is ensured if $k_p(t)$ and $k_q(t)$ vary dynamically as:

$$\dot{k}_p(t) = \begin{cases} \mu_1 \sqrt{\frac{\beta_1}{2}} sign(|\sigma| - \epsilon), & \text{if } k_p > k_0 \\ \alpha, & \text{otherwise} \end{cases}$$

$$k_q(t) = \left(\frac{\omega k_p}{\hat{a}_2} \right) \tag{6.21}$$

where $|\sigma(0)| > \epsilon$ and k_0 is a small positive constant with $|k_p(0)| > k_0$. ω, β_1, α, and μ_1 are arbitrary positive constants.

Proof: Suppose $e_1 = \sigma$ and $e_2 = \hat{a}_2 \tilde{x}_2$, (6.20) and (6.13) can be rewritten as:

$$\dot{e}_1 = e_2 - k_1(t)|e_1|^{1/2} sign(e_1) - k_2(t) e_1 + F_1(x,t,u)$$

$$\dot{e}_2 = -k_{3t}(t)sign(e_1) + k_{4t}(t)|e_1|^{1/2}sign(e_1) - k_{5t}(t)e_1 + F_2(x,t,u) \tag{6.22}$$

where $k_{it}(t) = \hat{a}_2 k_i(t)$ and $F_t(x,t,u) = \hat{a}_2 F_2(x,t,u)$. Eq. (6.22) can be rewritten as:

$$\dot{e}_1 = e_2 - k_p(t)[p_1|e_1|^{1/2}sign(e_1) + p_2 e_1] + F_1(x,t,u)$$

$$\dot{e}_2 = -k_{qt}(t)[0.5p_1^2 sign(e_1) + 1.5p_1p_2|e_1|^{1/2}sign(e_1) + p_2^2 e_1] + F_t(x,t,u) \tag{6.23}$$

where $k_{qt}(t) = \hat{a}_2 k_q(t)$.

Since $\hat{a}_2$ is positive and bounded, we have

$$|F_t(x,\hat{x},t,u)| \leq \delta_t(0.5p_1^2 + 1.5p_1p_2|\sigma|^{1/2} + p_2^2|\sigma|) \tag{6.24}$$

Consider

$$S = [s_1 \;\; s_2]^T = [\phi \;\; e_2]^T \tag{6.25}$$

where $\phi = p_1|e_1|^{1/2}sign(e_1) + p_2 e_1$, $|\phi| = p_1|e_1|^{1/2} + p_2|e_1|$, and $||S|| = \sqrt{\phi^2 + e_2^2}$. Differentiating ϕ with respect to e_1, we get Γ as

$$\Gamma = 0.5p_1|e_1|^{-1/2} + p_2 \tag{6.26}$$

In view of (6.25), (6.23) can be represented in state matrix form as:

$$\begin{bmatrix} \dot{s}_1 \\ \dot{s}_2 \end{bmatrix} = \Gamma \begin{bmatrix} -k_p(t) & 1 \\ -k_{qt}(t) & 0 \end{bmatrix} \begin{bmatrix} s_1 \\ s_2 \end{bmatrix} + \Gamma \begin{bmatrix} 1 & 0 \\ 0 & 1/\Gamma \end{bmatrix} \begin{bmatrix} F_1 \\ F_t \end{bmatrix} \tag{6.27}$$

Considering (6.16), (6.17) and (6.24), it can be said that there always exists $0 < \delta_p(x,t) \leq \delta_3$ and $0 < \delta_q(x,t) \leq \delta_t$ such that

$$F_1 = \delta_p[p_1|e_1|^{1/2} + p_2 e_1]sign(e_1) = \delta_p s_1$$

$$F_t = \delta_q[0.5p_1^2 + 1.5p_1p_2|e_1|^{1/2} + p_2^2|e_1|]sign(e_1) = \delta_q s_1 \Gamma \tag{6.28}$$

Using (6.28), (6.27) can be rewritten as:

$$\begin{bmatrix} \dot{s}_1 \\ \dot{s}_2 \end{bmatrix} = \Gamma \begin{bmatrix} -(k_p(t) - \delta_p) & 1 \\ -(k_{qt}(t) - \delta_q) & 0 \end{bmatrix} \begin{bmatrix} s_1 \\ s_2 \end{bmatrix} = \bar{A}(s_1) \begin{bmatrix} s_1 \\ s_2 \end{bmatrix} \tag{6.29}$$

It can be observed from (6.25) that the finite-time convergences of s_1 and s_2 ensures finite-time convergences of e_1 and e_2, and hence σ and $\tilde{x}_2$. To analyse the stability of (6.29), consider the Lyapunov function candidate as:

$$\Lambda(S, k_p, k_{qt}) = \Lambda_0(S) + \frac{1}{2\beta_1} k_r^2 + \frac{1}{2\beta_2} k_s^2 \tag{6.30}$$

where

$$k_r = k_p - k_p^*, \quad k_s = k_{qt} - k_{qt}^*,$$

$$\Lambda_0(S) = S^T P S,$$

$$P = \begin{bmatrix} \lambda + \omega^2 & -\omega \\ -\omega & 1 \end{bmatrix},$$

λ, k_p^* and k_{qt}^* are some positive constants [187]. Differentiating (6.30) with respect to time in both sides, we get

$$\dot{\Lambda}(S, k_p, k_{qt}) = S^T [\bar{A}^T P + P\bar{A}] S + \frac{1}{\beta_1} k_r \dot{k}_p + \frac{1}{\beta_2} k_s \dot{k}_{qt} \tag{6.31}$$

Using (6.29) and (6.30), the first term in right hand side (RHS) of (6.31) is computed and is as follows:

$$\dot{\Lambda}_0(S) = S^T [\bar{A}^T P + P\bar{A}] S \leq -\Gamma S^T Q S \tag{6.32}$$

where Q is a symmetric positive definite matrix given as:

$$Q = \begin{bmatrix} q_{11} & q_{12} \\ q_{21} & 2\omega \end{bmatrix}$$

with

$$q_{11} = 2\lambda k_p + 2\omega(\omega k_p - k_{qt}) - 2(\lambda + \omega^2)\delta_p + 2\omega\delta_q$$

$$q_{21} = q_{12} = (k_{qt} - \omega k_p - \lambda - \omega^2) + \omega\delta_p - \delta_q \tag{6.33}$$

It is seen that the following relationships ensure positive definiteness of Q with minimum eigenvalue value ω:

$$k_{qt} = \omega k_p \tag{6.34}$$

and

$$k_p > \frac{6\delta_3\omega(\lambda + \omega^2) - 3\omega^2(2\delta_t + 1) + (\omega\delta_3 - \delta_t - \lambda - \omega^2)^2}{6\omega\lambda} \tag{6.35}$$

In view of $\lambda_{min}(Q) \geq \omega$ and the well-known inequality

$$\lambda_{min}(P)||S||^2 \leq S^T P S \leq \lambda_{max}(P)||S||^2 \tag{6.36}$$

we can write

$$\dot{\Lambda}_0(S) \leq -\Gamma S^T Q S \leq -\omega\Gamma||S||^2 \tag{6.37}$$

Substituting Γ from (6.26) in (6.37), we get

$$\dot{\Lambda}_0(S) \leq -0.5\omega p_1|e_1|^{-1/2}||S||^2 - \omega p_2||S||^2 \tag{6.38}$$

Considering the fact that if $v_1 \leq -v_2 - v_3$, where v_2 and v_3 are positive, then both $v_1 \leq -v_2$ and $v_1 \leq -v_3$ are true, we can write

$$\dot{\Lambda}_0(S) \leq -0.5\omega p_1|e_1|^{-1/2}||S||^2 \tag{6.39}$$

Using (6.25), (6.30) and (6.36), we have

$$p_1|e_1|^{1/2} \leq |\phi| \leq ||S|| \leq \frac{\Lambda_0^{1/2}(S)}{\lambda_{min}^{1/2}(P)} \tag{6.40}$$

Using (6.36), (6.39) and (6.40), we can write

$$\dot{\Lambda}_0(S) \leq -n\Lambda_0^{1/2}(S) \tag{6.41}$$

where

$$n = \frac{\omega p_1^2 \lambda_{min}^{1/2}(P)}{2\lambda_{max}(P)}$$

Now, from (6.31) and (6.41), we have

$$\begin{aligned}\dot{\Lambda}(S, k_p, k_{qt}) &\leq -\Gamma S^T Q S + \frac{1}{\beta_1} k_r \dot{k}_p + \frac{1}{\beta_2} k_s \dot{k}_{qt} \\ &\leq -n\Lambda_0^{1/2}(S) - \frac{\mu_1}{\sqrt{2\beta_1}}|k_r| - \frac{\mu_2}{\sqrt{2\beta_2}}|k_s| + \frac{1}{\beta_1} k_r \dot{k}_p \\ &\quad + \frac{1}{\beta_2} k_s \dot{k}_{qt} + \frac{\mu_1}{\sqrt{2\beta_1}}|k_r| + \frac{\mu_2}{\sqrt{2\beta_2}}|k_s|\end{aligned} \tag{6.42}$$

Using the following well-known inequality

$$(v_1^2 + v_2^2 + v_3^2)^{1/2} \leq |v_1| + |v_2| + |v_3| \tag{6.43}$$

we can obtain the following from (6.30):

$$-n\Lambda_0^{1/2}(S) - \frac{\mu_1}{\sqrt{2\beta_1}}|k_r| - \frac{\mu_2}{\sqrt{2\beta_2}}|k_s| \leq -m\Lambda^{1/2}(S) \tag{6.44}$$

where $m = min(n, \mu_1, \mu_2)$.

In view of (6.44), (6.42) can be rewritten as:

$$\begin{aligned}\dot{\Lambda}(S, k_p, k_{qt}) &\leq -m\Lambda^{1/2}(S) + \frac{1}{\beta_1} k_r \dot{k}_p + \frac{1}{\beta_2} k_s \dot{k}_{qt} \\ &\quad + \frac{\mu_1}{\sqrt{2\beta_1}}|k_r| + \frac{\mu_2}{\sqrt{2\beta_2}}|k_s|\end{aligned} \tag{6.45}$$

Now, suppose $k_p(t)$ and $k_{qt}(t)$ are bounded with bounds k_p^* and k_{qt}^*, respectively (will be proven later in this section). Hence, $k_r < 0$ and $k_s < 0$, $\forall\ t > 0$.

Considering the boundedness of $k_p(t)$ and $k_{qt}(t)$, we can rewrite (6.45) as:

$$\dot{\Lambda}(S) \leq -m\Lambda^{1/2}(S) + D \tag{6.46}$$

where

$$D = -|k_r|\left(\frac{1}{\beta_1}\dot{k}_p - \frac{\mu_1}{\sqrt{2\beta_1}}\right) - |k_s|\left(\frac{1}{\beta_2}\dot{k}_{qt} - \frac{\mu_2}{\sqrt{2\beta_2}}\right) \tag{6.47}$$

In case when $|e_1| = |\sigma| \geq \epsilon$ and $k_p(t) > k_0$, considering (6.21) $D = 0$ can be ensured if

$$\omega = \frac{\mu_2}{\mu_1}\sqrt{\frac{\beta_2}{\beta_1}} \tag{6.48}$$

is chosen. Thus, finite-time convergence of s_1 and s_2 and hence e_1 and e_2 is guaranteed.

In case when $|e_1| \leq \epsilon$, D may be positive or negative. The negative value of D ensures finite-time convergence. However, its positive value may lead to e_1 greater than ϵ due to the decrease in control gains. As soon as e_1 becomes greater than ϵ, the control gains start increasing, and finite-time convergence is achieved as explained earlier. Hence, (6.21) always ensures finite-time convergence of e_1 and e_2. It is also guaranteed that e_1 always stays in a domain $|e_1| \leq \gamma_1$, $\gamma_1 \geq \epsilon$.

Now, we prove the boundedness of $k_p(t)$ and $k_{qt}(t)$ assumed earlier. For $\epsilon < e_1 \leq \gamma_1$, the solution to (6.21) can be obtained as:

$$k_p(t) = k_p(0) + \mu_1\sqrt{\frac{\beta_1}{2}}t, \quad 0 \leq t \leq T_f \tag{6.49}$$

where T_f is the convergence time. For $e_1 \leq \epsilon$, $k_p(t)$ can be increasing only till its value reaches k_0, otherwise it is always decreasing. Hence, in view of (6.21), $k_p(t)$ and $k_{qt}(t)$ are always bounded. Due to the boundedness of the RHS of (6.35) and the fact that $k_p(t)$ increases linearly with respect to time, the inequality in (6.35) is established in finite-time. Hence, as soon as the k_p starts satisfying (6.35), the finite-time convergence of the states is achieved. It can be easily seen that in case when σ and $\tilde{x}_2$ are at origin or in a small neighbourhood of origin, we have $\dot{\sigma} = 0$ or very close to zero. The $\tilde{x}_1$ also asymptotically converges to a small ball around origin. Since x_1 is an available state, its asymptotic convergence will not affect designing of any further control strategy using the system states.

6.5 Results and discussion

To validate the effectiveness of the proposed battery model parameter identification technique and the SOC observer, experiments are conducted on a LiPo battery using the test setup described in Section 4.5. The relationship between OCV and SOC given in that section is also utilized in the present work. In the following subsections, we present the results of implementation of the AFFRLS approach for battery model identification and AGISTO for SOC estimation. We also compare the obtained results of the estimated SOC with various well-established methods present in the current state-of-the-art.

6.5.1 Identification of battery model parameters

For identifying the BECM parameters, the current profile of a CDDS, as presented in Figure 4.4 (Chapter 4), is loaded to the battery. The battery terminal voltage thus obtained, shown in Figure 6.1, is recorded at every sampling instant and stored in the host computer. The relationships, as

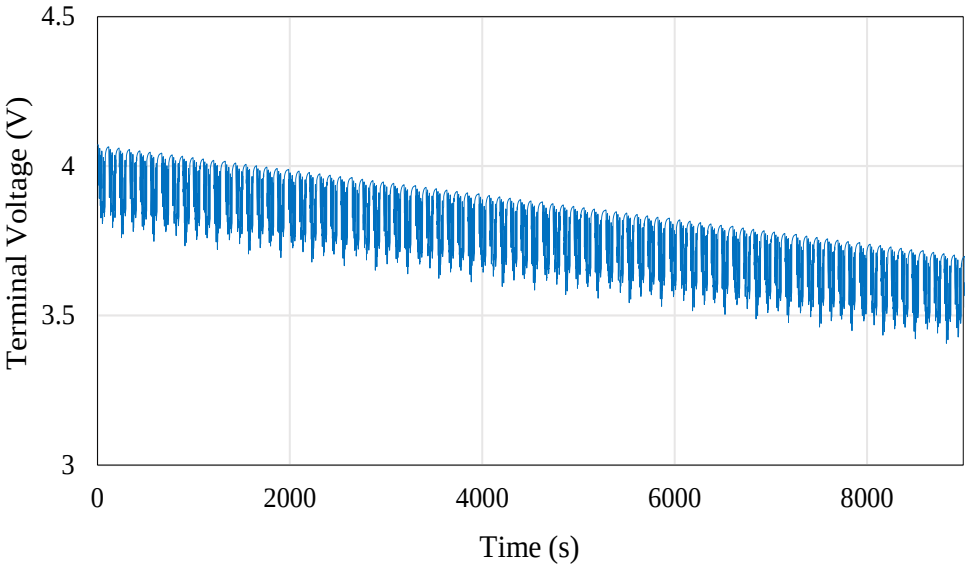

Figure 6.1: Actual terminal voltage.

given in (6.6) and (6.7), are used for recursive identification of real-time battery model resistances and capacitances. The forgetting factor in (6.7) varies according to (6.8) where $\lambda_{max} = 0.995$, $\lambda_{min} = 0.9$, $h = 0.9$, $e_{base} = 1.5 \times 10^{-5}$, and $M = 5$ are considered. The variation of real-time identified parameters of BECM can be seen in Figure 6.2. The prediction error in the process output is shown in Figure 6.3. It establishes the efficacy of the proposed BECM parameter identification approach. The forgetting

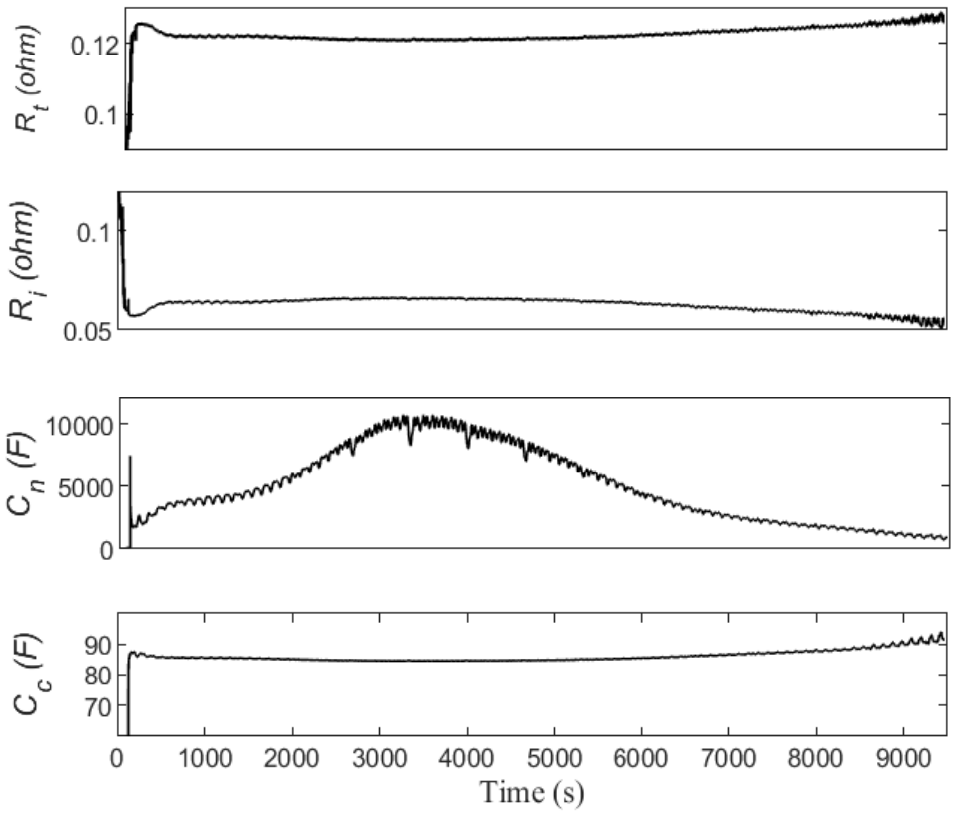

Figure 6.2: Variation of battery model parameters.

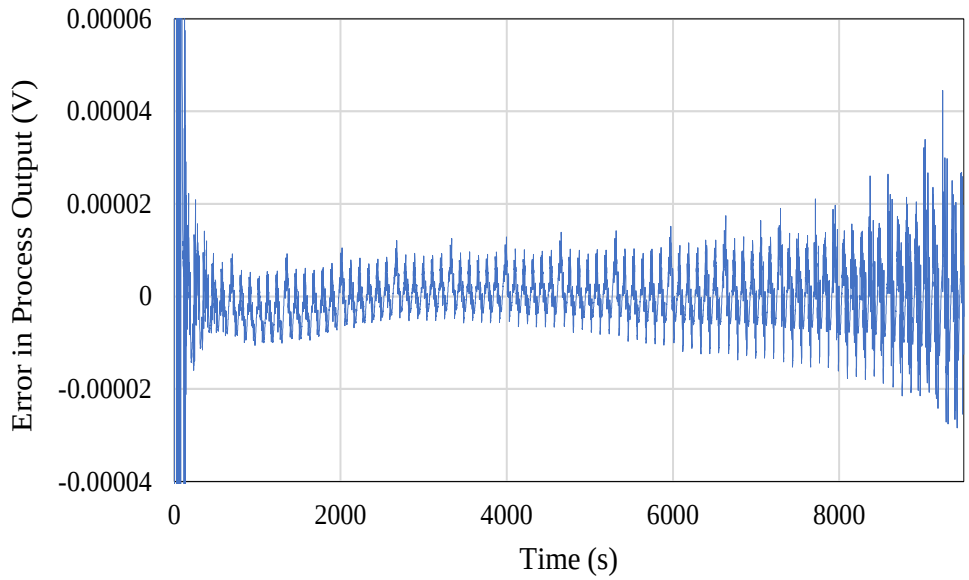

Figure 6.3: Estimation error between the actual output and predicted output by AFFRLS.

factor varies according to the RMS value of the prediction error in the window period, as shown in Figure 6.4. It is seen from Figure 6.3 and 6.4 that when the error is higher than the predefined value e_{base}, the value of forgetting factor decreases to track the parameters and increases again when the

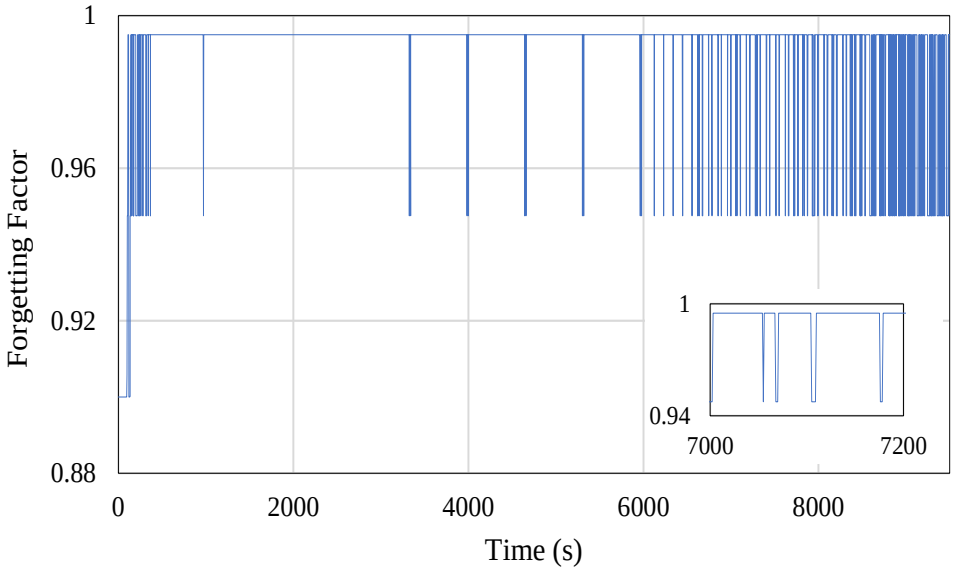

Figure 6.4: Variation of forgetting factor.

error becomes lower than e_{base}. Comparing the results obtained using AFFRLS with RSLF approach presented in Chapter 4, it is found that the convergence is faster in the proposed method. The convergence time of AFFRLS and RLSF are 124 s and 232 s, respectively. Moreover, the identified parameters are more stable in AFFRLS and their peak overshoot is also low.

6.5.2 SOC estimation using proposed approach and its comparative study

For estimation of SOC, the observer is designed using the a_1, b_1, q_1, and q_4 which are continuously obtained with the help of (6.4). In order to design the dynamics of adaptive gains of the proposed observer, we consider $p_1 = 2$, $p_2 = 1.5$, $\mu_1 = 0.05$, $\beta_1 = 0.2$, $\epsilon = 0.02$, $\alpha = 0.2$, $\omega = 1 \times 10^{-7}$, and $k_0 = 0.05$. To verify the efficacy of the proposed observer, the same current profile loaded to the battery is injected as input to the observer. Using the proposed observer and (6.18), the sliding variable is estimated. The convergence speed of sliding variables for the proposed method and ALSTO having same initial values (IVs) are compared in Figure 6.5. It can be inferred from the figure that the sliding variable converges to zero faster for the proposed method. It can also be observed from Figure 6.5 that the convergence time depends on the considered initial conditions and increases with increase in their absolute values. In case of known initial conditions, the sliding variable for the proposed method starts at zero itself and stays in its neighbourhood for all future times, as shown in Figure 6.6.

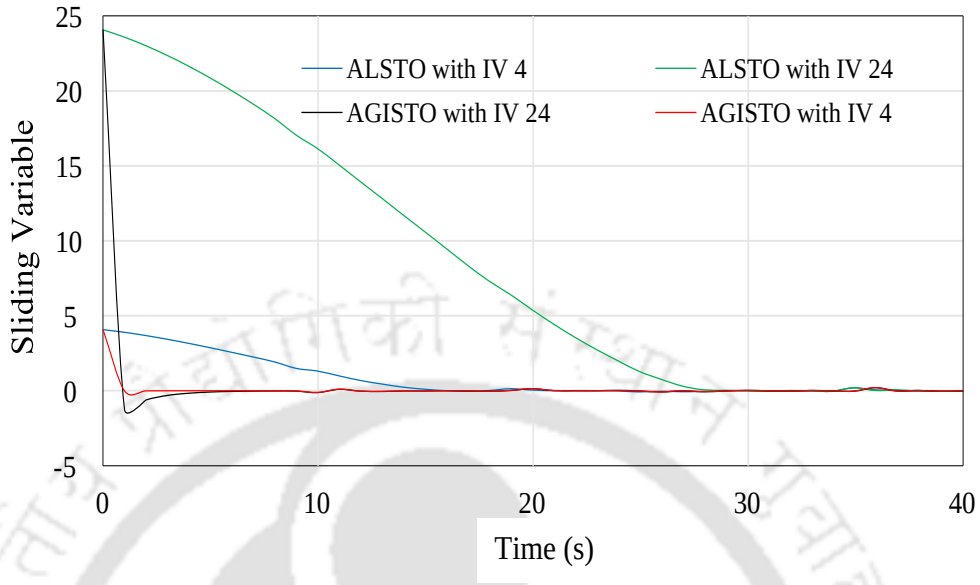

Figure 6.5: Comparison of convergence speed of sliding variable.

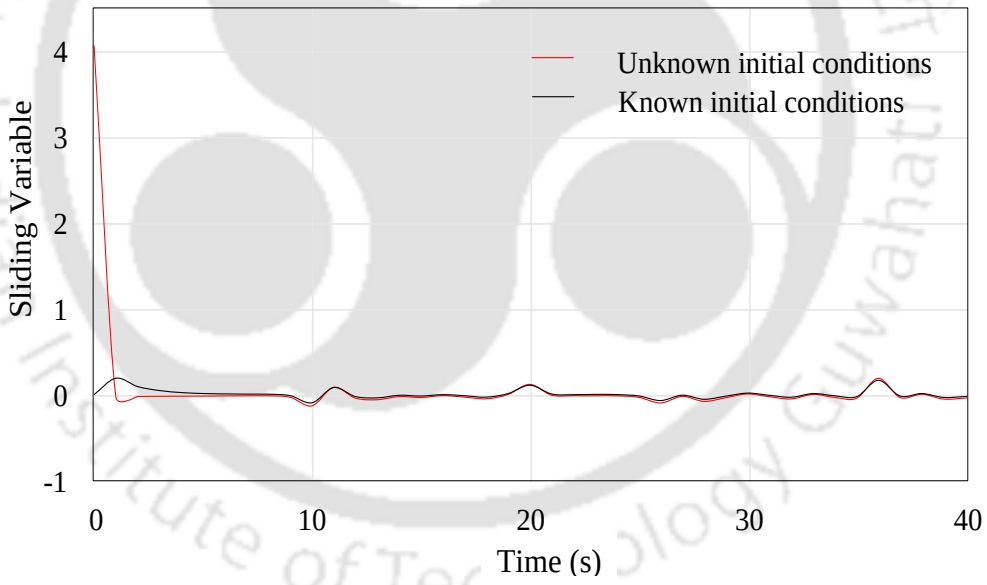

Figure 6.6: Convergence of sliding variable with known and unknown initial conditions.

For estimation of SOC, the initial SOC is considered with a 60% erroneous value. The estimated SOC from the proposed observer is presented in Figure 6.7. The proposed approach is also compared with some well-known methods such as AGSMO, TVDSMO, and PI observer in Figure 6.7 [125, 134, 189]. The observer parameters are tuned carefully for each approach. The reference SOC is derived from an inherent Ampere-hour counter present in BioLogic VMP3. The difference between the estimated SOC for each method and the actual SOC (% error) are shown in Figure 6.8. The

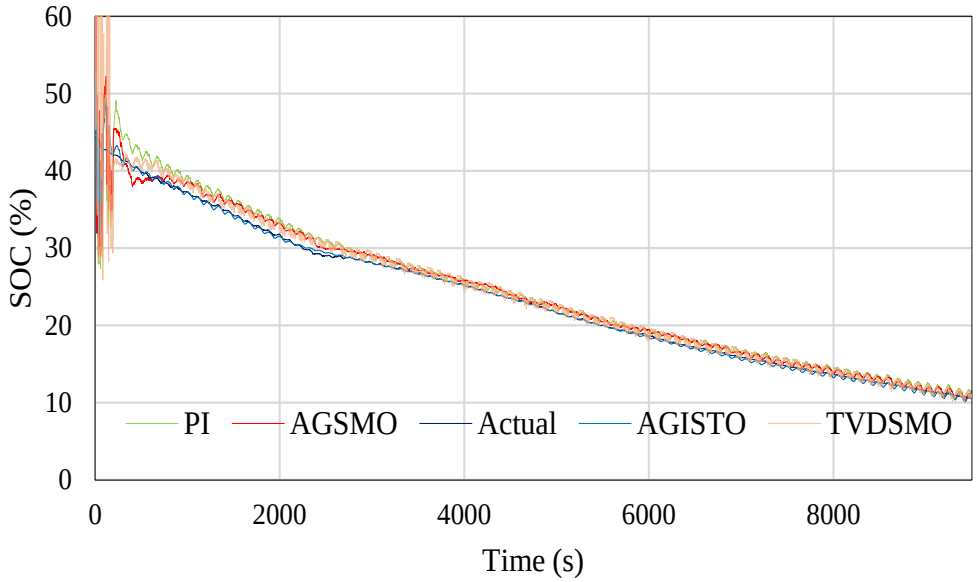

Figure 6.7: Comparative study of SOC estimation results.

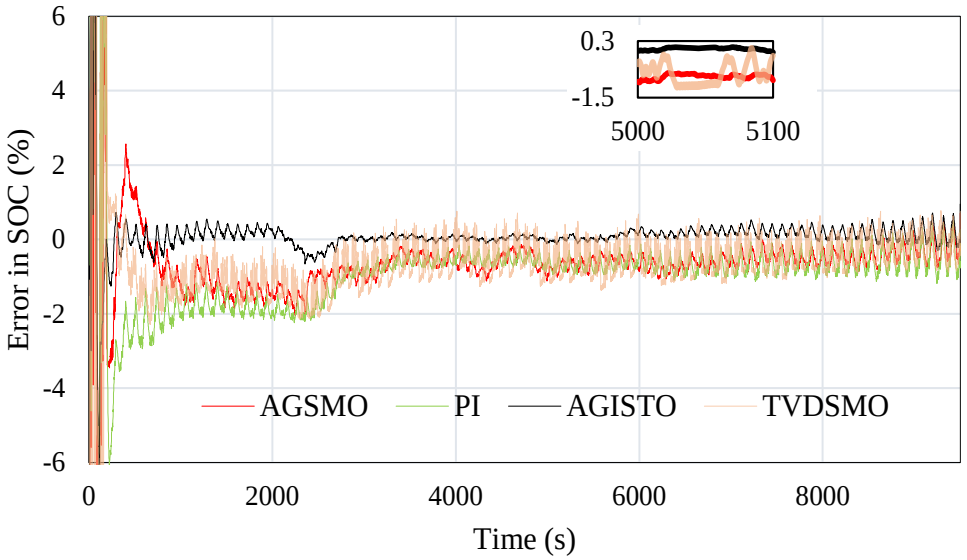

Figure 6.8: Error between actual and estimated SOC.

RMSE and MAE for each method can be found in Table 6.1. The results obtained in Chapter 4 and 5 in identical conditions are also included in this table for comparison. The table establishes the higher accuracy of the proposed approach. It can be observed from Figure 6.8 that the predicted SOC for each method has large error at the beginning of the experiment due to the erroneous initial conditions. But for the proposed observer, it converges fastest to the true SOC profile compared to the other methods. It is inferred from Figure 6.8 and the results obtained in Chapter 4 and 5 that the chattering is reduced in the proposed method. Between 5000-5100 s, the chattering width for

Table 6.1: Comparative study of SOC estimation methods

Method	MAE (%)	RMSE (%)	Computational time (s)	Convergence time (s)
AGISTO (Proposed)	0.95	0.36	2.92	275
AGSMO	2.05	0.88	24.45	429
TVDSMO	2.29	0.91	2.23	374
PI	2.58	1.06	2.01	713
SLSTO (Chapter 4)	1.38	0.70	2.52	589
ALSTO (Chapter 5)	1.29	0.44	2.71	392

AGSMO, TVDSMO, ALSTO, SLSTO, and AGISTO are 0.33%, 1.27%, 0.14%, 0.19%, and 0.10%, respectively. Table 6.1 demonstrates the computational time for each method. It can be seen that the computational time is small for each method except AGSMO. In the following subsections, the effectiveness of the proposed approach under various working conditions are discussed.

6.5.3 Effect of current and voltage measurement noise

In real-time system, the voltage and current sensors are generally associated with considerable amount of noise. Therefore, for investigating the robustness of each method, experiments are performed by considering the presence of white noise having standard deviation of 0.04 and 0.08 in voltage and current channels, respectively. The estimated SOC from each method under noisy environment are compared, as depicted in Figure 6.9, and the corresponding errors in estimating SOC are shown in Figure 6.10. The MAE and RMSE for each method including the methods explained in Chapter 4 and 5 in identical condition are given in Table 6.2. It is observed from the table that the proposed approach has better accuracy even under noisy conditions and also it takes least time to converge to the true SOC value. Moreover, Figure 6.10 and the results in previous chapters show that the chattering is least in the proposed approach. Between 5000-5100 s, the chattering width for AGSMO, TVDSMO, ALSTO, SLSTO, and AGISTO are found to be 1.05%, 2.24%, 0.59%, 0.62%, and 0.41%, respectively. Hence, it can be said that the proposed approach performs well even in the presence of current and voltage sensor noise.

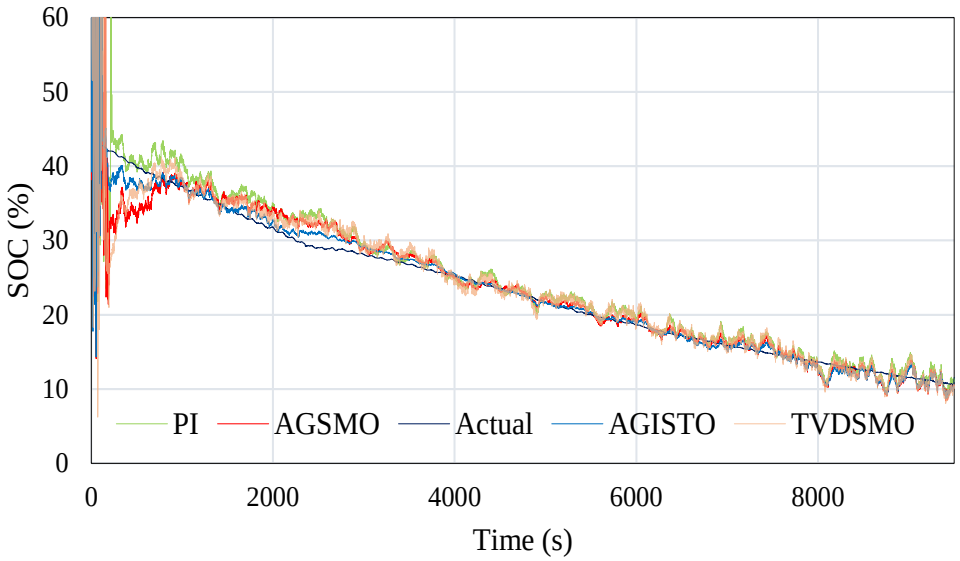

Figure 6.9: Comparative study of SOC estimation results with added noise.

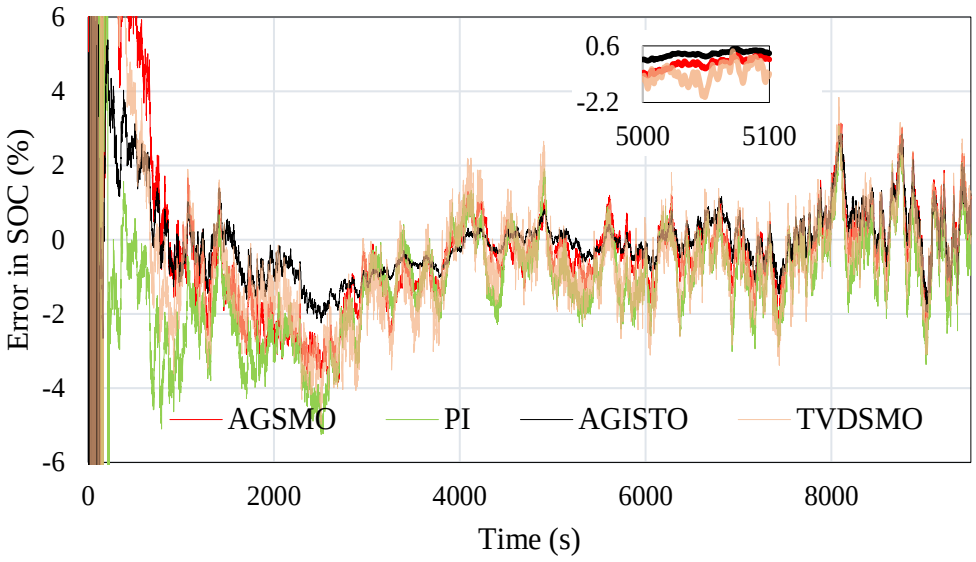

Figure 6.10: Error between actual and estimated SOC for added noise case.

6.5.4 Robustness study against identification error for the proposed observer

To verify the efficacy of the proposed approach in mitigating the effect of erroneous battery model parameters, the BECM resistances and capacitances with 10% identification error are considered in the present study. In order to illustrate the impact of ageing, the resistances are increased and the capacitances are decreased by 10%. The estimated SOC from each method with inaccurate BECM parameters are compared, as shown in Figure 6.11, and the corresponding errors in estimating SOC

Table 6.2: Comparison of SOC estimation with added noise

Method	MAE (%)	RMSE (%)	Computational time (s)	Convergence time (s)
AGISTO (Proposed)	2.86	0.84	2.98	414
AGSMO	4.01	1.30	25.8	662
TVDSMO	4.96	1.52	2.27	514
PI	5.24	1.77	2.06	790
SLSTO (Chapter 4)	2.97	0.93	2.57	622
ALSTO (Chapter 5)	2.98	0.83	2.75	505

are depicted in Figure 6.12. Figure 6.12 shows that the proposed approach provides better accuracy

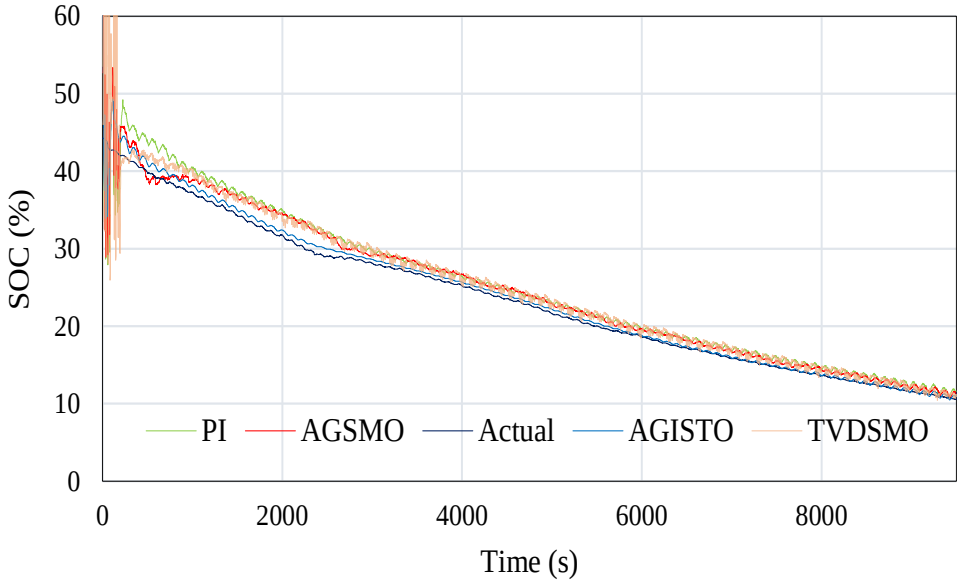

Figure 6.11: Estimated SOC from proposed approach with added identification error.

in estimating SOC than the other methods even with inaccurate identification results. For AGISTO, AGSMO, TVDSMO and PI, the MAEs are 1.86%, 3.58%, 3.74% and 3.87%, and the RMSEs are 0.56%, 1.47%, 1.61% and 1.81%, respectively. Under identical condition, the MAEs and RMSEs for ALSTO and SLSTO presented in Chapter 5 and 4 have been found to be 2.17% and 2.23%, and 0.59% and 1.15%, respectively. Hence, the proposed SOC estimation approach can provide satisfactory results even when the identification scheme provides inaccurate BECM parameters.

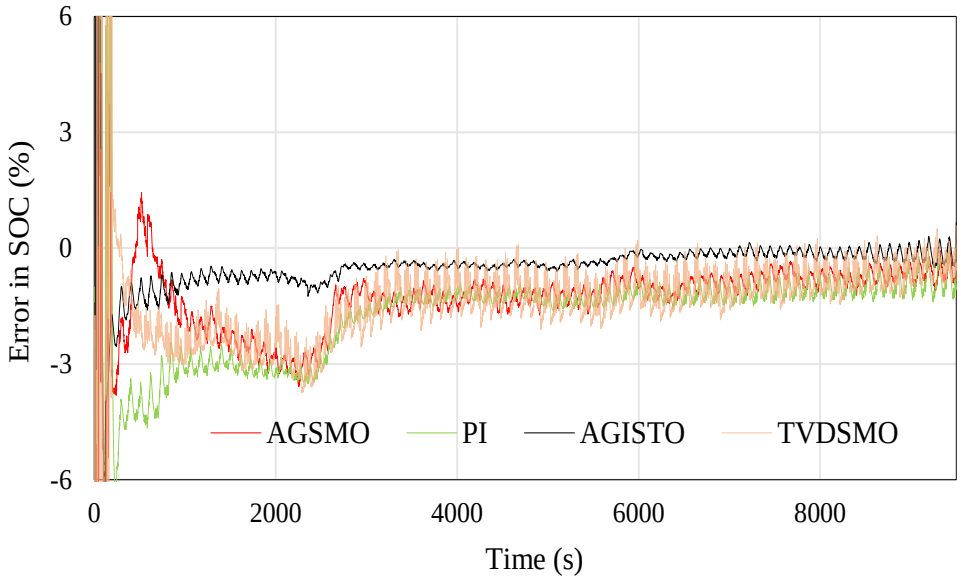

Figure 6.12: Error between actual and estimated SOC for added identification error case.

6.5.5 Study of combined effect of measurement noise and identification error

The effectiveness of the proposed observer is also analysed in presence of various noises and modelling uncertainties together. The estimated SOC from each method under such condition are compared, as shown in Figure 6.13, and the corresponding errors in estimating SOC are depicted in Figure 6.14. For AGISTO, AGSMO, TVDSMO and PI, MAEs are 2.99%, 5.01%, 5.76% and 6.24%, and

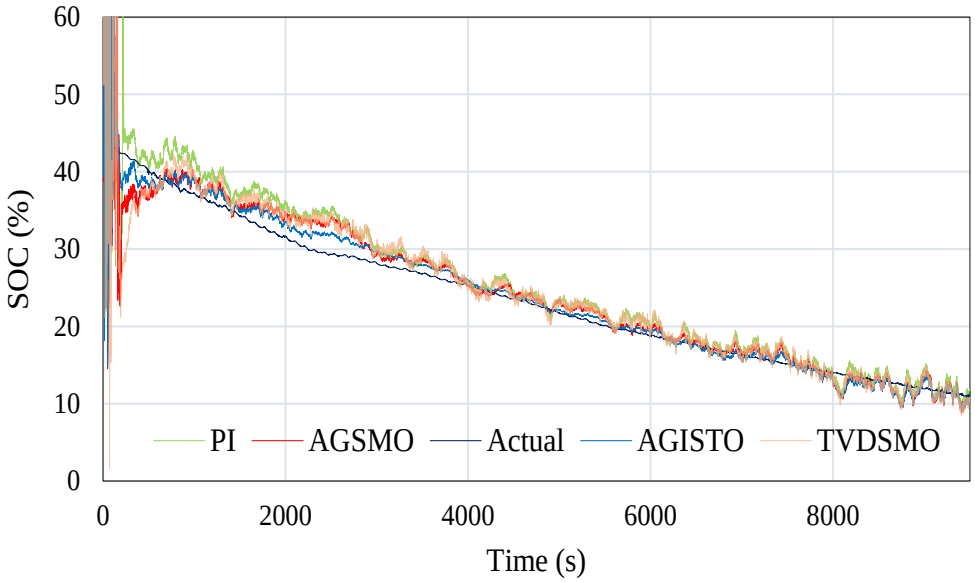

Figure 6.13: Comparison of actual and estimated SOC with added noise and identification errors together.

RMSEs are 1.14%, 1.60%, 1.96% and 2.36%, respectively. Under identical condition, the MAEs and

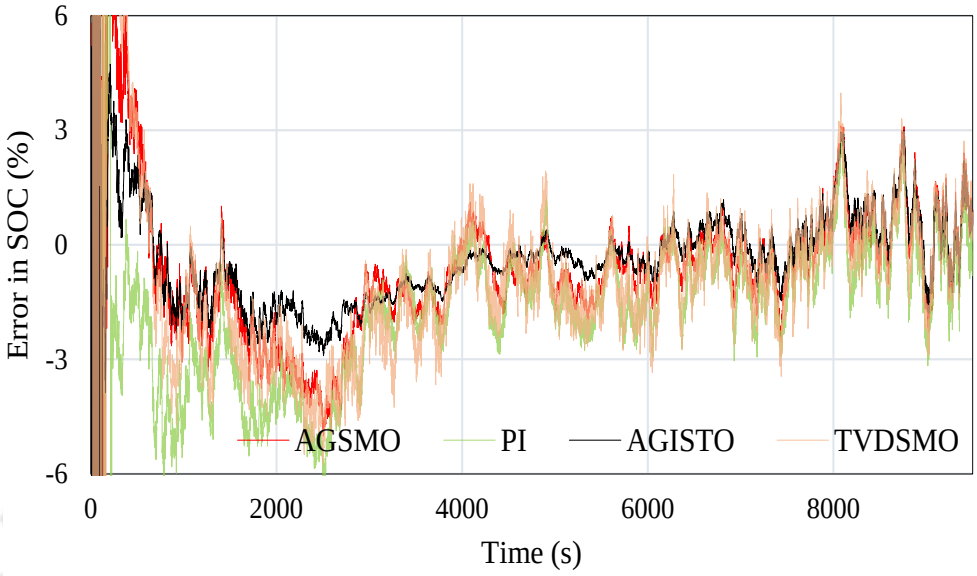

Figure 6.14: Error between actual and estimated SOC for added noise and identification errors together.

RMSEs of ALSTO and SLSTO presented in Chapter 5 and 4 have been found to be 3.06% and 3.14%, and 1.13% and 1.21%, receptively. Hence, in the presence of modelling uncertainties and various noises together, the proposed SOC estimation method outperforms the other methods.

6.6 Summary

In this chapter, the advantages of GSTA, adaptive algorithms, and integral sliding mode algorithm have been combined together to develop a new and improved SOC estimation method. The convergence of the proposed observer has been proven using a strong Lyapunov function. The required battery model parameters to design the observer have been identified by developing an improved recursive least square approach with adaptive forgetting factor. This identification approach enhances the stability, convergence, and tracking ability of RLSF approach by varying the forgetting factor with the RMS value of the prediction error for a window period. To establish the superiority of the proposed approach over ALSTO, SLSTO, and other well-established methods used for SOC estimation, experiments have been performed under different working conditions. By analysing the results of the experiments, we have observed that the proposed approach shows high SOC estimation accuracy, low computational time, high convergence speed, and improved robustness against measurement noise and modelling uncertainties compared to other well-established methods. The chattering is also minimum for the proposed approach.

7

Conclusions and Future Scope

7.1 Conclusions

The objective of this thesis is to develop efficient SOC estimation algorithms in real-time that enhance the performance of BMS and boost the usage of LIBs in future EVs by making them a more appealing and safer choice. For that purpose, four different techniques for SOC estimation have been progressively proposed and developed to improve upon the various state-of-the-art algorithms for SOC estimation. The proposed estimation methods in this thesis are model based consisting of two steps: (i) modelling of LIB and its identification, and (ii) state observer design for battery SOC estimation. The proposed approaches utilize only the available measurable quantities of the battery. The algorithms presented in this thesis provide high accuracy, good robustness against uncertainties, low computation time, high convergence speed, and adapt to the variation of different operating conditions. The low computational effort makes these approaches suitable for a low cost BMS. This research provides a new simple pathway for the SOC estimation without the need for time-consuming and tedious characterization tests which are non-ideal in a practical sense.

The first work in this thesis, as presented in Chapter 3, employs CSTO for estimating SOC of the LIB. It is a special type of SOSMO that strives to resolve the various issues related to existing sliding mode based SOC observers such as chattering, discontinuous control injection, more number of sensors requirement, and the need for low pass filters. It also ensures finite-time convergence of the observer states to the actual states. A geometrical approach using majorant curve is presented for establishing the finite-time convergence of the battery SOC observer. A novel approach for parameter identification of type 1, second order, and minimum phase system using the state-space based relay feedback approach is proposed. This offline approach is then utilized to identify the battery model parameters required for the observer design. This is a closed loop approach and provides good identification accuracy. The efficacy of the proposed method is established using numerical simulations. The OCV obtained from CSTO is compared with that of SOSMO and it is found that the proposed approach provides better estimation accuracy and lower chattering compared to SOSMO. Despite the good accuracy of the method, it is also associated with a few shortcomings. In this algorithm, the robustness of the observer can be ensured for a very limited class of uncertainties. Moreover, the battery model parameters are assumed to be fixed. However, these parameters vary with several operating conditions, such as C-rate, SOC, temperature, and ageing. Another shortcoming of this method is the need for an additional setup for identification test and additional memory in BMS to store the

battery model parameters data for their further use.

In the second work presented in Chapter 4, a new approach is proposed based on SLSTA for improved estimation of SOC of the LIB, which overcomes the shortfalls associated with CSTO. Besides enjoying the various advantages associated with CSTO, the proposed SOC observer guarantees the robustness for a more comprehensive class of uncertainties than CSTO. A strict Lyapunov function is used to prove the robust finite-time convergence of the proposed battery SOC observer. In order to design the observer, the required battery model parameters are identified using a standard online approach known as RLSF. It can keep track the changes in the battery model parameters with various operating conditions. Hence, their effect can be avoided in battery modelling which provided an opportunity to use a simple battery model. Unlike the offline identification methods, it does not require any additional setup or memory to perform the identification test. To verify the efficacy of the proposed method, the experiments are performed on a LiPo battery with a real-time driving cycle (CDDS) current profile. The proposed method is compared with AGSMO and PI observer for SOC estimation in various work environments. The reduction of the chattering for SLSTO compared to the AGSMO is also demonstrated. The robustness against measurement noise, computational and the convergence time are also compared which established the overall effectiveness of the proposed method. The proposed approach also efficiently deals with identification errors enabling it to provide satisfactory results under the impact of external factors such as ageing, which may influence the identification parameters. Despite the several advantages, the proposed observer in this work requires the information of the upper bounds of uncertainties that are not always available for a physical system such as battery. In general, it leads to the overestimation of the observer gains.

To address the shortcomings of the method presented in Chapter 4, the third work, as presented in Chapter, 5 has proposed a new SOC estimation algorithm based on ALSTO which is combined with RLSF approach for battery model identification. The main advantage of the proposed method is that unlike the CSTO and SLSTO, it does not demand any information on boundaries of the various uncertainties except for their existence. The ALSTO adaptively minimizes the associated gains in such a way that the sliding is maintained without overestimation of the observer gains. This further helps to reduce the chattering significantly. ALSTO can also deal with a more comprehensive class of uncertainties compared to conventional STA based observer. The finite-time convergence of estimation error and robustness of the battery SOC observer are demonstrated using Lyapunov stability theory.

The battery setup used in Chapter 4 is also utilized in this work to perform the required experiments to establish the efficacy of the proposed method. By comparing the proposed method with various well-established methods of SOC estimation, it is demonstrated that ALSTO shows better estimation accuracy, reduced chattering, low computational time, low convergence time, high robustness against measurement noise, and better handling of model identification errors. In general, super twisting algorithm including ALSTA has strong behaviour only against the disturbances around the origin, but weak for far states from origin. The convergence is slow if the trajectory is far from origin. In addition, the dynamic identification ability and convergence speed of RLSF in identifying the BECM parameters will be affected in case of frequent change in charging and discharging currents. RLSF does not provide adequate robustness when the algorithm is poorly excited or interfered. The fixed forgetting factor is unable to provide either high stability, fast convergence, or good tracking ability.

To overcome the limitations associated with the work presented in Chapter 5, the advantages of GSTA, adaptive algorithms, and integral sliding mode algorithm are combined together to develop a new and improved SOC estimation method in Chapter 6. Apart from standard nonlinear terms, GSTA algorithm also includes additional linear terms and converges faster even when the trajectory is far from origin. It guarantees a more comprehensive class of uncertainties than the ALSTO for finite-time convergence. Due to the adaptiveness offered by the algorithm, it works efficiently even without the knowledge of the upper bounds of various uncertainties. The integral sliding mode can eliminate the reaching phase in the cases where initial conditions of the system are known. GSTA forces the state trajectory to the sliding surface in finite time in case of unknown or erroneous initial conditions. The convergence of the proposed observer is proven using a strong Lyapunov function. The required battery model parameters to design the observer are identified by developing an improved recursive least square approach with adaptive forgetting factor. This identification approach enhances the stability, convergence, and tracking ability of RLSF approach by varying the forgetting factor with the RMS value of the prediction error for a window period. The battery setup used for experiments is identical to the one used in Chapter 4. To establish the superiority of the proposed approach over ALSTO and other popular methods used for SOC estimation, experiments are performed under different working conditions. By analyzing the results of the experiments, it is observed that the proposed approach shows high SOC estimation accuracy, low computational time, less convergence time, and improved robustness against measurement noise and modelling uncertainties compared to

other well-established methods.

7.2 Future scope

There are several works related to this thesis that can be done to further boost the commercialization of the LIB. The potential works which require further investigation are listed as follows:

- This thesis only focuses on the problem of SOC estimation of LIB. The proposed SOC estimation approaches can be extended further to predict other important BMS states such as health prediction (SOH) and peak power capability (SOP) of a battery. The optimum charging of the battery and the cell balancing using the knowledge of estimated SOC can be investigated. Subsequently, an integrated battery management system with estimation of SOC, SOH, and SOP, cell balancing, and optimal charging can be developed for EV application.
- In order to further improve the SOC estimation accuracy, the effect on hysteresis due to temperature and ageing can be studied in more detail since it can significantly affect the performance of some LIBs such as lithium phosphate.
- The estimation approach developed in this thesis is for a single battery cell. Although it is economically possible to have a management board for each cell, one worthwhile direction of future work would be to verify the effectiveness of developed techniques for a large battery pack. This could potentially help to reduce the cost of the hardware required for a complete system.
- The employment of the techniques presented in this thesis can be explored for other energy storage system applications, especially in smartgrids and microgrids. It is believed that the outcome of this thesis is applicable to other types of rechargeable batteries, nevertheless, validations are recommended in future work. The efficacy of the presented techniques can also be checked for other battery electrochemistry as well as supercapacitors.

References

[1] M. Venkataramanan *et al.*, "Causes and effects of global warming," *Indian Journal of Science and Technology*, vol. 4, no. 3, pp. 226–229, 2011.

[2] USEPA, "Sources of greenhouse gas emissions," Available: https://www.epa.gov/ghgemissions/sources-greenhouse-gas-emissions, Accessed: 2021-12-27.

[3] S. Boudoudouh and M. Maâroufi, "Real-time battery state of charge estimation in smart grid application by multi agent system," *International Journal of Hydrogen Energy*, vol. 42, no. 30, pp. 19 487–19 495, 2017.

[4] M. Faisal, M. A. Hannan, P. J. Ker, A. Hussain, M. B. Mansor, and F. Blaabjerg, "Review of energy storage system technologies in microgrid applications: Issues and challenges," *IEEE Access*, vol. 6, pp. 35 143–35 164, 2018.

[5] BloombergNEF, "Lithium-ion battery prices," Available: https://about.bnef.com/blog/behind-scenes-take-lithium-ion-battery-prices/, Accessed: 2021-12-27.

[6] M. Hannan, M. M. Hoque, A. Mohamed, and A. Ayob, "Review of energy storage systems for electric vehicle applications: Issues and challenges," *Renewable and Sustainable Energy Reviews*, vol. 69, pp. 771–789, 2017.

[7] F. Schipper and D. Aurbach, "A brief review: Past, present and future of lithium ion batteries," *Russian Journal of Electrochemistry*, vol. 52, no. 12, pp. 1095–1121, 2016.

[8] T. Sasaki, Y. Ukyo, and P. Novák, "Memory effect in a lithium-ion battery," *Nature materials*, vol. 12, no. 6, pp. 569–575, 2013.

[9] Y. Liang, C. Z. Zhao, H. Yuan, Y. Chen, W. Zhang, J.-Q. Huang, D. Yu, Y. Liu, M.-M. Titirici, Y.-L. Chueh, H. Yu, and Q. Zhang, "A review of rechargeable batteries for portable electronic devices," *InfoMat*, vol. 1, no. 1, pp. 6–32, 2019.

[10] T. B. Reddy, *Linden's handbook of batteries*. McGraw-Hill Education, 2011.

[11] M. Wu, B. Xu, and C. Ouyang, "Physics of electron and lithium-ion transport in electrode materials for Li-ion batteries," *Chinese Physics B*, vol. 25, no. 1, p. 018206, 2015.

[12] L. Xiubin, L. Yue, W. Nantian, Z. Qingqi, and L. Tingpeng, "The diffusion polarization model of lithium-ion battery relaxation effect," in *12th IEEE International Conference on Electronic Measurement & Instruments (ICEMI), Qingdao*, vol. 1. IEEE, 2015, pp. 131–135.

[13] B. Pattipati, B. Balasingam, G. Avvari, K. Pattipati, and Y. Bar-Shalom, "Open circuit voltage characterization of lithium-ion batteries," *Journal of Power Sources*, vol. 269, pp. 317–333, 2014.

[14] M. Team *et al.*, "A guide to understanding battery specifications," *Massachusetts Institute of technology, USA, Tech. Rep.*, 2008.

[15] H. Tian, P. Qin, K. Li, and Z. Zhao, "A review of the state of health for lithium-ion batteries: Research status and suggestions," *Journal of Cleaner Production*, vol. 261, p. 120813, 2020.

[16] C. Zou, A. Klintberg, Z. Wei, B. Fridholm, T. Wik, and B. Egardt, "Power capability prediction for lithium-ion batteries using economic nonlinear model predictive control," *Journal of Power Sources*, vol. 396, pp. 580–589, 2018.

[17] C. Wu, J. Sun, C. Zhu, Y. Ge, and Y. Zhao, "Research on overcharge and overdischarge effect on lithium-ion batteries," in *IEEE Vehicle Power and Propulsion Conference (VPPC), Montreal*. IEEE, 2015, pp. 1–6.

[18] D. Lisbona and T. Snee, "A review of hazards associated with primary lithium and lithium-ion batteries," *Process Safety and Environmental Protection*, vol. 89, no. 6, pp. 434–442, 2011.

[19] N. Togasaki, T. Yokoshima, Y. Oguma, and T. Osaka, "Prediction of overcharge-induced serious capacity fading in nickel cobalt aluminum oxide lithium-ion batteries using electrochemical impedance spectroscopy," *Journal of Power Sources*, vol. 461, p. 228168, 2020.

[20] D. Ouyang, Y. He, M. Chen, J. Liu, and J. Wang, "Experimental study on the thermal behaviors of lithium-ion batteries under discharge and overcharge conditions," *Journal of Thermal Analysis and Calorimetry*, vol. 132, no. 1, pp. 65–75, 2018.

[21] D. Zhang, B. Haran, A. Durairajan, R. E. White, Y. Podrazhansky, and B. N. Popov, "Studies on capacity fade of lithium-ion batteries," *Journal of Power Sources*, vol. 91, no. 2, pp. 122–129, 2000.

[22] X. Feng, M. Ouyang, X. Liu, L. Lu, Y. Xia, and X. He, "Thermal runaway mechanism of lithium ion battery for electric vehicles: A review," *Energy Storage Materials*, vol. 10, pp. 246–267, 2018.

[23] J. R. Belt, C. D. Ho, T. J. Miller, M. A. Habib, and T. Q. Duong, "The effect of temperature on capacity and power in cycled lithium ion batteries," *Journal of power sources*, vol. 142, no. 1-2, pp. 354–360, 2005.

[24] C. Yuqin, L. Hong, W. Lie, and L. Tianhong, "Irreversible capacity loss of graphite electrode in lithium-ion batteries," *Journal of power sources*, vol. 68, no. 2, pp. 187–190, 1997.

[25] D. I. Stroe, M. Swierczynski, S. K. Kær, and R. Teodorescu, "Degradation behavior of lithium-ion batteries during calendar ageing-the case of the internal resistance increase," *IEEE Transactions on Industry Applications*, vol. 54, no. 1, pp. 517–525, 2017.

[26] D. Anseán, V. M. García, M. González, C. Blanco-Viejo, J. C. Viera, Y. F. Pulido, and L. Sánchez, "Lithium-ion battery degradation indicators via incremental capacity analysis," *IEEE Transactions on Industry Applications*, vol. 55, no. 3, pp. 2992–3002, 2019.

[27] L. Su, J. Zhang, J. Huang, H. Ge, Z. Li, F. Xie, and B. Y. Liaw, "Path dependence of lithium ion cells aging under storage conditions," *Journal of Power Sources*, vol. 315, pp. 35–46, 2016.

[28] P. A. Cassani and S. S. Williamson, "Significance of battery cell equalization and monitoring for practical commercialization of plug-in hybrid electric vehicles," in *24th Annual IEEE Applied Power Electronics Conference and Exposition, Washington, DC.* IEEE, 2009, pp. 465–471.

[29] I. Zilberman, J. Schmitt, S. Ludwig, M. Naumann, and A. Jossen, "Simulation of voltage imbalance in large lithium-ion battery packs influenced by cell-to-cell variations and balancing systems," *Journal of Energy Storage*, vol. 32, p. 101828, 2020.

[30] D. J. Docimo and H. K. Fathy, "Analysis and control of charge and temperature imbalance within a lithium-ion battery pack," *IEEE Transactions on Control Systems Technology*, vol. 27, no. 4, pp. 1622–1635, 2018.

[31] K. Liu, K. Li, Q. Peng, and C. Zhang, "A brief review on key technologies in the battery management system of electric vehicles," *Frontiers of Mechanical Engineering*, vol. 14, no. 1, pp. 47–64, 2019.

[32] K. W. E. Cheng, B. Divakar, H. Wu, K. Ding, and H. F. Ho, "Battery-management system (BMS) and SOC development for electrical vehicles," *IEEE Transactions on Vehicular Technology*, vol. 60, no. 1, pp. 76–88, 2010.

[33] M. U. Cuma and T. Koroglu, "A comprehensive review on estimation strategies used in hybrid and battery electric vehicles," *Renewable and Sustainable Energy Reviews*, vol. 42, pp. 517–531, 2015.

[34] A. A.-H. Hussein and I. Batarseh, "An overview of generic battery models," in *IEEE Power and Energy Society General Meeting, Detroit.* IEEE, 2011, pp. 1–6.

[35] S. Moore and M. Eshani, "An empirically based electrosource horizon lead-acid battery model," *SAE Transactions*, pp. 421–424, 1996.

[36] H. Fang, X. Zhao, Y. Wang, Z. Sahinoglu, T. Wada, S. Hara, and R. A. De Callafon, "State-of-charge estimation for batteries: A multi-model approach," in *American Control Conference, Portland*. IEEE, 2014, pp. 2779–2785.

[37] L. E. Unnewehr and S. A. Nasar, *Electric vehicle technology*. New York: Wiley, 1982.

[38] H. He, R. Xiong, H. Guo, and S. Li, "Comparison study on the battery models used for the energy management of batteries in electric vehicles," *Energy Conversion and Management*, vol. 64, pp. 113–121, 2012.

[39] G. L. Plett, "Extended Kalman filtering for battery management systems of LiPB-based HEV battery packs: Part 3. State and parameter estimation," *Journal of Power Sources*, vol. 134, no. 2, pp. 277–292, 2004.

[40] O. Tremblay, L.-A. Dessaint, and A.-I. Dekkiche, "A generic battery model for the dynamic simulation of hybrid electric vehicles," in *IEEE Vehicle Power and Propulsion Conference (VPPC), Texas*. IEEE, 2007, pp. 284–289.

[41] O. Tremblay and L. A. Dessaint, "Experimental validation of a battery dynamic model for EV applications," *World Electric Vehicle Journal*, vol. 3, no. 2, pp. 289–298, 2009.

[42] C. Seitl, J. Kathan, G. Lauss, and F. Lehfuß, "Power hardware-in-the-loop implementation and verification of a real time capable battery model," in *23rd IEEE International Symposium on Industrial Electronics (ISIE), Istanbul*. IEEE, 2014, pp. 2285–2290.

[43] V. Srinivasan, J. W. Weidner, and J. Newman, "Hysteresis during cycling of nickel hydroxide active material," *Journal of the Electrochemical Society*, vol. 148, no. 9, p. A969, 2001.

[44] G. L. Plett, *Battery management systems, Volume I: Battery modeling*. Artech House, 2015.

[45] A. Jokar, B. Rajabloo, M. Désilets, and M. Lacroix, "Review of simplified pseudo-two-dimensional models of lithium-ion batteries," *Journal of Power Sources*, vol. 327, pp. 44–55, 2016.

[46] J. Newman and W. Tiedemann, "Porous-electrode theory with battery applications," *AIChE Journal*, vol. 21, no. 1, pp. 25–41, 1975.

[47] T.-S. Dao, C. P. Vyasarayani, and J. McPhee, "Simplification and order reduction of lithium-ion battery model based on porous-electrode theory," *Journal of Power Sources*, vol. 198, pp. 329–337, 2012.

[48] W. Sung and C. B. Shin, "Electrochemical model of a lithium-ion battery implemented into an automotive battery management system," *Computers & Chemical Engineering*, vol. 76, pp. 87–97, 2015.

[49] K. A. Smith, C. D. Rahn, and C.-Y. Wang, "Model-based electrochemical estimation and constraint management for pulse operation of lithium ion batteries," *IEEE Transactions on Control Systems Technology*, vol. 18, no. 3, pp. 654–663, 2009.

[50] D. Di Domenico, A. Stefanopoulou, and G. Fiengo, "Lithium-ion battery state of charge and critical surface charge estimation using an electrochemical model-based extended Kalman filter," *Journal of Dynamic Systems, Measurement, and Control*, vol. 132, no. 6, 2010.

[51] D. Zhang, B. N. Popov, and R. E. White, "Modeling lithium intercalation of a single spinel particle under potentiodynamic control," *Journal of the Electrochemical Society*, vol. 147, no. 3, p. 831, 2000.

[52] H. Fang, Y. Wang, Z. Sahinoglu, T. Wada, and S. Hara, "State of charge estimation for lithium-ion batteries: An adaptive approach," *Control Engineering Practice*, vol. 25, pp. 45–54, 2014.

[53] S. K. Rahimian, S. Rayman, and R. E. White, "Extension of physics-based single particle model for higher charge–discharge rates," *Journal of Power Sources*, vol. 224, pp. 180–194, 2013.

[54] H. Chan, "A new battery model for use with battery energy storage systems and electric vehicles power systems," in *IEEE Power Engineering Society Winter Meeting Conference Proceedings, Singapore*, vol. 1. IEEE, 2000, pp. 470–475.

[55] Y. C. Hsieh, T. D. Lin, R. J. Chen, and H. Y. Lin, "Electric circuit modelling for lithium-ion batteries by intermittent discharging," *IET Power Electronics*, vol. 7, no. 10, pp. 2672–2677, 2014.

[56] H. He, R. Xiong, and J. Fan, "Evaluation of lithium-ion battery equivalent circuit models for state of charge estimation by an experimental approach," *Energies*, vol. 4, no. 4, pp. 582–598, 2011.

[57] Y. Zheng, W. Gao, M. Ouyang, L. Lu, L. Zhou, and X. Han, "State-of-charge inconsistency estimation of lithium-ion battery pack using mean-difference model and extended Kalman filter," *Journal of Power Sources*, vol. 383, pp. 50–58, 2018.

[58] Y. Wang, Z. Chen, and C. Zhang, "On-line remaining energy prediction: A case study in embedded battery management system," *Applied Energy*, vol. 194, pp. 688–695, 2017.

[59] R. Xiong, H. He, and K. Zhao, "Research on an online identification algorithm for a Thevenin battery model by an experimental approach," *International journal of Green Energy*, vol. 12, no. 3, pp. 272–278, 2015.

[60] H. He, R. Xiong, X. Zhang, F. Sun, and J. Fan, "State-of-charge estimation of the lithium-ion battery using an adaptive extended Kalman filter based on an improved Thevenin model," *IEEE Transactions on Vehicular Technology*, vol. 60, no. 4, pp. 1461–1469, 2011.

[61] X. Chen, W. Shen, M. Dai, Z. Cao, J. Jin, and A. Kapoor, "Robust adaptive sliding-mode observer using RBF neural network for lithium-ion battery state of charge estimation in electric vehicles," *IEEE Transactions on Vehicular Technology*, vol. 65, no. 4, pp. 1936–1947, 2015.

[62] T. K. Nizami, Y. V. Karteek, A. Chakravarty, N. Alam, and S. K. Nayak, "Relay approach for parameter extraction of Li-ion battery and SOC estimation using finite time observer," in *Indian Control Conference (ICC), Guwahati*. IEEE, 2017, pp. 59–64.

[63] M. Partovibakhsh and G. Liu, "An adaptive unscented Kalman filtering approach for online estimation of model parameters and state-of-charge of lithium-ion batteries for autonomous mobile robots," *IEEE Transactions on Control Systems Technology*, vol. 23, no. 1, pp. 357–363, 2014.

[64] X. Liu, W. Li, and A. Zhou, "PNGV equivalent circuit model and SOC estimation algorithm for lithium battery pack adopted in AGV vehicle," *IEEE Access*, vol. 6, pp. 23 639–23 647, 2018.

[65] P. Li, "An improved PNGV modeling and SOC estimation for lithium iron phosphate batteries," in *IOP Conference Series: Earth and Environmental Science*, vol. 94, no. 1. IOP Publishing, 2017, p. 012012.

[66] J. Xu, C. C. Mi, B. Cao, and J. Cao, "A new method to estimate the state of charge of lithium-ion batteries based on the battery impedance model," *Journal of Power Sources*, vol. 233, pp. 277–284, 2013.

[67] V. H. Johnson, A. A. Pesaran, and T. Sack, "Temperature-dependent battery models for high-power lithium-ion batteries," National Renewable Energy Lab., Golden, CO (US), Tech. Rep., 2001.

[68] K. S. Ng, C. S. Moo, Y. P. Chen, and Y. C. Hsieh, "Enhanced Coulomb counting method for estimating state-of-charge and state-of-health of lithium-ion batteries," *Applied Energy*, vol. 86, no. 9, pp. 1506–1511, 2009.

[69] B. Zine, K. Marouani, M. Becherif, and S. Yahmedi, "Estimation of battery SOC for hybrid electric vehicle using Coulomb counting method," *International Journal of Emerging Electric Power Systems*, vol. 19, no. 2, 2018.

[70] W. Waag, C. Fleischer, and D. U. Sauer, "Critical review of the methods for monitoring of lithium-ion batteries in electric and hybrid vehicles," *Journal of Power Sources*, vol. 258, pp. 321–339, 2014.

[71] S. Hoenig, H. Singh, and T. G. Palanisamy, "Method for determining state of charge of a battery by measuring its open circuit voltage," 2002, 6,366,054.

[72] V. Pop, H. Bergveld, P. Notten, J. O. het Veld, and P. P. Regtien, "Accuracy analysis of the state-of-charge and remaining run-time determination for lithium-ion batteries," *Measurement*, vol. 42, no. 8, pp. 1131–1138, 2009.

[73] F. Huet, "A review of impedance measurements for determination of the state-of-charge or state-of-health of secondary batteries," *Journal of Power Sources*, vol. 70, no. 1, pp. 59–69, 1998.

[74] A. Hammouche, E. Karden, and R. W. De Doncker, "Monitoring state-of-charge of Ni–MH and Ni–Cd batteries using impedance spectroscopy," *Journal of Power Sources*, vol. 127, no. 1, pp. 105–111, 2004.

[75] S. Rodrigues, N. Munichandraiah, and A. Shukla, "AC impedance and state-of-charge analysis of a sealed lithium-ion rechargeable battery," *Journal of Solid State Electrochemistry*, vol. 3, no. 7-8, pp. 397–405, 1999.

[76] D. N. How, M. Hannan, M. H. Lipu, and P. J. Ker, "State of charge estimation for lithium-ion batteries using model-based and data-driven methods: A review," *IEEE Access*, vol. 7, pp. 136 116–136 136, 2019.

[77] J. Zou, Y. Han, and S. S. So, "Overview of artificial neural networks," *Artificial Neural Networks*, pp. 14–22, 2008.

[78] J. Li and M. Liu, "State-of-charge estimation of lithium-ion batteries using composite multi-dimensional features and a neural network," *IET Power Electronics*, vol. 12, no. 6, pp. 1470–1478, 2019.

[79] C. Bo, B. Zhifeng, and C. Binggang, "State of charge estimation based on evolutionary neural network," *Energy Conversion and Management*, vol. 49, no. 10, pp. 2788–2794, 2008.

[80] H. Chaoui, C. C. Ibe-Ekeocha, and H. Gualous, "Aging prediction and state of charge estimation of a LiFePO4 battery using input time-delayed neural networks," *Electric Power Systems Research*, vol. 146, pp. 189–197, 2017.

[81] L. Kang, X. Zhao, and J. Ma, "A new neural network model for the state-of-charge estimation in the battery degradation process," *Applied Energy*, vol. 121, pp. 20–27, 2014.

[82] W. Y. Chang, "Estimation of the state of charge for a LFP battery using a hybrid method that combines a RBF neural network, an OLS algorithm and AGA," *International Journal of Electrical Power & Energy Systems*, vol. 53, pp. 603–611, 2013.

[83] E. Chemali, P. J. Kollmeyer, M. Preindl, and A. Emadi, "State-of-charge estimation of li-ion batteries using deep neural networks: A machine learning approach," *Journal of Power Sources*, vol. 400, pp. 242–255, 2018.

[84] H. Chaoui and C. C. Ibe-Ekeocha, "State of charge and state of health estimation for lithium batteries using recurrent neural networks," *IEEE Transactions on Vehicular Technology*, vol. 66, no. 10, pp. 8773–8783, 2017.

[85] X. Song, F. Yang, D. Wang, and K. L. Tsui, "Combined CNN-LSTM network for state-of-charge estimation of lithium-ion batteries," *IEEE Access*, vol. 7, pp. 88 894–88 902, 2019.

[86] M. Charkhgard and M. Farrokhi, "State-of-charge estimation for lithium-ion batteries using neural networks and EKF," *IEEE Transactions on Industrial Electronics*, vol. 57, no. 12, pp. 4178–4187, 2010.

[87] Z. Liu, Y. Wang, J. Du, and C. Chen, "RBF network-aided adaptive unscented Kalman filter for lithium-ion battery soc estimation in electric vehicles," in *IEEE Conference on Industrial Electronics and Applications (ICIEA), Singapore*. IEEE, 2012, pp. 1673–1677.

[88] J. C. A. Anton, P. J. G. Nieto, C. B. Viejo, and J. A. V. Vilán, "Support vector machines used to estimate the battery state of charge," *IEEE Transactions on Power Electronics*, vol. 28, no. 12, pp. 5919–5926, 2013.

[89] J. Á. Antón, P. G. Nieto, F. de Cos Juez, F. S. Lasheras, M. G. Vega, and M. R. Gutiérrez, "Battery state-of-charge estimator using the SVM technique," *Applied Mathematical Modelling*, vol. 37, no. 9, pp. 6244–6253, 2013.

[90] J. Meng, G. Luo, and F. Gao, "Lithium polymer battery state-of-charge estimation based on adaptive unscented Kalman filter and support vector machine," *IEEE Transactions on Power Electronics*, vol. 31, no. 3, pp. 2226–2238, 2016.

[91] A. J. Salkind, C. Fennie, P. Singh, T. Atwater, and D. E. Reisner, "Determination of state-of-charge and state-of-health of batteries by fuzzy logic methodology," *Journal of Power Sources*, vol. 80, no. 1-2, pp. 293–300, 1999.

[92] M. F. Samadi and M. Saif, "State-space modeling and observer design of Li-ion batteries using Takagi–Sugeno fuzzy system," *IEEE Transactions on Control System Technology*, vol. 25, no. 1, pp. 301–308, 2016.

[93] P. Singh, R. Vinjamuri, X. Wang, and D. Reisner, "Design and implementation of a fuzzy logic-based state-of-charge meter for Li-ion batteries used in portable defibrillators," *Journal of Power Sources*, vol. 162, no. 2, pp. 829–836, 2006.

[94] F. Behrooz, N. Mariun, M. H. Marhaban, M. A. Mohd Radzi, and A. R. Ramli, "Review of control techniques for HVAC systems: Nonlinearity approaches based on Fuzzy cognitive maps," *Energies*, vol. 11, no. 3, p. 495, 2018.

[95] W. Zhou, Y. Zheng, Z. Pan, and Q. Lu, "Review on the battery model and SOC estimation method," *Processes*, vol. 9, no. 9, p. 1685, 2021.

[96] L. Xu, J. Wang, and Q. Chen, "Kalman filtering state of charge estimation for battery management system based on a stochastic fuzzy neural network battery model," *Energy Conversion and Management*, vol. 53, no. 1, pp. 33–39, 2012.

[97] I. H. Li, W. Y. Wang, S. F. Su, and Y. S. Lee, "A merged fuzzy neural network and its applications in battery state-of-charge estimation," *IEEE Transactions on Energy Conversion*, vol. 22, no. 3, pp. 697–708, 2007.

[98] H. Sheng and J. Xiao, "Electric vehicle state of charge estimation: Nonlinear correlation and fuzzy support vector machine," *Journal of Power Sources*, vol. 281, pp. 131–137, 2015.

[99] Z. Chen, Y. Fu, and C. C. Mi, "State of charge estimation of lithium-ion batteries in electric gdrive vehicles using extended Kalman filtering," *IEEE Transactions on Vehicular Technology*, vol. 62, no. 3, pp. 1020–1030, 2012.

[100] G. Pérez, M. Garmendia, J. F. Reynaud, J. Crego, and U. Viscarret, "Enhanced closed loop state of charge estimator for lithium-ion batteries based on Extended Kalman Filter," *Applied Energy*, vol. 155, pp. 834–845, 2015.

[101] X. Wu, X. Li, and J. Du, "State of charge estimation of lithium-ion batteries over wide temperature range using unscented Kalman filter," *IEEE Access*, vol. 6, pp. 41 993–42 003, 2018.

[102] C. Nguyen Van and T. Nguyen Vinh, "SOC Estimation of the lithium-ion battery pack using a sigma point Kalman filter based on a cells second order dynamic model," *Applied Science*, vol. 10, no. 5, p. 1896, 2020.

[103] Y. Tian, B. Xia, W. Sun, Z. Xu, and W. Zheng, "A modified model based state of charge estimation of power lithium-ion batteries using unscented Kalman filter," *Journal of Power Sources*, vol. 270, pp. 619–626, 2014.

[104] W. He, N. Williard, C. Chen, and M. Pecht, "State of charge estimation for electric vehicle batteries using unscented Kalman filtering," *Microelectronics Reliability*, vol. 53, no. 6, pp. 840–847, 2013.

[105] D. J. Xuan, Z. Shi, J. Chen, C. Zhang, and Y. X. Wang, "Real-time estimation of state-of-charge in lithium-ion batteries using improved central difference transform method," *Journal of Cleaner Production*, vol. 252, p. 119787, 2020.

[106] Z. Chen, X. Li, J. Shen, W. Yan, and R. Xiao, "A novel state of charge estimation algorithm for lithium-ion battery packs of electric vehicles," *Energies*, vol. 9, no. 9, p. 710, 2016.

[107] R. Xiong, H. He, F. Sun, and K. Zhao, "Evaluation on state of charge estimation of batteries with adaptive extended Kalman filter by experiment approach," *IEEE Transactions on Vehicular Technology*, vol. 62, no. 1, pp. 108–117, 2012.

[108] S. Sepasi, R. Ghorbani, and B. Y. Liaw, "A novel on-board state-of-charge estimation method for aged Li-ion batteries based on model adaptive extended Kalman filter," *Journal of Power Sources*, vol. 245, pp. 337–344, 2014.

[109] S. Peng, C. Chen, H. Shi, and Z. Yao, "State of charge estimation of battery energy storage systems based on adaptive unscented Kalman filter with a noise statistics estimator," *IEEE Access*, vol. 5, pp. 13 202–13 212, 2017.

[110] H. He, R. Xiong, and J. Peng, "Real-time estimation of battery state-of-charge with unscented Kalman filter and RTOS μCOS-II platform," *Applied Energy*, vol. 162, pp. 1410–1418, 2016.

[111] A. Tulsyan, Y. Tsai, R. B. Gopaluni, and R. D. Braatz, "State-of-charge estimation in lithium-ion batteries: A particle filter approach," *Journal of Power Sources*, vol. 331, pp. 208–223, 2016.

[112] D. Zhou, K. Zhang, A. Ravey, F. Gao, and A. Miraoui, "Online estimation of lithium polymer batteries state-of-charge using particle filter-based data fusion with multimodels approach," *IEEE Transactions on Industry Applications*, vol. 52, no. 3, pp. 2582–2595, 2016.

[113] S. Schwunk, N. Armbruster, S. Straub, J. Kehl, and M. Vetter, "Particle filter for state of charge and state of health estimation for lithium–iron phosphate batteries," *Journal of Power Sources*, vol. 239, pp. 705–710, 2013.

[114] F. Liu, J. Ma, and W. Su, "Unscented particle filter for SOC estimation algorithm based on a dynamic parameter identification," *Mathematical Problems in Engineering*, vol. 2019, 2019.

[115] M. Ye, H. Guo, R. Xiong, and Q. Yu, "A double-scale and adaptive particle filter-based online parameter and state of charge estimation method for lithium-ion batteries," *Energy*, vol. 144, pp. 789–799, 2018.

[116] C. Lin, H. Mu, R. Xiong, and W. Shen, "A novel multi-model probability battery state of charge estimation approach for electric vehicles using H-infinity algorithm," *Applied Energy*, vol. 166, pp. 76–83, 2016.

[117] Q. Zhu, L. Li, X. Hu, N. Xiong, and G.-D. Hu, "H-∞ based nonlinear observer design for state of charge estimation of lithium-ion battery with polynomial parameters," *IEEE Transactions on Vehicular Technology*, vol. 66, no. 12, pp. 10 853–10 865, 2017.

[118] R. Xiong, Q. Yu, L. Y. Wang, and C. Lin, "A novel method to obtain the open circuit voltage for the state of charge of lithium ion batteries in electric vehicles by using H-infinity filter," *Applied Energy*, vol. 207, pp. 346–353, 2017.

[119] W. Li, M. Rentemeister, J. Badeda, D. Jöst, D. Schulte, and D. U. Sauer, "Digital twin for battery systems: Cloud battery management system with online state-of-charge and state-of-health estimation," *Journal of Energy Storage*, vol. 30, p. 101557, 2020.

[120] Y. Zhang, R. Xiong, H. He, and W. Shen, "Lithium-ion battery pack state of charge and state of energy estimation algorithms using a hardware-in-the-loop validation," *IEEE Transactions on Power Electronics*, vol. 32, no. 6, pp. 4421–4431, 2016.

[121] Q. Yu, R. Xiong, C. Lin, W. Shen, and J. Deng, "Lithium-ion battery parameters and state-of-charge joint estimation based on H-infinity and unscented Kalman filters," *IEEE Transactions on Vehicular Technology*, vol. 66, no. 10, pp. 8693–8701, 2017.

[122] J. Qi, A. F. Taha, and J. Wang, "Comparing Kalman filters and observers for power system dynamic state estimation with model uncertainty and malicious cyber attacks," *IEEE Access*, vol. 6, pp. 77 155–77 168, 2018.

[123] D. Luenberger, "Observers for multivariable systems," *IEEE Transactions on Automatic Control*, vol. 11, no. 2, pp. 190–197, 1966.

[124] X. Hu, F. Sun, and Y. Zou, "Estimation of state of charge of a lithium-ion battery pack for electric vehicles using an adaptive Luenberger observer," *Energies*, vol. 3, no. 9, pp. 1586–1603, 2010.

[125] J. Xu, C. C. Mi, B. Cao, J. Deng, Z. Chen, and S. Li, "The state of charge estimation of lithium-ion batteries based on a proportional-integral observer," *IEEE Transactions on Vehicular Technology*, vol. 63, no. 4, pp. 1614–1621, 2014.

[126] X. Tang, Y. Wang, and Z. Chen, "A method for state-of-charge estimation of LiFePO4 batteries based on a dual-circuit state observer," *Journal of Power Sources*, vol. 296, pp. 23–29, 2015.

[127] S. K. Spurgeon, "Sliding mode observers: A survey," *International Journal of Systems Science*, vol. 39, no. 8, pp. 751–764, 2008.

[128] A. Levant, "Robust exact differentiation via sliding mode technique," *Automatica*, vol. 34, no. 3, pp. 379–384, 1998.

[129] I. S. Kim, "Nonlinear state of charge estimator for hybrid electric vehicle battery," *IEEE Transactions on Power Electronics*, vol. 23, no. 4, pp. 2027–2034, 2008.

[130] J. K. Barillas, J. Li, C. Günther, and M. A. Danzer, "A comparative study and validation of state estimation algorithms for Li-ion batteries in battery management systems," *Applied Energy*, vol. 155, pp. 455–462, 2015.

[131] V. Utkin and H. Lee, "Chattering problem in sliding mode control systems," in *International Workshop on Variable Structure Systems*. IEEE, 2006, pp. 346–350.

[132] H. Lee and V. I. Utkin, "Chattering suppression methods in sliding mode control systems," *Annual Reviews in Control*, vol. 31, no. 2, pp. 179–188, 2007.

[133] Y. B. Shtessel, L. Fridman, and A. Zinober, "Higher order sliding modes," *International Journal of Robust and Nonlinear Control: IFAC-Affiliated Journal*, vol. 18, no. 4-5, pp. 381–384, 2008.

[134] B. Ning, B. Cao, B. Wang, and Z. Zou, "Adaptive sliding mode observers for lithium-ion battery state estimation based on parameters identified online," *Energy*, vol. 153, pp. 732–742, 2018.

[135] J. Du, Z. Liu, Y. Wang, and C. Wen, "An adaptive sliding mode observer for lithium-ion battery state of charge and state of health estimation in electric vehicles," *Control Engineering Practice*, vol. 54, pp. 81–90, 2016.

[136] J. J. Ren, Y. C. Liu, N. Wang, and S. Y. Liu, "Sensorless control of ship propulsion interior permanent magnet synchronous motor based on a new sliding mode observer," *ISA Transactions*, vol. 54, pp. 15–26, 2015.

[137] B. Veselic, B. Perunicic-Drazenovic, and Č. Milosavljevic, "Improved discrete-time sliding-mode position control using euler velocity estimation," *IEEE Transactions on Industrial Electronics*, vol. 57, no. 11, pp. 3840–3847, 2010.

[138] J. M. Foucaut and M. Stanislas, "Some considerations on the accuracy and frequency response of some derivative filters applied to particle image velocimetry vector fields," *Measurement Science and Technology*, vol. 13, no. 7, p. 1058, 2002.

[139] A. Vasebi, S. Bathaee, and M. Partovibakhsh, "Predicting state of charge of lead-acid batteries for hybrid electric vehicles by extended Kalman filter," *Energy Conversion and Management*, vol. 49, no. 1, pp. 75–82, 2008.

[140] W. J. Rugh, *Linear system theory*. Prentice-Hall, Inc., 1996.

[141] K. J. Åström and P. Eykhoff, "System identification: A survey," *Automatica*, vol. 7, no. 2, pp. 123–162, 1971.

[142] A. K. Tangirala, *Principles of system identification: Theory and practice*. CRC Press, 2018.

[143] S. Barcellona and L. Piegari, "Lithium-ion battery models and parameter identification techniques," *Energies*, vol. 10, no. 12, p. 2007, 2017.

[144] W. Xue-Zhe, S. Ze-Chang, and T. Jia-Qing, "Parameter identification and state estimation of Li-ion power battery in hybrid electric vehicle," *Journal of Tongji University Natural Science*, vol. 2, 2008.

[145] S. Orcioni, L. Buccolini, A. Ricci, and M. Conti, "Lithium-ion battery electrothermal model, parameter estimation, and simulation environment," *Energies*, vol. 10, no. 3, p. 375, 2017.

[146] J. Liu, J. Wu, Z. Xiong, and X. Zhu, "Servo system identification using relay feedback: A time-domain approach," *Journal of Manufacturing Science and Engineering*, vol. 134, no. 6, 2012.

[147] W. Stefanutti, P. Mattavelli, S. Saggini, and M. Ghioni, "Autotuning of digitally controlled DC–DC converters based on relay feedback," *IEEE Transactions on Power Electronics*, vol. 22, no. 1, pp. 199–207, 2007.

[148] S. L. Chen, K. K. Tan, and S. Huang, "Friction modeling and compensation of servomechanical systems with dual-relay feedback approach," *IEEE Transactions on Control Systems Technology*, vol. 17, no. 6, pp. 1295–1305, 2009.

[149] S. Majhi, *Advanced control theory: A relay feedback approach*. Cengage Learning Asia, 2009.

[150] G. Marchetti, C. Scali, and D. Lewin, "Identification and control of open-loop unstable processes by relay methods," *Automatica*, vol. 37, no. 12, pp. 2049–2055, 2001.

[151] P. K. Padhy and S. Majhi, "Relay based PI–PD design for stable and unstable FOPDT processes," *Computers & Chemical Engineering*, vol. 30, no. 5, pp. 790–796, 2006.

[152] S. Majhi, "Relay based identification of processes with time delay," *Journal of Process Control*, vol. 17, no. 2, pp. 93–101, 2007.

[153] S. Majhi and D. Atherton, "Online tuning of controllers for an unstable FOPDT process," *IEE Proceedings-Control Theory and Applications*, vol. 147, no. 4, pp. 421–427, 2000.

[154] J. Y. Hung, W. Gao, and J. C. Hung, "Variable structure control: A survey," *IEEE Transactions on Industrial Electronics*, vol. 40, no. 1, pp. 2–22, 1993.

[155] S. Emelyanov, *Variable structure control systems*. Moscow: Nouka, 1967.

[156] U. Itkis, *Control systems of variable structure*. John Wiley & Sons, 1976.

[157] V. Utkin, "Variable structure systems with sliding modes," *IEEE Transactions on Automatic Control*, vol. 22, no. 2, pp. 212–222, 1977.

[158] Y. Shtessel, C. Edwards, L. Fridman, and A. Levant, *Sliding mode control and observation*. Springer, 2014, vol. 10.

[159] R. Ghazali, Y. M. Sam, M. F. Rahmat, A. W. I. M. Hashim *et al.*, "Performance comparison between sliding mode control with PID sliding surface and PID controller for an electro-hydraulic positioning system," *International Journal on Advanced Science, Engineering and Information Technology*, vol. 1, no. 4, pp. 447–452, 2011.

[160] R.-E. Tudoroiu, W. Kecs, M. Dobritoiu, and N. Ilias, "UML-RT hybrid control strategy approach of DC servomotor angular speed by using an embedded sliding mode control," *International Journal of Computer Science and Applications*, vol. 13, no. 2, pp. 61–88, 2016.

[161] G. Bartolini, A. Ferrara, A. Levant, and E. Usai, "On second order sliding mode controllers," in *Variable structure systems, sliding mode and nonlinear control*. Springer, 1999, pp. 329–350.

[162] A. Levant, "Sliding order and sliding accuracy in sliding mode control," *International Journal of Control*, vol. 58, no. 6, pp. 1247–1263, 1993.

[163] V. Utkin, "On convergence time and disturbance rejection of super-twisting control," *IEEE Transactions on Automatic Control*, vol. 58, no. 8, 2013.

[164] J. Davila, L. Fridman, and A. Levant, "Second-order sliding-mode observer for mechanical systems," *IEEE Transactions on Automatic Control*, vol. 50, no. 11, pp. 1785–1789, 2005.

[165] T. Floquet and J.-P. Barbot, "Super twisting algorithm-based step-by-step sliding mode observers for nonlinear systems with unknown inputs," *International Journal of Systems Science*, vol. 38, no. 10, pp. 803–815, 2007.

[166] K. Zhang, T. Hatano, T. T. Nguyen, C. Edwards, G. Herrmann, S. Burgess, M. Antognozzi, S. Khan, R. Harniman, and M. Miles, "A super-twisting observer for atomic-force reconstruction in a probe microscope," *Control Engineering Practice*, vol. 94, p. 104191, 2020.

[167] E. Cruz-Zavala, J. A. Moreno, and L. M. Fridman, "Uniform robust exact differentiator," *IEEE Transactions on Automatic Control*, vol. 56, no. 11, pp. 2727–2733, 2011.

[168] Y. Feng, C. Xue, Q. L. Han, F. Han, and J. Du, "Robust estimation for state-of-charge and state-of-health of lithium-ion batteries using integral-type terminal sliding-mode observers," *IEEE Transactions on Industrial Electronics*, vol. 67, no. 5, pp. 4013–4023, 2019.

[169] A. F. Filippov, *Differential equations with discontinuous righthand sides: Control systems*. Springer Science & Business Media, 2013, vol. 18.

[170] Y. Huangfu, J. Xu, D. Zhao, Y. Liu, and F. Gao, "A novel battery state of charge estimation method based on a super-twisting sliding mode observer," *Energies*, vol. 11, no. 5, p. 1211, 2018.

[171] Z. Wei, K. J. Tseng, N. Wai, T. M. Lim, and M. Skyllas-Kazacos, "Adaptive estimation of state of charge and capacity with online identified battery model for vanadium redox flow battery," *Journal of Power Sources*, vol. 332, pp. 389–398, 2016.

[172] M. Wielitzka, M. Dagen, and T. Ortmaier, "Joint unscented Kalman filter for state and parameter estimation in vehicle dynamics," in *IEEE Conference on Control Applications (CCA), Sydney*. IEEE, 2015, pp. 1945–1950.

[173] L. Pei, C. Zhu, T. Wang, R. Lu, and C. Chan, "Online peak power prediction based on a parameter and state estimator for lithium-ion batteries in electric vehicles," *Energy*, vol. 66, pp. 766–778, 2014.

[174] J. Hou, Y. Yang, and T. Gao, "A normal-gamma-based adaptive dual unscented Kalman filter for battery parameters and state-of-charge estimation with heavy-tailed measurement noise," *International Journal of Energy Research*, vol. 44, no. 5, pp. 3510–3525, 2020.

[175] J. Brand, Z. Zhang, and R. K. Agarwal, "Extraction of battery parameters of the equivalent circuit model using a multi-objective genetic algorithm," *Journal of Power Sources*, vol. 247, pp. 729–737, 2014.

[176] R. Zhu, B. Duan, C. Zhang, and S. Gong, "Accurate lithium-ion battery modeling with inverse repeat binary sequence for electric vehicle applications," *Applied Energy*, vol. 251, p. 113339, 2019.

[177] X. Lai, W. Gao, Y. Zheng, M. Ouyang, J. Li, X. Han, and L. Zhou, "A comparative study of global optimization methods for parameter identification of different equivalent circuit models for Li-ion batteries," *Electrochimica Acta*, vol. 295, pp. 1057–1066, 2019.

[178] J. Zhang, Y. Wei, and H. Qi, "State of charge estimation of LiFePO4 batteries based on online parameter identification," *Applied Mathematical Modelling*, vol. 40, no. 11-12, pp. 6040–6050, 2016.

[179] S. Zhang and X. Zhang, "A comparative study of different online model parameters identification methods for lithium-ion battery," *Science China Technological Sciences*, vol. 64, no. 10, pp. 2312–2327, 2021.

[180] M. Verbrugge, "Adaptive, multi-parameter battery state estimator with optimized time-weighting factors," *Journal of Applied electrochemistry*, vol. 37, no. 5, pp. 605–616, 2007.

[181] T. Feng, L. Yang, X. Zhao, H. Zhang, and J. Qiang, "Online identification of lithium-ion battery parameters based on an improved equivalent-circuit model and its implementation on battery state-of-power prediction," *Journal of Power Sources*, vol. 281, pp. 192–203, 2015.

[182] H. Rahimi-Eichi, F. Baronti, and M. Y. Chow, "Online adaptive parameter identification and state-of-charge coestimation for lithium-polymer battery cells," *IEEE Transactions on Industrial Electronics*, vol. 61, no. 4, pp. 2053–2061, 2013.

[183] A. Vahidi, A. Stefanopoulou, and H. Peng, "Recursive least squares with forgetting for online estimation of vehicle mass and road grade: Theory and experiments," *Vehicle System Dynamics*, vol. 43, no. 1, pp. 31–55, 2005.

[184] P. C. Young, "Recursive least squares estimation," in *Recursive Estimation and Time-Series Analysis*. Springer, 2011, pp. 29–46.

[185] J. A. Moreno and M. Osorio, "Strict Lyapunov functions for the super-twisting algorithm," *IEEE Transactions on Automatic Control*, vol. 57, no. 4, pp. 1035–1040, 2012.

[186] R. Lairenlakpam, G. Thakre, P. Gupta, Y. Singh, and P. Kumar, "Electric conversion of a polluting gasoline vehicle into an electric vehicle and its performance and drive cycle analysis," in *IEEE International Conference on Power Electronics, Drives, and Energy System (PEDES), Chennai*. IEEE, 2018, pp. 1–6.

[187] Y. Shtessel, M. Taleb, and F. Plestan, "A novel adaptive-gain supertwisting sliding mode controller: Methodology and application," *Automatica*, vol. 48, no. 5, pp. 759–769, 2012.

[188] Y. B. Shtessel, J. A. Moreno, F. Plestan, L. M. Fridman, and A. S. Poznyak, "Super-twisting adaptive sliding mode control: A Lyapunov design," in *49th IEEE Conference on Decision Control (CDC), Atlanta*. IEEE, 2010, pp. 5109–5113.

[189] K. Dai, J. Wang, and H. He, "An improved SOC estimator using time-varying discrete sliding mode observer," *IEEE Access*, vol. 7, pp. 115 463–115 472, 2019.

[190] J. A. Moreno, "A linear framework for the robust stability analysis of a generalized super-twisting algorithm," in *Proceedings of 6th International Conference on Electrical Engineering, Computer Science and Automatic Control (CCE 2009), Toluca*. IEEE, 2009, pp. 1–6.

[191] Q. Song, Y. Mi, and W. Lai, "A novel variable forgetting factor recursive least square algorithm to improve the anti-interference ability of battery model parameters identification," *IEEE Access*, vol. 7, pp. 61 548–61 557, 2019.

[192] X. Sun, J. Ji, B. Ren, C. Xie, and D. Yan, "Adaptive forgetting factor recursive least square algorithm for online identification of equivalent circuit model parameters of a lithium-ion battery," *Energies*, vol. 12, no. 12, p. 2242, 2019.

[193] T. Fortescue, L. S. Kershenbaum, and B. E. Ydstie, "Implementation of self-tuning regulators with variable forgetting factors," *Automatica*, vol. 17, no. 6, pp. 831–835, 1981.

[194] T. Kim, Y. Wang, H. Fang, Z. Sahinoglu, T. Wada, S. Hara, and W. Qiao, "Model-based condition monitoring for lithium-ion batteries," *Journal of Power Sources*, vol. 295, pp. 16–27, 2015.

[195] V. H. Duong, H. A. Bastawrous, K. Lim, K. W. See, P. Zhang, and S. X. Dou, "Online state of charge and model parameters estimation of the LiFePO4 battery in electric vehicles using multiple adaptive forgetting factors recursive least-squares," *Journal of Power Sources*, vol. 296, pp. 215–224, 2015.

[196] D. J. Park, B. E. Jun, and J. H. Kim, "Fast tracking RLS algorithm using novel variable forgetting factor with unity zone," *Electronics Letters*, vol. 27, no. 23, pp. 2150–2151, 1991.

[197] E. Jiménez-Rodríguez, E. Mejía-Estrada, Ó. Jaramillo-Zuluaga, and J. D. Sánchez-Torres, "An integral sliding mode observer for linear systems," *International Federation of Automatic Conttrol*, 2016.

[198] P. V. Surjagade, S. Shimjith, and A. Tiwari, "Second order integral sliding mode observer and controller for a nuclear reactor," *Nuclear Engineering and Technology*, vol. 52, no. 3, pp. 552–559, 2020.

[199] I. L. G. Borlaug, K. Y. Pettersen, and J. T. Gravdahl, "Tracking control of an articulated intervention AUV in 6DOF using the generalized super-twisting algorithm," in *American Control Conference (ACC), Philadelphia*. IEEE, 2019, pp. 5705–5712.